Characterization of the Vocal Fold Lamina Propria towards Voice Restoration

by

Mariah Somer Hahn
B.S. Chemical Engineering
University of Texas at Austin, May 1998
M.S. Electrical Engineering
Stanford University, January 2001

Submitted to the Department of Electrical Engineering and Computer Science
in Partial Fulfillment of the Requirements for the Degree of
Doctor of Philosophy in Electrical Engineering and Computer Science.

September 2004

Signature of Author: _____ 07/20/2004
Department of Electrical Engineering and Computer Science
July 21, 2004

Certified by: _____
Robert S. Langer
Germeshausen Professor, Chemical and Biomedical Engineering
Dissertation Supervisor

Accepted by: _____
Arthur C. Smith
Professor Emeritus of Electrical Engineering and Computer Science
Chairman, Committee for Graduate Students

Characterization of the Vocal Fold Lamina Propria towards Voice Restoration

by

Mariah Somer Hahn

Submitted to the Department of Electrical Engineering and Computer Science
on July 21, 2004 in Partial Fulfillment of the Requirements for the Degree of
Doctor of Philosophy in Electrical Engineering and Computer Science

ABSTRACT

During normal speech, human vocal folds sustain greater than 100 high impact collisions each second. When the pliability of this complex biomechanical system is reduced by scarring, voice quality may be compromised. Currently, little can be done to treat patients affected with voice loss or chronic voice impairment due to scarring. Because of the size of the patient population suffering from voice impairment secondary to scarring, alternate treatment methods are currently being actively investigated. An implant-based approach is one strategy for treating lamina propria scarring.

To rationally design an implant material for this purpose, it is important to have a more complete understanding of lamina propria biochemistry and microstructure than is currently in literature. This dissertation presents the following critical insights into normal human lamina propria biochemical structure:

1.) quantitative analysis of collagen, elastin, hyaluronan, and proteoglycan presence;
2.) quantitative examination of the spatial distributions of collagen, elastin, and hyaluronan, and qualitative investigation of the spatial distributions of specific proteoglycan types; and
3.) assessment of total cellularity and spatial variations in extracellular matrix turnover.

Similar analyses have been carried out on the vocal fold lamina propria of normal dog, pig, and ferret towards identifying an appropriate animal model for implant trials.

Dissertation Supervisor: Robert S. Langer
Title: Germeshausen Professor, Chemical & Biomedical Engineering

Vita

Mariah Hahn was born to Janet and Larry Douglas in 1977. She received her Bachelors of Science in chemical engineering from the University of Texas at Austin in May 1998. With her husband's encouragement, she decided to pursue a long-standing interest and apply to graduate school in electrical engineering. She received her Masters of Science in electrical engineering from Stanford in January 2001. In February 2001, she began her doctoral work in electrical engineering and computer science at MIT.

Dedication

To my husband, Juergen, who supported me when I chose to go to graduate school in a different state, even though our time apart was a hardship for us both, and who provided constant encouragement throughout my graduate work. In so many ways, the honor of this degree belongs to us both.

Acknowledgements

I would like to express my gratitude to Prof. Robert Langer and Dr. Steven Zeitels for their personal and financial support during my research program. I would also like to thank the other members of my dissertation committee, Prof. Freeman and Prof. Grodzinsky, for their time and assistance in helping me complete this work, and the National Science Foundation for financial support during my first three years as a graduate student. I would also like to extend a special thanks to Dr. Rox Anderson, who has often gone out of his way for me, and to Prof. Barry Starcher for analyzing the desmosine levels reported in this dissertation.

A number of people have helped me in this journey – each contributing in substantial ways, even if our interactions were brief. Among these individuals are: Prof. James Kobler, Prof. Robert Hillman, and Diane Jones of the Massachusetts Eye and Ear Infirmary; Constance Beal, Ilda Moura, Prof. Martha Gray, Dr. Robert Marini, Kathyrn Madden, and Kathleen Cormier of MIT. I am indebted to all my colleagues in the Langer lab, but in particular to Jason Fuller, Xinqiao Jia, Joe Seidel, Erin Lavik, Shulamit Levenberg, Ben Teply, Akin Akinc, Greg Zugates, David Lavan, Hyoungshin Park, Thanh-Nga Tran, Tommy Thomas, and Elise Westmeyer. I have also had the help of several great undergraduate researchers, including Cindy Jao, Johanna Salazar-Lazaro, Leila Agha, Rachel Livingston, and Andy Lin.

Outside of academia, Deborah Dowd, Nisha Abraham, and Jenny McDonald have encouraged and supported me through difficult times during my PhD and have been wonderful friends. And always, always behind the scenes supporting me has been my husband, Juergen. So many people have come into play to make this day happen for me, and all of them are in my heart.

Table of Contents

List of Figures

List of Tables

Chapter 1. Motivation and Approach

1.1 Introduction to vocal fold anatomy and scarring

The human vocal folds are paired structures roughly 10-15 mm in length and 5mm thick, which are brought into apposition across the airway for sound production. Each vocal fold is a laminated structure consisting of pliable vibratory layer of connective tissue, known as the lamina propria (LP), sandwiched between epithelium and muscle [1]. (See Figure 1.1).

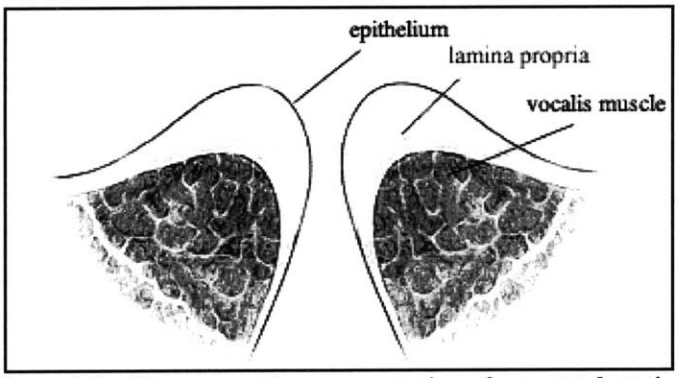

Figure 1.1 : Diagrammatic representation of a coronal section through the midmembranous human vocal folds

The human LP is often further subdivided into the superficial (SLP), intermediate (ILP), and deep (DLP) layers [2]. These subdivisions have traditionally been based on histologically-observed changes in elastin and collagen concentration within human LP [3]. The intermediate and deep layers, also known as the vocal ligament, are thought to be involved in balancing the tension present in the vocalis muscle with that in the SLP [4]. The SLP is believed to be the region of the vocal fold that sustains the most stress during vibration [5], and most patients suffering from vocal fold scarring have trauma limited to this layer [6].

As air is forced out of the lungs, the muscle and overlying LP of the vocal folds are driven into vibration, creating a quasi-periodic valving of air flow. During normal speech, human vocal folds sustain greater than 100 high impact collisions per second [7]. Thus, the vocal folds are vulnerable to mechanical damage or scarring from overuse and abuse of the voice. Scarred SLP can also result from benign and malignant disease processes requiring ablative surgery or radiation therapy, or from prolonged endotracheal intubation [8]. The altered geometry and increased tissue stiffness associated with vocal fold scarring cause voice changes ranging from hoarseness to complete voice loss. Since little can currently be done to treat patients suffering from voice impairment secondary to scarring and because of the size of this patient population, alternate treatment methods are currently being actively pursued [6,

9-18]. One such alternate approach, and the one which has formed the underlying basis for this project, is the use of an implant to restore normal function.

This intricate vibratory system has an additional layer of complexity that arises from the high levels of neurological control needed to express emotional states through voice [19]. In fact, voice and mind are so connected that psychological dysfunction can create voice dysfunction in the absence of any vocal fold defect [20]. Or vice versa, the effects of LP abnormalities on fold vibration can be markedly reduced by this same neurological input. This situation has significant implications for the potential of implant-based strategies to restore functionally normal voice as well as for methods that can be used to assess restoration quality. Specifically, LP restoration does not need to be complete for near-complete functional restoration to occur. At the same time, the intimate neurological control of the vocal folds creates ambiguity in the use of phonation-based assessment tools for implant evaluation.

1.2 Current methods in scar treatment

Aspects of vocal fold scarring are currently addressed with a variety of surgical techniques, from scar lysis to tissue replacement with flaps, grafts, and injectable materials [6, 14]. Whereas scar lysis, flaps, and grafts attempt to remove the scar tissue and/or replace it with new tissue, injectable materials are used to augment the amount of "functional" tissue, reducing the impact of the scarred portion on the overall vibration. Effectively, the implant is meant to alter the mass distribution in and pliability of the scarred region of the LP so that normal functionality is restored. Synthetic materials such as Teflon and silicone [21], and biologically-related or derived materials, such as fascia [22], fat [23], and collagen [24], have previously been used as augmentation substances. More recently, patients have been injected with hylaform (hylan b), a modified form of hyaluronan [17].

Important starting points can be gained from these previous research studies, including that: 1.) biodegradable implant materials have generally been resorbed prior to generation of lasting replacement tissue, and as such restoration has often been temporary; 2.) non-biodegradable implant strategies have generally resulted in foreign body responses over the long term, often exacerbating the scarring and voice dysfunction originally present [6, 14]. Beyond this, however, how voice outcome specifically relates to the chemical and structural properties of a given implant material remains largely unclear, limiting the ability to predict how modification of a given implant material will affect functional outcome.

This lack of clarity arises in part from the reliance on phonation-based assessment tools as common measures of "success" in most of these implant trials. Although these criteria have an intuitive appeal in that the desired output of the implant-"input" into the "host-implant interactions" black-box is functional restoration of voice, relating these phonation-based measures back to the implant material is complicated by the diverse variables that impact voice. The result is that observed vocal range and quality and vibratory behavior cannot be unambiguously correlated with the implant material and, thus, do not clearly indicate how a

material should be changed to improve outcome. This additional level of insight requires objective information concerning cellular level implant-host interactions. It is a goal of this thesis is to identify and develop measurable "outputs" which not only are correlated with vibratory function but also give key insight into implant-host interactions at the cellular and microstructural level.

Two possible "outputs" sets that meet these joint criteria are: 1.) combined quantitative biochemical and histological implant assessment, or 2.) combined biomechanical and histological implant examination. These two sets are linked through the structure-function relationship [25], which essentially states that, given appropriate biochemical composition and microstructural information, a tissue's biomechanical properties can be predicted. Results from implant analysis using either of these "output" sets could then be compared to established benchmarks for normal LP, allowing objective evaluation of implant success and insight into possible implant alterations to improve outcome.

A final comment needs to be made concerning the above listed "output" evaluation sets. It is important to differentiate the biomechanical properties of the LP from vocal fold vibratory behavior. Vocal fold vibration is a complex interplay between the underlying muscle, the geometry and pliability of the LP, and neurological input. The biomechanical properties of the LP would ideally be independent of the muscle vibratory behavior, vocal fold geometry, and neurological input.

1.3. Current understanding of LP biochemistry and microstructure

In recent decades, a number of histological studies have been published which have significantly advanced the understanding of LP biochemical composition and microstructure. For example, the distributions of total collagen [26-31], elastin, [29, 30, 32-35], and general mucopolysaccharides [34, 36] throughout the human LP have been well studied. Since these molecules have key biomechanical functions, these studies have increased the insight into the structure-function relationship of this tissue [4]. However, quantitative information is still needed to better complete the functional picture sketched by this histological data. In fact, all currently published protein-based biochemical studies of the LP have been qualitative, to the author's knowledge.

A number of researchers have attempted to assess the mechanical properties of the LP. Most of these studies have performed traditional bulk tensile tests on the LP or have assessed low frequency LP viscoelasticity using cone and plate rheometry [29, 37-40]. However, it is not clear how relevant these biomechanical measurements are in the context of the actual stresses and strains sustained by the vocal fold lamina propria in its normal operating frequency range. For example, it is unclear whether low frequency (<10Hz) data can be extrapolated to make high frequency (>~100Hz) functional assessments. In addition, the relatively complex macroscopic geometry of the LP makes the results from traditional bulk mechanical testing techniques difficult to interpret reliably.

1.4 Method of approach

Based on initial feasibility studies of biomechanical versus biochemical lamina propria analyses, it was decided to pursue development of biochemical and microstructural / histological benchmarks for normal vocal fold LP towards implant evaluation. Important outcomes from these feasibility studies are discussed in Appendix A.

There are two approaches generally taken to studying tissue biochemistry: protein-based and mRNA-based biochemical techniques. Although mRNA measures have substantial value in elucidating the dynamic state of tissue cellular physiology, there is generally not a one-to-one correlation between mRNA levels of a specific extracellular matrix (ECM) molecule and the concentration of that molecule within the ECM [41]. With respect to first-order implant evaluation schemes, understanding what is quantitatively present in the normal vocal fold LP ECM is arguably of higher priority than elucidating the dynamic state of the cells. As such, this thesis will focus on protein-based ECM biochemical quantitation.

The concentration and distribution of the following major biomolecules in the normal human LP will be investigated: (1) total collagen, (2) elastin, (3) hyaluronan, and (4) proteoglycan / associated sulfated glycosaminoglycan side chains. Fibrous proteins, such as collagen and elastin, are of interest in part due to the strong roles these molecules generally play in determining tissue biomechanical function. In particular, collagen contributes to the tensile response of tissue, while elastin tends to dominate the elastic response. Hyaluronan impacts tissue viscous response, and proteoglycans not only serve important regulatory functions by sequestering bioactive molecules [42], but also contribute to tissue biomechanical properties [25]. Therefore, quantitative study of these ECM molecules should yield insight into the biomechanics of the LP. In addition, since tissue cellularity is altered in a number of physiological and pathological processes, normal human LP total cellularity has been examined.

Since the appropriate choice of animal model is integral to development of restoration strategies applicable to humans, the LPs of several potential animal models have been similarly studied and compared to the human LP. Dogs and pigs are currently two standard animal models in vocal fold research, and hence these animals have been investigated. Ferrets have also been analyzed in the present work for their potential as a small animal model for LP implant studies. Although ferrets have not previously been used for vocal fold research, their large airway relative to their size makes controlled surgical access to their vocal folds feasible. In addition, ferrets appear to phonate more frequently and with greater range than rabbits [43], a small animal that has been used in several recent vocal fold research studies [10, 44].

Chapters 3 and 4 present results from biochemical and immunohistochemical studies of LP proteoglycans and LP collagen and fibronectin, respectively. Chapters 4 and 5 discuss biochemical and histological results for elastin and hyaluronan and for tissue cellularity and turnover, respectively.

Towards future in vitro studies of the interactions of LP cells with various implant materials, methods for isolating vocal fold LP fibroblasts and appropriate media types for LP cell growth and proliferation have been examined, as discussed in Appendix B.

1.5 Literature cited

1. Citardi, M.J., C.L. Gracco, and C.T. Sasaki, The Anatomy of the Human Larynx, in Diagnosis and Treatment of Voice Disorders, J.S. Rubin, R.T. Sataloff, and G.S. Korovin, Editors. 1995, Igaku-Shoin Medical Publishers, Inc.: New York.
2. Gray, S.D., Cellular physiology of the vocal folds. Otolaryngologic Clinics of North America, 2000. **33**(4): p. 679-+.
3. Kurita, S., et al., The Layer Structure of the Vocal Fold - Age-Dependent Variations. Folia Phoniatrica, 1980. **32**(3): p. 210-210.
4. Hirano, M. and Y. Kakita, eds. Cover-body theory of vocal fold vibration. Speech Science, ed. R. Daniloff. 1985, College-Hill Press: San Diego.
5. Gunter, H.E., A mechanical model of vocal-fold collision with high spatial and temporal resolutions. Journal of the Acoustical Society of America, 2003. **113**(2): p. 994-1000.
6. Rosen, C.A., Vocal fold scar - Evaluation and treatment. Otolaryngologic Clinics of North America, 2000. **33**(5): p. 1081-+.
7. Scherer, R.C., Laryngeal Function During Phonation, in Diagnosis and Treatment of Voice Disorders, J.S. Rubin, et al., Editors. 1995, Igaku-Shoin Medical Publishers, Inc: New York.
8. Zeitels, S.M. and G.B. Healy, Medical progress: Laryngology and phonosurgery. New England Journal of Medicine, 2003. **349**(9): p. 882-892.
9. Webb, K., et al., Comparison of human fibroblast ECM-related gene expression on elastic three-dimensional substrates relative to two-dimensional films of the same material. Biomaterials, 2003. **24**(25): p. 4681-4690.
10. Kriesel, K.J., et al., Treatment of vocal fold scarring: Rheological and histological measures of homologous collagen matrix. Annals of Otology Rhinology and Laryngology, 2002. **111**(10): p. 884-889.
11. Woo, P., R. Rahbar, and Z. Wang, Fat implantation into Reinke's space: A histologic and stroboscopic study in the canine. Annals of Otology Rhinology and Laryngology, 1999. **108**(8): p. 738-744.
12. Chan, R.W. and I.R. Titze, Hyaluronic acid (with fibronectin) as a bioimplant for the vocal fold mucosa. Laryngoscope, 1999. **109**(7): p. 1142-1149.
13. Chan, R.W. and I.R. Titze, Viscosities of implantable biomaterials in vocal fold augmentation surgery. Laryngoscope, 1998. **108**(5): p. 725-731.

14. Benninger, M.S., et al., Vocal fold scarring: Current concepts and management. Otolaryngology-Head and Neck Surgery, 1996. **115**(5): p. 474-482.
15. Thibeault, S.L., et al., Histologic and rheologic characterization of vocal fold scarring. Journal of Voice, 2002. **16**(1): p. 96-104.
16. Hallen, L., et al., DiHA (dextranomers in hyaluronan) injections for treatment of insufficient closure of the vocal folds: Early clinical experiences. Laryngoscope, 2001. **111**(6): p. 1063-1067.
17. Hertegard, S., et al., Cross-linked hyaluronan used as augmentation substance for treatment of glottal insufficiency: Safety aspects and vocal fold function. Laryngoscope, 2002. **112**(12): p. 2211-2219.
18. Huber, J.E., et al., Extracellular matrix as a scaffold for laryngeal reconstruction. Annals of Otology Rhinology and Laryngology, 2003. **112**(5): p. 428-433.
19. Benninger, M.S. and C. Schwimmer, Functional Neuroophysiology and Vocal Fold Paralysis, in Diagnosis and Treatment of Voice Disorders, J.S. Rubin, et al., Editors. 1995, Igaku-Shoin Medical Publishers, Inc.: New York.
20. Rosen, D.C. and R.T. Sataloff, Psychological Aspects of Voice Disorders, in Diagnosis and Treatment of Voice Disorders, J.S. Rubin, et al., Editors. 1995, Igaku-Shoin Medical Publishers, Inc.: New York.
21. Rosen, C.A., Phonosurgical vocal fold injection - Procedures and materials. Otolaryngologic Clinics of North America, 2000. **33**(5): p. 1087-+.
22. Duke, S.G., et al., Fascia augmentation of the vocal fold: Graft yield in the canine and preliminary clinical experience. Laryngoscope, 2001. **111**(5): p. 759-764.
23. Hsiung, M.W., et al., Autogenous fat injection for vocal fold atrophy. European Archives of Oto-Rhino-Laryngology, 2003. **260**(9): p. 469-474.
24. Staskowski, P.A., C.N. Ford, and K. Inagi, The histologic fate of autologous collagen injected into the canine vocal fold. Otolaryngology-Head and Neck Surgery, 1998. **118**(2): p. 187-190.
25. Fung, Y.C., Biomechanics: Mechanical Properties of Living Tissues. 2 ed. 1993, New York: Springer-Verlag.
26. Hammond, T.H., S.D. Gray, and J.E. Butler, Age- and gender-related collagen distribution in human vocal folds. Annals of Otology Rhinology and Laryngology, 2000. **109**(10): p. 913-920.
27. Madruga de Melo, E., et al., Distribution of collagen in the lamina propria of the human vocal fold. Laryngoscope, 2003. **113**(12): p. 2187-91.
28. Sato, K., M. Hirano, and T. Nakashima, Age-related changes of collagenous fibers in the human vocal fold mucosa. Annals of Otology Rhinology and Laryngology, 2002. **111**(1): p. 15-20.
29. Gray, S.D., et al., Biomechanical and histologic observations of vocal fold fibrous proteins. Annals of Otology Rhinology and Laryngology, 2000. **109**(1): p. 77-85.
30. Ishii, K., et al., Age-related development of the arrangement of connective tissue fibers in the lamina propria of the human vocal fold. Annals of Otology Rhinology and Laryngology, 2000. **109**(11): p. 1055-1064.
31. Sato, K., Reticular fibers in the vocal fold mucosa. Annals of Otology Rhinology and Laryngology, 1998. **107**(12): p. 1023-1028.

32. Sato, K. and M. Hirano, Age-related changes of elastic fibers in the superficial layer of the lamina propria of vocal folds. Annals of Otology Rhinology and Laryngology, 1997. **106**(1): p. 44-48.
33. Ximenes, J.A., et al., Histologic changes in human vocal folds correlated with aging: A histomorphometric study. Annals of Otology Rhinology and Laryngology, 2003. **112**(10): p. 894-898.
34. Hammond, T.H., et al., The intermediate layer: A morphologic study of the elastin and hyaluronic acid constituents of normal human vocal folds. Journal of Voice, 1997. **11**(1): p. 59-66.
35. Hammond, T.H., et al., Age- and gender-related elastin distribution changes in human vocal folds. Otolaryngology-Head and Neck Surgery, 1998. **119**(4): p. 314-322.
36. Pawlak, A.S., et al., Immunocytochemical study of proteoglycans in vocal folds. Annals of Otology Rhinology and Laryngology, 1996. **105**(1): p. 6-11.
37. Titze, I.R., Stresses in Vocal-Fold Tissues During Normal Phonation. Journal of the Acoustical Society of America, 1976. **60**: p. S64-S64.
38. Titze, I.R., The Physics of Small-Amplitude Oscillation of the Vocal Folds. Journal of the Acoustical Society of America, 1988. **83**(4): p. 1536-1552.
39. Chan, R.W. and I.R. Titze, Viscoelastic shear properties of human vocal fold mucosa: Measurement methodology and empirical results. Journal of the Acoustical Society of America, 1999. **106**(4): p. 2008-2021.
40. Chan, R.W. and I.R. Titze, Viscoelastic shear properties of human vocal fold mucosa: Theoretical characterization based on constitutive modeling. Journal of the Acoustical Society of America, 2000. **107**(1): p. 565-580.
41. Westermeier, R. and T. Naven, Proteomics in practice : a laboratory manual of proteome analysis. 2002, Weinheim: Wiley-VCH.
42. Iozzo, R.V., Matrix proteoglycans: From molecular design to cellular function. Annual Review of Biochemistry, 1998. **67**: p. 609-652.
43. Aitkin, L.M., J.E. Nelson, and R.K. Shepherd, Hearing, Vocalization and the External Ear of a Marsupial, the Northern Quoll, Dasyurus-Hallucatus. Journal of Comparative Neurology, 1994. **349**(3): p. 377-388.
44. Hertegard, S., et al., Viscoelastic properties of rabbit vocal folds after augmentation. Otolaryngology-Head and Neck Surgery, 2003. **128**(3): p. 401-406.

Chapter 2. Proteoglycans

2.1 Introduction

Proteoglycans (PGs) represent a large family of complex molecules composed of core proteins to which sulfated glycosaminoglycan (sGAG) side chains, such as dermatan sulfate (DS), chondroitin sulfate (CS), keratan sulfate (KS), or heparan sulfate (HS), are attached. PGs are known to regulate cell adhesion, cell growth, and matrix formation [1], and to influence tissue biomechanical properties [1, 2]. Both the absolute quantities and spatial distributions of PGs types are important in the maintenance of appropriate tissue physiology [3].

Histological studies on the PG/GAG content of the vocal fold lamina propria (LP) have been published [4, 5] which have advanced the understanding of the normal presence of these molecules. However, significant questions remain. Although the influence of PGs on LP biomechanics has been discussed [5, 6], the degree of this impact is difficult to assess, since the actual concentration of PGs in the LP is currently unknown. Pawlak et al.[5] immunohistochemically analyzed the distributions of decorin, CS, KS, and a heparan sulfate PG (HSPG) in normal human LP. A primary finding of this study was the intracellular localization of CS. This is an unusual result which warrants further investigation, since many other loose connective tissues contain this sGAG type throughout the ECM [7]. In addition, the antibody used by Pawlak et al.[5] to examine the presence of HSPGs appears to recognize only one molecule (Chemicon International, Technical Assistance) of the rich HSPG family. Garrett et al.[4] histologically evaluated overall GAG distributions in dog and pig LP, but not the distributions of specific PG/sGAG types. Thus, the quantity and distribution of PGs in human and animal model vocal fold LPs merit further study.

The present work examines and compares the PG/sGAG content of normal human vocal fold LP and that of dog, pig, and ferret. Specifically, LP PGs levels are quantitated indirectly by measuring the concentration of total sGAG side chains, and immunohistochemical analyses for specific PG/sGAG classes are presented for all four species.

2.2 Materials and methods

2.2.1 Tissue procurement

Eight human larynges were obtained within 24 hours post-mortem. The age, gender, source, and method of preservation of these specimens are described in Table 2.1. All human tissue included in this study appeared normal as assessed by a pathologist, and donors had no known medical history of vocal fold surgery or chronic voice disorders. Human tissue was procured with the approval and in accordance with the guidelines of the Massachusetts Institute of

Technology (MIT) and Massachusetts Eye and Ear Infirmary (MEEI) committees on human experimentation.

Six female beagle larynges (Marshall Farms, North Rose, NY) from 2-3 year old animals, six pig larynges (Research 87, Inc) from 6-12 month old animals of both genders, and four adult male ferret larynges (Marshall Farms, North Rose, NY) were recovered within 6 hours post-mortem. All animal specimens included in this study had macroscopically and microscopically normal vocal folds. For each animal laryngeal specimen, one hemi-larynx was snap-frozen and stored at -80°C for biochemical analysis and the second hemi-larynx was placed into neutral buffered formalin at 4°C for histochemical studies.

Epiglottis tissue from each species was processed histologically as a positive control tissue for immunohistochemical studies. Pig hyaline cartilage was used as a biochemical assay control. All animal tissue was procured with the approval and according to the guidelines of the MIT animal care committee.

Table 2.1: Human specimen information*

Specimen	Age	Gender	Source	Preservation	Analyses
S1	61	male	MEEI surgical	left vf: snap frozen right vf: formalin fixed	biochemical histological
S2	57	female	Clinomics autopsy	formalin fixed	biochemical histological
S3	49	male	Clinomics autopsy	formalin fixed	histological
S4	48	male	Clinomics autopsy	formalin fixed	biochemical histological
S5	47	female	Clinomics autopsy	formalin fixed	histological
S6	40	female	MGH autopsy	snap frozen	biochemical
S7	55	female	MGH autopsy	snap frozen	biochemical
S8	66	male	MGH autopsy	snap frozen	biochemical

*MEEI, Massachusetts Eye and Ear Infirmary; MGH, Massachusetts General Hospital; Clinomics, Clinomics Biosciences, Inc. Formalin-fixed human tissue was fixed in hemi-larynx form.

2.2.2 Tissue preparation for biochemical and histological analysis

Each snap-frozen animal or human (S1, S6, S7, S8) hemi-larynx was briefly thawed in sterile PBS, and the middle third of the vocal fold was excised for biochemical analysis. The formalin-fixed human (S1, S2, S3, S4, S5) and animal hemi-larynges, after overnight fixation, were transferred to 70% ethanol at 4°C for 16 hours, after which the middle third of each vocal fold was retrieved. In human specimens S2 and S4, the anterior half of this middle third was processed for histological analysis and the posterior half was further processed for biochemical assays. Control samples were run to ensure that the formalin-fixation of the S2 and S4 portions reserved for biochemical analysis was not significantly altering measurements for the biomolecules of interest.

Histological specimens were paraffin embedded, and serial 5μm sections transverse to the vocal fold free edge were cut. Epiglottis controls were exposed to the same histological preparation conditions as the associated vocal fold tissue.

In tissue portions reserved for biochemistry, the muscular layer and superior and inferior glandular regions were microdissected away. The remaining LP was then lyophilized and stored at -80°C until further analysis. At time of analysis, approximately 200μL of 50 μg/mL filter-sterilized proteinase K (Worthington Biochemical, Lakewood, NJ) in 100mM sodium acetate buffer, pH 7.0 was added to each biochemical sample per 1 mg tissue dry weight. Digestion proceeded at 60°C for 24 hrs, with fresh proteinase K being added after 12 hrs and again after 18 hrs. Hyaline cartilage controls were exposed to the same digestion conditions and biochemical assays as the vocal fold LP specimens.

2.2.3 Biochemical analyses

2.2.3.1 Total protein quantification

As a measure of total protein in each sample digest, total amino acids, excluding tryptophan and cysteins, were quantitated in triplicate by AAA Service Laboratory, Inc (Boring, Oregon). The total amount of proteinase K added to each sample was approximately 30μg per 1mg dry weight. Since protein appears to comprise approximately 75-85% of the LP dry weight (unpublished observations), the contribution of proteinase K to total measured protein levels will be considered negligible in comparison to the tissue contribution.

2.2.3.2 sGAG quantification

Total sGAG was measured using the Blyscan assay (Accurate Chemical and Scientific Corp., Westbury, NY), a modified dimethylmethylene blue assay. Each human, pig, and dog vocal fold sample was measured in triplicate. Due to the small size of the ferret vocal fold, portions of the ferret digests had to be pooled to bring the sGAG quantity into the range of the assay. These pooled samples were measured in duplicate.

2.2.4 Immunohistochemical analyses

2.2.4.1 Antibodies

As previously mentioned, each PG contains a core protein and at least one GAG side chain. Common side chain types include HS, DS, KS, and CS, with CS being further subdivided into 0-, 4-, and 6-sulfate forms. The type and length of sGAG side chains associated with a particular PG core protein are often altered in tissue pathology, as are the levels of individual core proteins [8]. Therefore, both the core proteins and side chains types in the LP are important to characterizing its normal PG content. This study has analyzed the LP distributions of decorin, biglycan, versican, and aggrecan core proteins and of chondroitin 6-sulfate (C6S), chondroitin 4-sulfate (C4S), KS, and HS side chains. The antibodies, epitope

retrieval methods, and dilutions used are listed in Table 2.2. Antibodies which require further comment are described below.

Antibody clone 2B1 (Calbiochem, LaJolla, CA) has been shown to bind PG-M/versican [9, 10], and clone 6B6 (Calbiochem, LaJolla, CA) recognizes decorin, but not biglycan [11]. Thus, throughout the remainder of this paper, the staining resulting from antibodies 2B1 and 6B6 will be referred to as versican and decorin staining, respectively. For ferrets, the versican antibody did not bind to the epiglottis positive control, implying the antibody to be non-reactive with this species (data not shown). Similarly, the biglycan antibody was only applied to human specimens, since initial tests with animal tissues seemed to indicate that antibody binding was non-specific for biglycan in these species (data not shown).

Antibody clone 3G10 recognizes unsaturated uronic acid residues attached to HSPG core proteins following heparitinase I digestion [9]. Antibody 3G10 has been shown to bind not only cell-associated HSPGs, such as syndecans [9], but also matrix HSPGs, such as perlecan [12]. The keratan sulfate antibody 5D4 (Calbiochem, LaJolla, CA) appears to recognize highly sulfated corneal and skeletal KS PGs with high affinity and poorly sulfated or unsulfated KS PGs with significantly lower affinity [13].

Table 2.2: Pre-treatment and antibody dilution factors

Antibody	Clone	Epitope Retrieval	Human Dilution	Dog Dilution	Pig Dilution	Ferret Dilution
Aggrecan	HAG5B11	Trypsin	1:400 Dako	1:400 Dako	1:400 Dako	1:300 Dako
Biglycan	Courtesy of Peter Roughley	ABC	1:2400 Sniper	N/A	N/A	N/A
ΔDi-4S	2B6	ACII	1:100 Dako	1:40 Dako	1:100 Dako	1:40 Dako
ΔDi-6S	3B3	ABC	1:400 Dako	1:400 Dako	1:300 Dako	1:400 Dako
Heparan sulfate	F69-3G10	heparitinase I	1:900 Dako	1:1000 Dako	1:3000 Dako	1:1000 Dako
Decorin	6B6	ABC	1:300 Dako	1:400 Dako	1:300 Dako	1:400 Dako
Versican	2B1	ABC	1:800 Dako	1:400 Dako	1:300 Dako	N/A
Keratan sulfate	5D4	ABC	1:450 Dako	1:450 Dako	1:150 Dako	1:200 Dako

The ΔDi-6S antibody recognizes C6S oligosaccharide stubs attached to PG core protein following chondroitinase ABC (ABC) digestion of the tissue [7]. Similarly, antibody ΔDi-4S binds stubs of DS and CS side chains bound to core proteins following ABC digestion [7]. In this study, tissues receiving the ΔDi-4S antibody were treated with chondroitinase ACII (ACII) rather than ABC. ACII cleaves CS-containing chains but not DS-containing chains,

and, under these conditions, ΔDi-4S antibody staining emphasizes the distribution of C4S side chains [7].

Several variants of aggrecan exist [1]. For example, the G1 domain and KS side chains associated with cartilaginous aggrecan appear to be largely absent in the aggrecan form present in the tensioned regions of tendon [14]. Thus, the aggrecan antibody (Accurate Chemical and Scientific Corp., Westbury, NY) used in this study was selected for the ability to bind most aggrecan variants. Specifically, the aggrecan antibody used does not bind the recombinant bacterial fragments corresponding to the G1 or KS-bearing region of the aggrecan core protein. Transmission electron microscopy (TEM) seems to indicate that the antibody binds within the N-terminal portion of the chondroitin sulfate-attachment region (Technical information, Accurate Chemical and Scientific Corp., Westbury, NY).

2.2.4.2 Immunohistochemical procedure

Unless otherwise stated, immunohistochemical steps took place in a humidified environment at room temperature, and immunohistochemical reagents were purchased from Biocare Medical (Walnut Creek, CA). Tissue sections were deparaffinized in xylene, taken to water using graded ethanol baths, and then exposed to peroxidase block for 10 minutes.

Heparitinase I (Calbiochem, La Jolla, CA) was applied to the appropriate tissues at 0.02 U/mL in 50 mM Tris acetate, 5mM calcium acetate pH 7.0 for 2 hours at 37°C. Tissues receiving the ΔDi-4S antibody were treated with 0.1 U/mL ACII (Seikagaku America, Falmouth, MA) in 50mM sodium acetate, 5mM calcium acetate pH 6.0 for 1hr at 37°C. ABC (Seikagaku America, Falmouth, MA) was applied at 0.1 U/mL dissolved in 100mM Tris, 10mM EDTA buffer, pH 8.0 for 30 minutes at 37°C. For aggrecan antibody staining, tissues were digested with 0.19% trypsin for 7 minutes at room temperature.

All tissues were subsequently treated with Avidin-Biotin block. After 10 minute incubation with the blocking agent Terminator, tissue sections were lightly drained and the appropriate antibody diluted either in Sniper or Dako antibody diluent (Dako Cytomation, Carpinteria, CA), as specified in Table 2.2, was applied. Biglycan antibody was applied overnight at 4°C, whereas all other antibodies were applied for 1 hr at room temperature.

Following antibody application, goat anti-mouse IgG or goat anti-rabbit IgG secondary antibody and streptavidin-HRP were applied sequentially for 10 minutes each. Antibody binding was detected using chromagen DAB, after which slides were dipped in hematoxylin, taken to xylene, and coverslipped.

Species-specific epiglottis sections served as positive controls for each antibody. Negative control vocal fold sections for decorin, versican, biglycan, aggrecan, and KS involved application of negative control serum in place of primary antibody following appropriate enzymatic pretreatment. According to methodologies of Couchman et al.[7] and David et al.

[9], negative controls for ΔDi-6S, ΔDi-4S, and 3G10 antibodies did not receive ABC, ACII, or heparitinase I pretreatment, respectively, although primary antibody was applied.

2.2.5 Immunohistochemical image analysis

2.2.5.1 Image capture

An Axiolab microscope (Zeiss, Thornwood, NY) coupled to an Axiocam CCD camera (Zeiss, Thornwood, NY) and to an Axiovision image analysis system was used for image recording. For all slides, full spectrum 1030x1300 8-bit color images were recorded. Background correction was performed prior to image capture by interactively referencing a blank field using the Axiovision software.

2.2.5.2 Schematic development

A common LP microstructural organization appears to exist for all normal LP specimens of given species, and recognition of this organization can facilitate intraspecies comparison of LP staining patterns. Thus, schematics emphasizing repeatedly observed microstructural subdivisions in the LP of each species have been developed and are displayed in Figure 2.1.

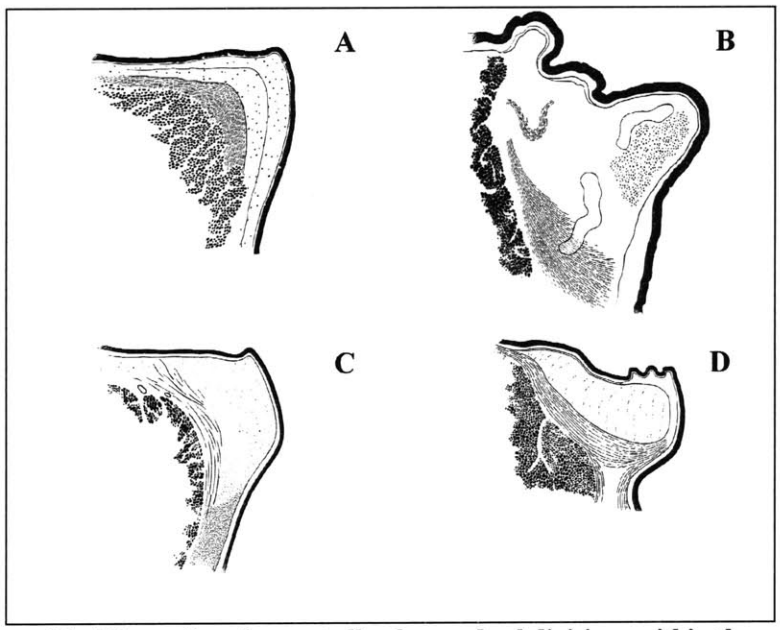

Figure 2.1: Schematics of repeatedly observed subdivisions within the vocal fold LP by species. (A): human; (B): dog; (C): pig; (D): ferret.

To gain insight into the origin of the LP subdivisions depicted within these schematics, examine the staining for C6S and versican in dog LP as shown in Figures 2.2a,c. Regions

within these immunohistochemical images corresponding to the LP subdivisions present in the dog LP schematic have been outlined using specific colors. Versican and C6S stained specimens were selected to demonstrate dog LP subdivisions since each antibody highlights/emphasizes different LP features. Although the exact placement and dimensions of these dog LP subdivisions varies from specimen to specimen, as indicated in Figures 2.2g,h, the subdivisions noted in the schematic have been observed in each dog LP examined in this study. Figures 2.3, 2.4, and 2.5 illustrate the correspondence of subdivisions within the LP schematics for human, pig, and ferret, respectively, to regions within actual specimen LPs.

For humans, the regions in Figures 2.3d-f outlined in red correspond to what laryngologists have termed the superficial LP [15], whereas the blue-delineated regions correspond to the deep LP. These designations of the LP region nearest the epithelium as the superficial LP, the LP region nearest the muscle as deep LP, and the LP region in between these as the intermediate LP, have been extended to the animal models (Figure 2.6) to facilitate qualitative verbal descriptions of staining patterns.

It should be noted that the schematics illustrate gross LP morphology post-excision from the larynx structure. Some alterations in the overall size and shape of each species' LP from its in vivo state due to the excision of the midmembranous portion from its attachments post-fixation should be anticipated.

2.2.5.3 Semi-quantitative image analysis

Consistent interspecies variations in LP staining patterns for specific molecules can give insight into important LP microstructural or compositional differences across species. However, interspecies comparison of antibody staining can be difficult, since the observed intensity range for DAB staining varies with antibody, species, and with specimen within a given species. Therefore, in seeking to compare LP antibody staining patterns across species, relative staining intensity, rather than absolute intensity, should be examined. Relative staining intensity within different LP subregions has been analyzed on a specimen-by-specimen basis for each antibody as follows: LP regions within a specific specimen of maximum staining intensity were assigned a 6 while regions of background staining intensity were assigned a 1. Subregions with staining intensities between these extremes were assigned numbers between 1 and 6, as appropriate, with an intermediate degree of staining being assigned a 3-4. For a specific antibody, the numeric assignments for each LP region were then averaged across all specimens of a given species and rounded to the nearest integer. The resulting number was matched with a color code: 6=red, 5=yellow, 4=green, 3=light blue, 2=dark blue, 1=purple. These colors were then applied to the appropriate subregions within the LP schematics.

The average relative staining intensities for C6S and KS in the human LP were not assessed, due to the relatively high variability among human specimens in staining patterns for these antibodies. This variability made average relative intensity evaluations of unclear utility for these molecules.

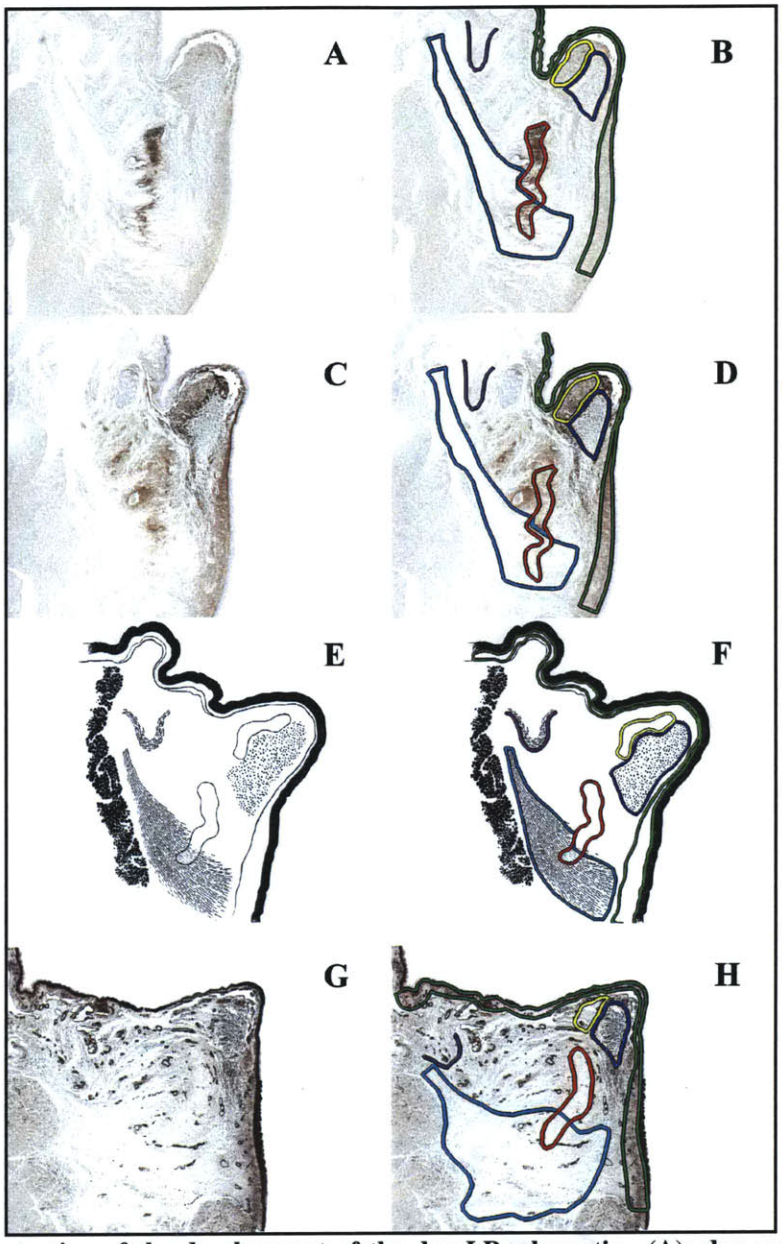

Figure 2.2: Demonstration of the development of the dog LP schematic. (A): dog specimen stained for C6S; (C): same dog specimen stained for versican; (E): dog LP schematic; (B, D, F): images (A, C, E), respectively, with major dog LP features delineated with specific colors; (G): HS staining of a different dog specimen; (H): image (G) with same major features delineated as in (B, D, F). Images (G, H) have been included to demonstrate the variability in feature location and size among dog specimens.

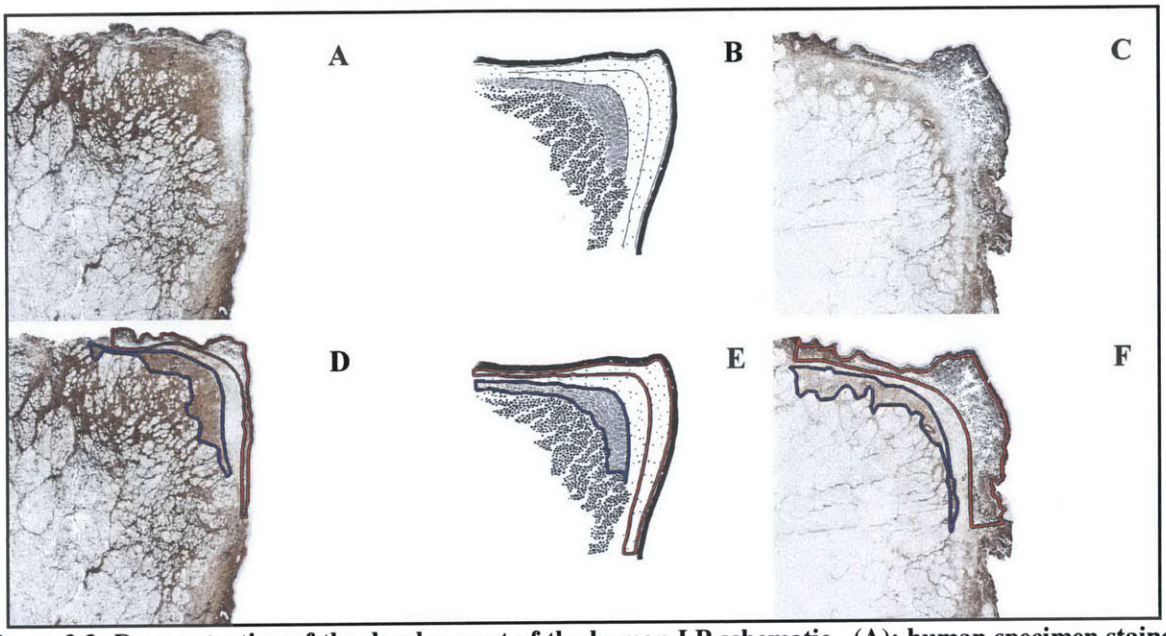

Figure 2.3: Demonstration of the development of the human LP schematic. (A): human specimen stained for decorin; (B): human LP schematic; (D, E): images (A, B), respectively, with major human LP features delineated with specific colors; (C): decorin staining of a different human specimen; (F): image (C) with same major features delineated as in (D, E). Images (C, F) have been included to demonstrate the variability in feature location and size among human specimens.

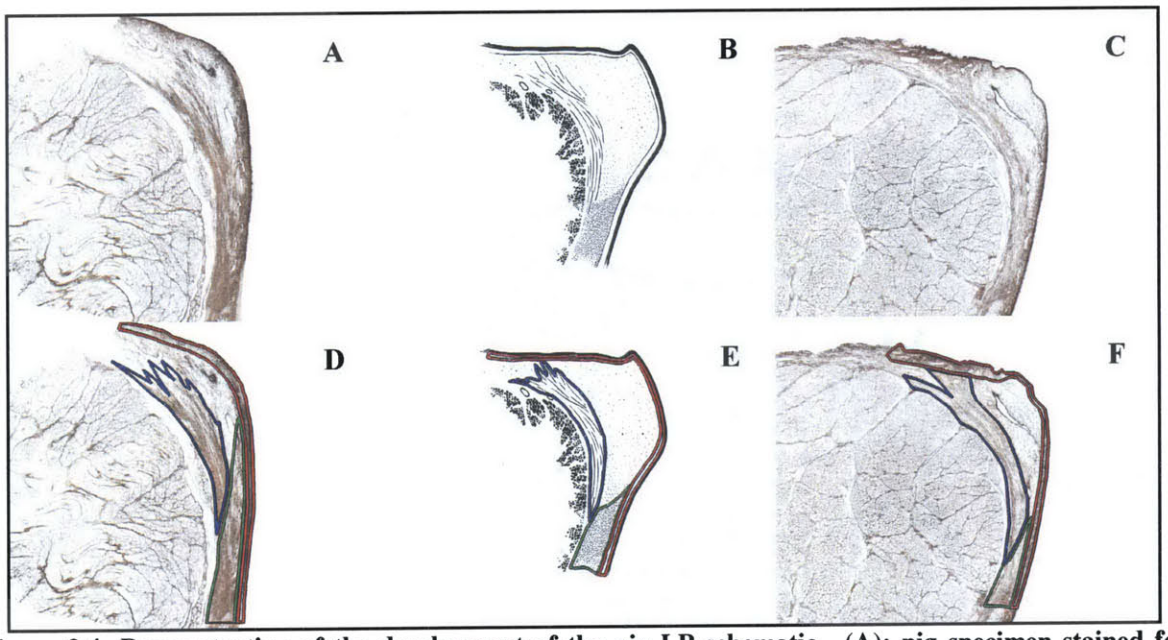

Figure 2.4: Demonstration of the development of the pig LP schematic. (A): pig specimen stained for decorin; (B): pig LP schematic; (D, E): images (A, B), respectively, with major pig LP features delineated with specific colors; (C): HS staining of a different pig specimen; (F): image (C) with same major features delineated as in (D, E). Images (C, F) have been included to demonstrate the variability in feature location and size among pig specimens.

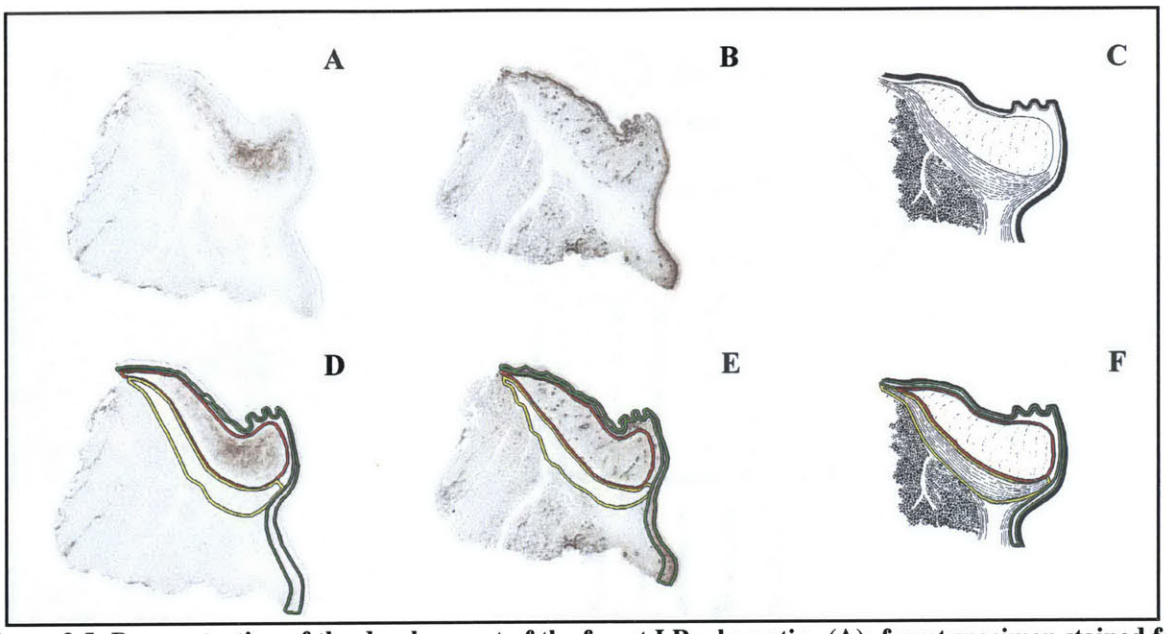

Figure 2.5: Demonstration of the development of the ferret LP schematic. (A): ferret specimen stained for C6S; (B): same ferret specimen stained for HS; (C): ferret LP schematic; (D, E, F): images (A, B, C), respectively, with major ferret LP features delineated with specific colors.

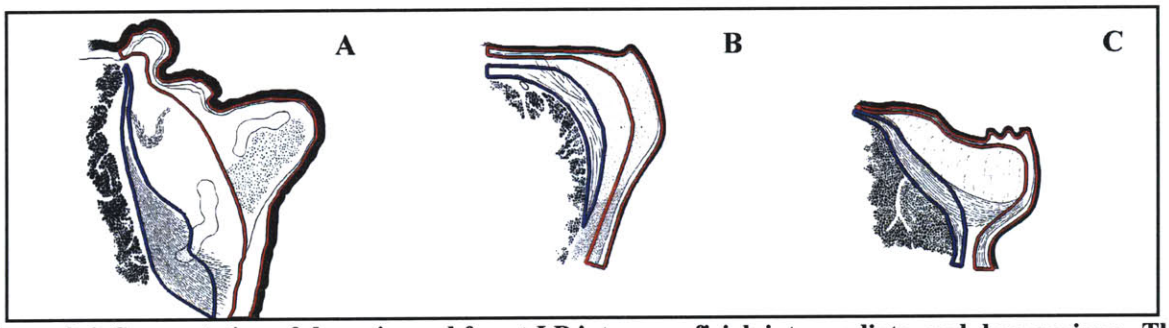

Figure 2.6: Segmentation of dog, pig, and ferret LP into superficial, intermediate, and deep regions. The region designated as superficial LP is outlined for each species in red, and the region designated as deep LP is delineated in blue. (A): dog; (B): pig; (C): ferret.

2.2.6 Statistical analysis

Average LP sGAG levels for each animal species were compared to average human results using an unpaired student t-test. Differences were considered statistically significant at a level of $p<0.05$. Standard deviations (SDs) were calculated to include the SDs within and among specimens of a given species. Since aliquots of the ferret specimens were pooled for the sGAG assay, interspecimen variations in sGAG levels are not represented in the ferret SD, although such variations are represented in human, dog, and pig sGAG SDs. Therefore, the mean ferret sGAG concentration could not be strictly compared to that of humans by a student t-test.

2.3 Results

2.3.1 Biochemical results

Figure 2.7 shows total sGAG per mg tissue total protein for each species. Results are reported as average ± standard error of the mean. Dog and pig LP total sGAG concentrations were not statistically different from that of human specimens ($p>0.05$), and total sGAG levels in ferret LP appeared to be of the same order of magnitude as in human LP. No statistically significant difference in human LP sGAG content with gender was noted (data not shown), although this result is likely a reflection of the limited human specimen set.

For hyaline cartilage controls, the measured sGAG levels were within the range cited in literature for normal hyaline cartilage [16] (data not shown).

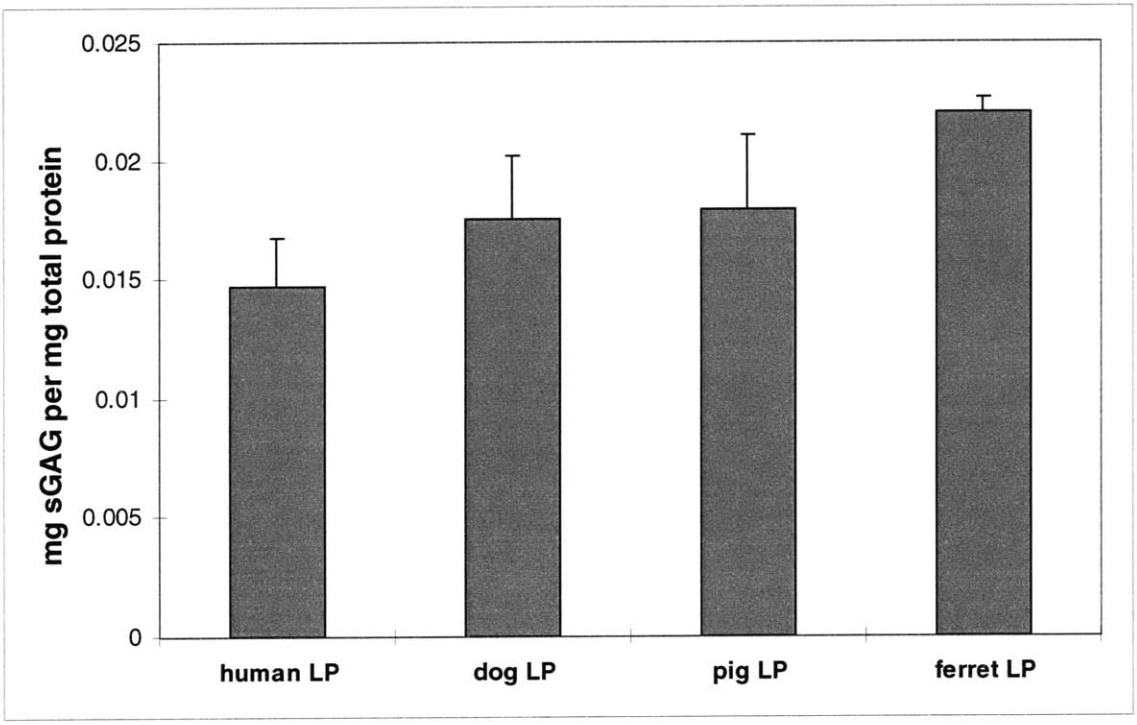

Figure 2.7: Total sGAG content by species. No statistically significant differences were found between the mean sGAG for pig and dog and that of humans, $p>0.05$. Ferrets were not statistically compared to humans, as discussed in Materials and Methods.

2.3.2 Immunohistochemical results

Figure 2.8 depicts representative images of vocal fold LP staining for versican, decorin, and

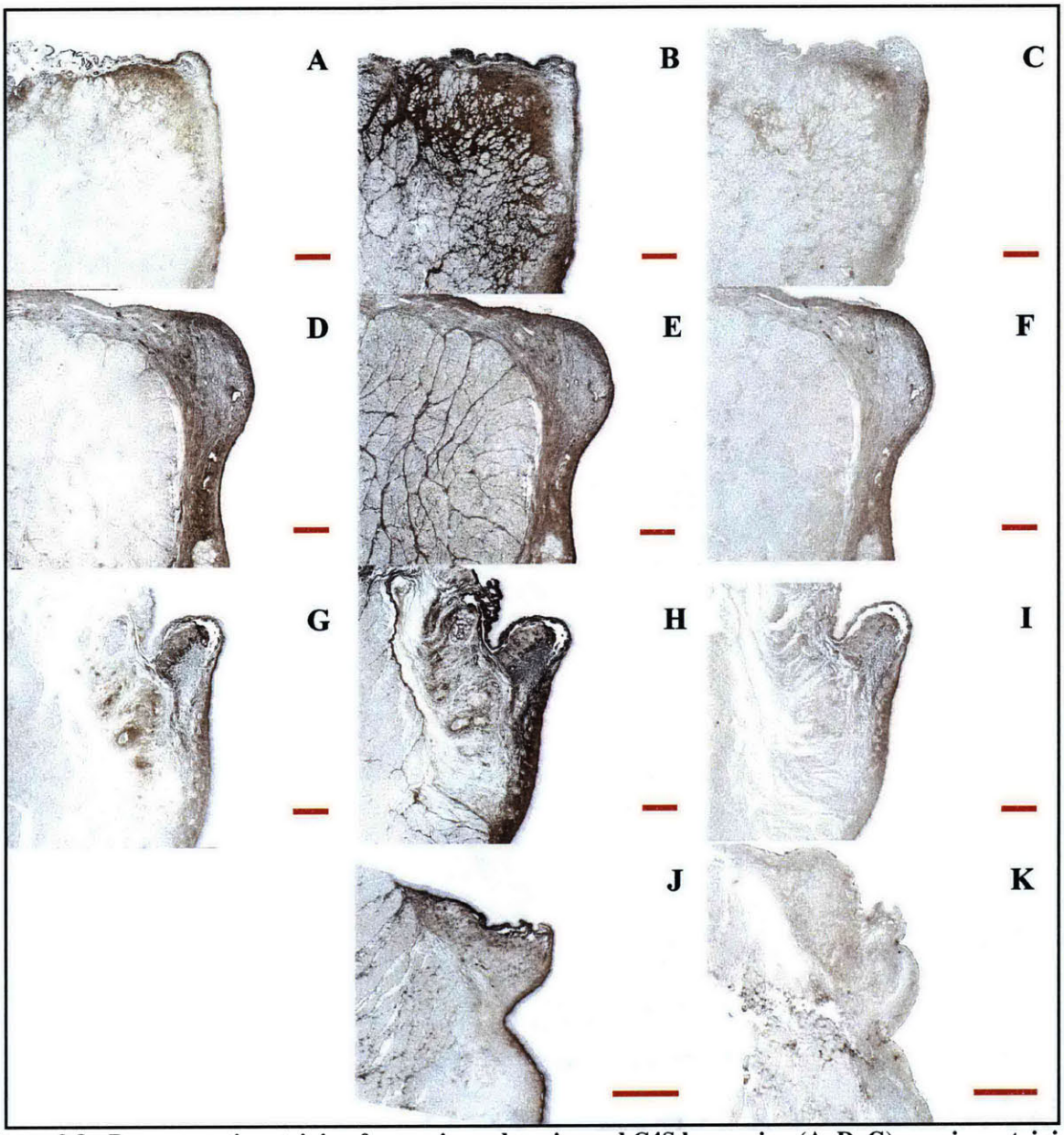

Figure 2.8: Representative staining for versican, decorin, and C4S by species. (A, D, G): versican staining in human, pig, and dog, respectively; (B, E, H, J): decorin staining in human, pig, dog, and ferret, respectively; (C, F, I, K): C4S staining in human, pig, dog, and ferret, respectively. Scale bars =500 μm.

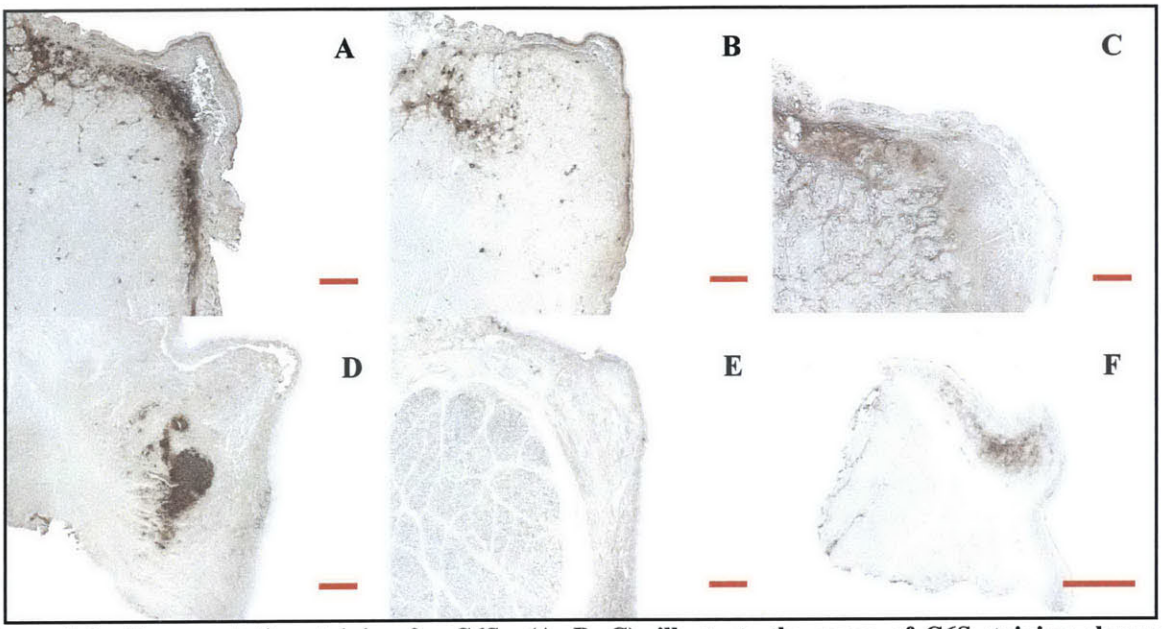

Figure 2.9: Representative staining for C6S. (A, B, C): illustrate the range of C6S staining observed among human specimens; (D, E, F): C6S staining in dog, pig, and ferret, respectively. Scale bars = 500 μm.

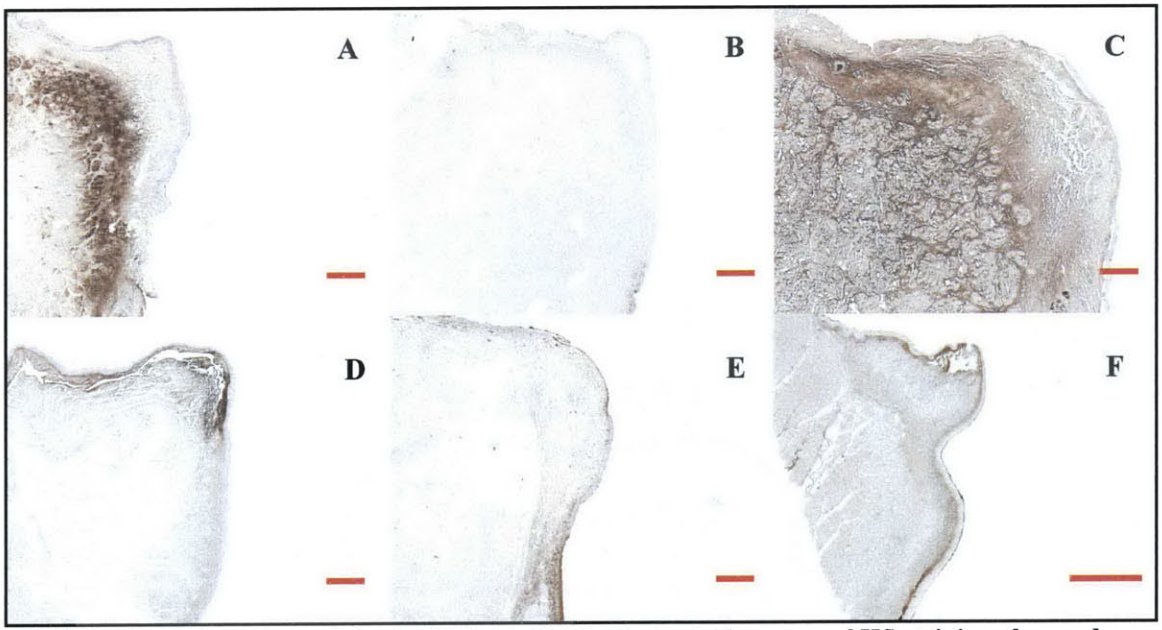

Figure 2.10: Representative staining for KS. (A, B, C): illustrate the range of KS staining observed among human specimens; (D, E, F): KS staining in dog, pig, and ferret, respectively. Scale bars = 500 μm.

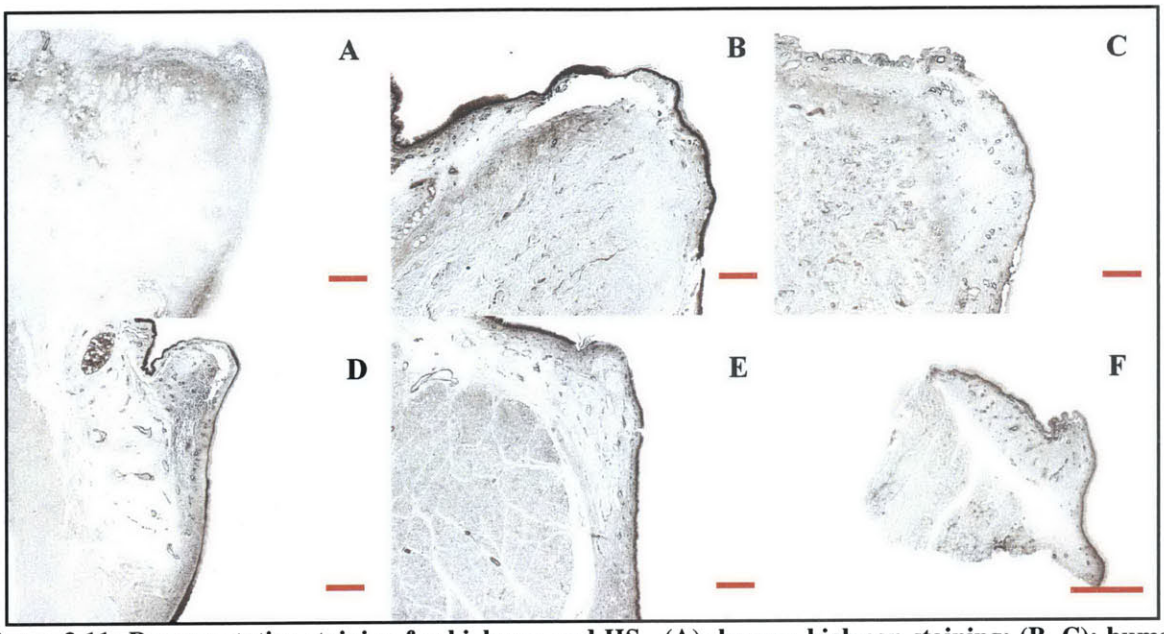

Figure 2.11: Representative staining for biglycan and HS. (A): human biglycan staining; (B, C): human HS staining; (D, E, F): HS staining in dog, pig, and ferret, respectively. Scale bars = 500 μm.

C4S for all four species. Figures 2.9 and 2.10 illustrate C6S and KS staining, respectively. Three images of human LP C6S and KS staining have been included illustrate the variability in staining observed among human specimens for these antibodies. Representative HS staining in two human specimens and in the animal models is shown in Figure 2.11. Also included in Figure 2.11 is a representative image of human LP biglycan staining. Aggrecan staining could not be distinguished from background in any of the LP specimens, although staining in the elastic cartilage epiglottis controls was intense (data not shown).

Semi-quantitative results for the average relative staining intensities of versican, decorin, and C4S are displayed with respect to the species-specific LP schematics in Figure 2.12. Similar analyses were carried out for C6S, KS, and HS staining, and the results are shown in Figure 2.13. Also contained in Figure 2.13 is the average relative intensity image for human LP biglycan staining.

From Figure 2.12, it can be seen C4S staining was prevalent throughout the LP of each species, although in humans, the staining was most intense in the deep LP. The distribution of decorin in humans was primarily localized in the superficial and deep regions of the LP. Versican staining, although also present in the superficial and deep layers, extended into the human intermediate LP. The versican, decorin, and C4S distributions in pigs were very similar, with staining being relatively intense in the deep and inferior LP and along the epithelial-LP border. In dogs, the oblong subregion of the intermediate LP of relatively intense versican staining corresponded to a region of low decorin and C4S staining. For ferrets, decorin staining was most intense in the superficial region.

C6S staining in humans showed several different patterns. In some specimens, staining for this molecule was highest in the deep LP. In other specimens, C6S staining appeared to be primarily localized to the superficial and intermediate layers. Some specimens showed staining intermediate between the extremes represented by the above two cases.

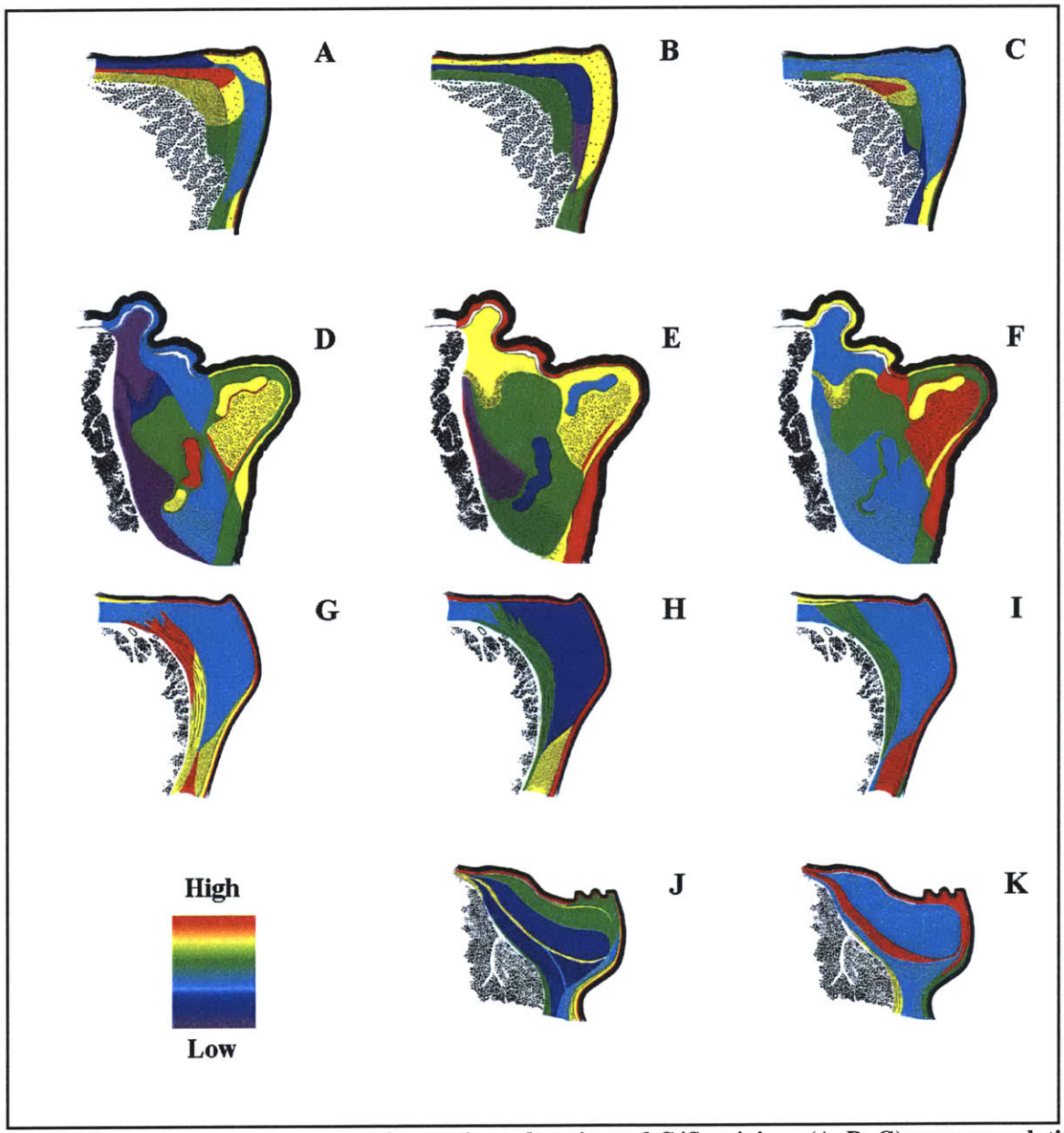

Figure 2.12: Semi-quantitative images for versican, decorin, and C4S staining. (A, D, G): average relative versican staining in human, dog, and pig, respectively; (B, E, H, J): average relative decorin staining in human, dog, pig, and ferret, respectively; (C, F, I, K): average relative C4S staining in human, dog, pig, and ferret, respectively.

KS staining in humans also varied from specimen to specimen, with some specimens showing very intense deep LP staining and others showing minimal non-glandular related staining. In other specimens, the staining was intermediate between the above two extremes. In dog and ferret, the oblong region of intense C6S staining in the intermediate LP corresponded to a

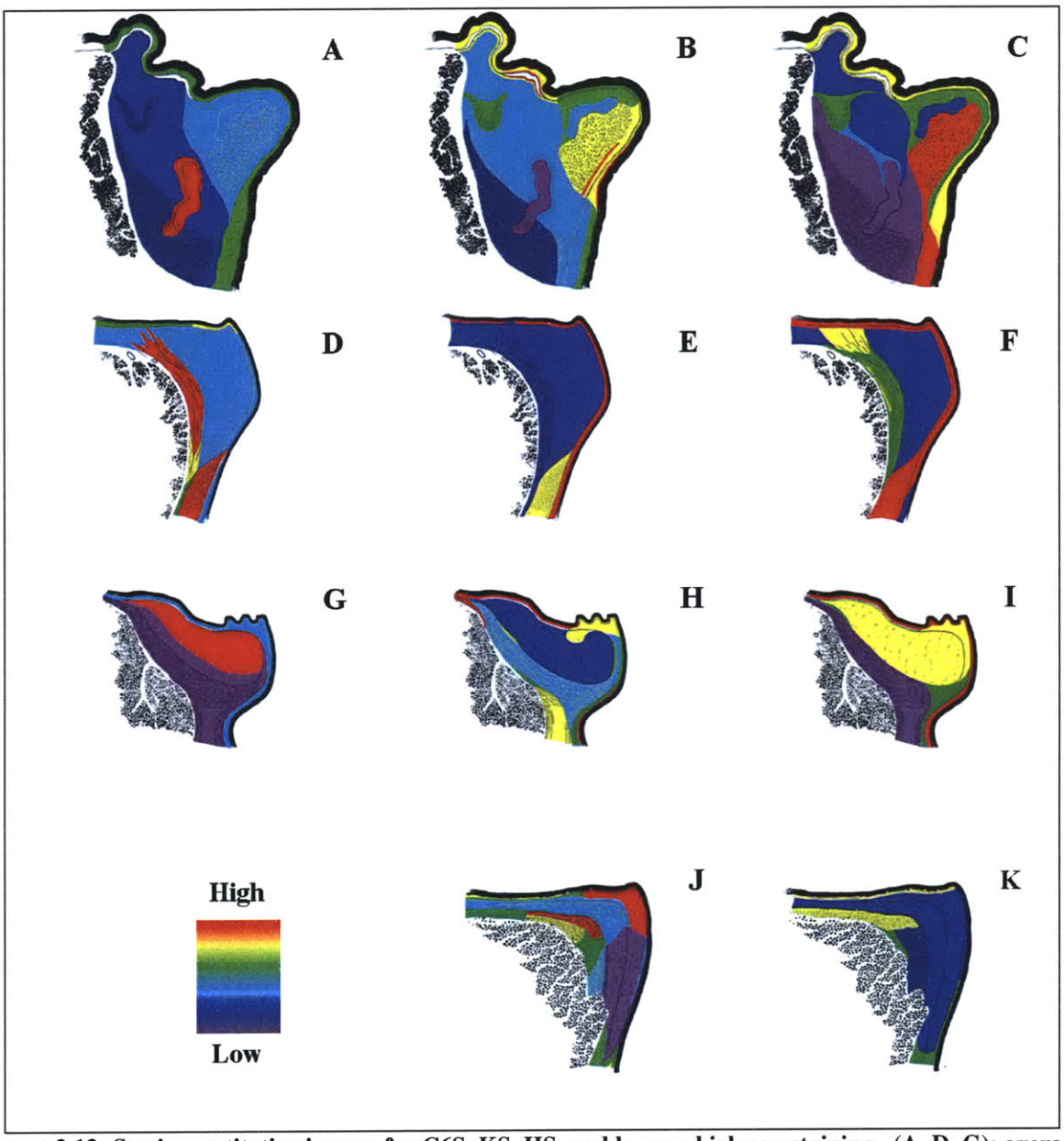

Figure 2.13: Semi-quantitative images for C6S, KS, HS, and human biglycan staining. (A, D, G): average relative C6S staining in dog, pig, and ferret respectively; (B, E, H): average relative KS staining in dog, pig, ferret respectively; (C, F, I, K): average relative HS staining in dog, pig, ferret, and human respectively. (J): average relative human biglycan staining.

region of low observed KS staining. For pigs, KS staining was primarily superficially oriented, whereas C6S seemed to follow a staining pattern similar to that with of versican.

Staining for HS in the human LP was relatively intense in the superior portion of the deep LP. In some specimens, this staining extended throughout the deep LP. In dogs, HS staining appeared to be primarily localized to the superficial LP, whereas in pigs HS staining was distributed throughout the LP in the staining pattern similar to that of decorin. Ferret staining for HS extended into the intermediate regions of the LP, although staining was highest near the epithelial-LP boundary.

Human biglycan staining was highest in the superior region of the deep LP, with staining extending throughout the deep LP in varying intensities depending on the specimen. Also, biglycan staining was observed in the superior portion of the superficial LP in approximately half of the human specimens examined.

2.4 Discussion

The present study has immunohistochemically analyzed the distribution of specific PG core proteins and side chains in the midmembranous vocal fold LP of normal humans, dogs, pigs, and ferrets. In addition, the PG levels in normal LP have been indirectly assessed by quantifying levels of associated sGAG side chains relative to tissue total protein.

2.4.1 Biochemical results

The total sGAG concentration in the human LP was 0.015 ± 0.002 mg per mg total protein, with the total sGAG content in the three animal model LPs being similar to that of human. The human LP total sGAG concentration is over an order of magnitude lower than that of hyaline cartilage [16] and is similar to that of dermis [17]. These quantitative sGAG measures, therefore, place the vocal fold LP in the context of other biochemically and biomechanically well-characterized tissues and place bounds on the expected contribution of PGs to LP biomechanical properties [18]. In addition, since PG/sGAG levels are frequently altered in scar and disease states [3, 19], comparison of the total sGAG concentrations presented here with those characteristic of abnormal LP states may yield insight into vocal fold scarring and pathology and possible methods of restoring the normal tissue state.

2.4.2 Immunohistochemical results

Decorin staining in human specimens was intense in the superficial and deep LP, although slightly less intense in the deep LP. These human decorin staining results correspond well with those of Pawlak et al. [5] Among decorin's properties is the ability inhibit collagen fibrillogenesis in vitro [20]. Previous histological work on the distribution of collagen in the human LP has shown collagen levels to be, in general, markedly higher in the deep LP than in the superficial LP [6, 21, 22]. In addition, the fibers in the human deep LP tend to be of

greater thickness than those in the superficial LP [22]. The higher relative intensity of decorin staining in the superficial LP in comparison to the relative intensity of collagen staining in this region may in part account for these documented variations in collagen fiber density and thickness within the human LP.

Biglycan staining in normal human LP appeared to be most intense in the deep LP and did not show the same degree of superficial LP presence as that seen for decorin. The density of biglycan relative to decorin appears to be altered in certain scar states [23], with the alteration being dependent of scar type. Histological studies of rabbit vocal fold LP have shown decorin to be reduced in LP scar[24], and a future concomitant study of biglycan alterations should yield further insight into the nature of vocal fold scarring.

Versican, a large aggregating PG which binds to hyaluronan (HA) [1] and which is frequently associated with elastic networks [25], was present in LP ECM of each species (Figure 2.8). The highly hydrated versican-HA complex appears to inhibit cell-matrix interactions [26], to play a role in dissipation of impact and compressive stresses [27], and to affect tissue turgor [27]. In addition, versican has been implicated in the formation of interstitial lung edema[28] and may similarly contribute to human Reinke's edema. Like versican, aggrecan is a large aggregating PG which can associate with HA to form highly hydrated complexes and is a characteristic PG in cartilage and fibrocartilage. The results of the present study seem to indicate that aggrecan is not one of the primary PGs in the midmembranous LP (data not shown).

KS staining varied significantly among human specimens, with the consistent KS staining of the vocal ligament noted by Pawlak et al. [5] not being observed in this study. Similar interspecimen variations in KS staining were not noted in the animal models. The reasons for the discrepancy with the KS results of Pawlak et al.[5] are at present unclear, since the same antibody was used in both studies. However, the interspecimen variations in human KS staining observed in the present study may be in part attributable to the properties of the 5D4 antibody used to detect KS PG. As previously mentioned, poorly sulfated or unsulfated KS PGs show low affinity for this antibody. Therefore, the human variability in 5D4 staining may reflect interspecimen differences in KS sulfation levels rather than differences in total KS PG present.

Although the KS PG fibromodulin has been identified in human [29] and rabbit [24] vocal LPs, it is not clear if this is the only or most prevalent KS PG in the LP. Both lumican and fibromodulin are among the more abundant KS PGs in non-corneal,-scleral, and -cartilaginous connective tissues, and both are involved in regulation of collagen fibrillogenesis and maintenance of tissue tensile strength [30]. Further analysis would be required to determine the identities of the KS PGs in the vocal fold LP. If lumican does, however, prove to be a constituent of the LP, its presence may not be represented in the 5D4 KS staining patterns observed in this study, since lumican in non-corneal tissues is generally present in poorly sulfated or non-sulfated forms [30].

As with KS, marked interspecimen variations in C6S staining patterns were noted in the human LP, although similar interspecimen variations were not noted for the animal models. Possible physiological grounds for the observed variations in C6S staining among human specimens are at present unclear. In addition, linking the observed C6S and C4S staining patterns with specific PG core proteins is complex. For example, decorin, biglycan, and versican core proteins are known to have CS and/or DS side chains. The relative fractions of these side chains as well as the sulfation of the CS chains attached to the decorin, biglycan, and versican core proteins varies with tissue type and region [31] and with health [8]. It is likely that all three of these core proteins contribute to the observed C4S and C6S staining patterns.

The results for human versican, C6S, and C4S appear to revise previously published results on the PG composition of the human vocal folds [5]. Although the presence of versican was hypothesized by Pawlak et al. [5] based on observed CS staining, this molecule and other C6S- and C4S-bearing PGs were believed to be present primarily intracellularly. These deductions were based on observed LP staining with ΔDi-6S antibody [5], the same antibody used in the present work to detect C6S. The distinction between the present results and those of Pawlak et al.[5] likely results from differences in tissue pretreatment prior to antibody ΔDi-6S application. Pawlak et al. [5] appears to have used the ΔDi-6S antibody without chondroitinase pretreatment of the tissue. However, due to the nature of this antibody, such enzymatic pretreatment is necessary for evaluation of C6S bearing PG in the ECM [7].

HSPG was observed to be present in the LP ECM, in addition to cell- and basement - membranes (Figure 2.11). The association of HSPG staining with the superior portion of the human LP vocal ligament was particularly striking. The presence of HSPG separate from cell- or basement-membranes in the LP is in contrast to the results of Pawlak et al.[5], where LP HSPG was reported to be intracellularly or basement membrane localized. This discrepancy likely results from the antibodies selected to detect HSPG. The antibody used in the present study recognizes a range of cell-associated and matrix-associated HSPG, whereas the antibody used by Pawlak et al.[5] appears to recognize a single HSPG type. Matrix HSPGs are generally most abundant in basement membranes, regions that bear high shear stresses, and certain HSPGs have been found to be critical to maintaining basement membrane integrity in response to stress [32]. Thus, the presence of HSPG in the LP ECM may be a reflection of the shear stresses sustained by this tissue.

Among the biological functions of many PG types is the ability to bind growth factors. For example, decorin, biglycan, and fibromodulin, are known to modulate TGF-β activity [32]. Certain matrix HSPGs appear to modulate bFGF activity[1], and highly sulfated HS has been shown to potentiate the activity of TGF-β1 [32]. bFGF has been shown to inhibit elastogenesis in rat lung fibroblasts [33], whereas TGF-β1 increases elastin and collagen synthesis in dermal fibroblasts [34] and lysyl oxidase activity [35] in lung fibroblasts. Thus, the observed spatial variations in PG presence may imply that a region-specific balance of various PG groups is critical to the development /maintenance of the layered structure

characteristic of normal adult human LP and of the subdivisions characteristic of each animal LP.

To the author's knowledge, this work presents the first quantitative measures of the total sGAG content of human and animal model vocal fold LP. It also clarifies and expands upon previous studies of specific PG/sGAG types present in the human LP. In particular, versican, C6S, C4S, and HSPG, molecules previously believed to be intracellularly or basement membrane-localized, have been identified in the LP ECM. An in depth study of dog, pig, and ferret LP PG/sGAG content has also been conducted, and significant interspecies differences in the distributions of specific PG/sGAG types have been noted.

2.5 Literature cited

1. Iozzo, R.V., Matrix proteoglycans: From molecular design to cellular function. Annual Review of Biochemistry, 1998. **67**: p. 609-652.
2. Wight, T.N., D.K. Heinegard, and V.C. Hascall, Proteoglycans: structure and function. 2nd ed. Cell Biology of Extracellular Matrix, ed. E.D. Hay. 1991, NY: Prenum Press.
3. Poole, A.R., Proteoglycans in Health and Disease - Structures and Functions. Biochemical Journal, 1986. **236**(1): p. 1-14.
4. Garrett, C.G., J.R. Coleman, and L. Reinisch, Comparative histology and vibration of the vocal folds: Implications for experimental studies in microlaryngeal surgery. Laryngoscope, 2000. **110**(5): p. 814-824.
5. Pawlak, A.S., et al., Immunocytochemical study of proteoglycans in vocal folds. Annals of Otology Rhinology and Laryngology, 1996. **105**(1): p. 6-11.
6. Gray, S.D., et al., Biomechanical and histologic observations of vocal fold fibrous proteins. Annals of Otology Rhinology and Laryngology, 2000. **109**(1): p. 77-85.
7. Couchman, J.R., et al., Mapping by Monoclonal-Antibody Detection of Glycosaminoglycans in Connective Tissues. Nature, 1984. **307**(5952): p. 650-652.
8. Theocharis, A.D., et al., Altered content composition and structure of glycosaminoglycans and proteoglycans in gastric carcinoma. International Journal of Biochemistry & Cell Biology, 2003. **35**(3): p. 376-390.
9. David, G., et al., Developmental-Changes in Heparan-Sulfate Expression - Insitu Detection with Mabs. Journal of Cell Biology, 1992. **119**(4): p. 961-975.
10. Sobue, M., et al., Production and Immunohistochemical Characterization of a Monoclonal-Antibody Raised to Proteoglycan Purified from a Human Yolk-Sac Tumor. Histochemical Journal, 1989. **21**(8): p. 455-&.
11. Sobue, M., et al., Production and Characterization of Monoclonal-Antibody to Dermatan Sulfate Proteoglycan. Journal of Histochemistry & Cytochemistry, 1988. **36**(5): p. 479-485.
12. Erickson, A.C. and J.R. Couchman, Basement membrane and interstitial proteoglycans produced by MDCK cells correspond to those expressed in the kidney cortex. Matrix Biology, 2001. **19**(8): p. 769-778.

13. Caterson, B., J.E. Christner, and J.R. Baker, Identification of a Monoclonal-Antibody That Specifically Recognizes Corneal and Skeletal Keratan Sulfate - Monoclonal-Antibodies to Cartilage Proteoglycan. Journal of Biological Chemistry, 1983. **258**(14): p. 8848-8854.
14. Vogel, K.G., et al., Aggrecan in Bovine Tendon. Matrix Biology, 1994. **14**(2): p. 171-179.
15. Kurita, S., et al., The Layer Structure of the Vocal Fold - Age-Dependent Variations. Folia Phoniatrica, 1980. **32**(3): p. 210-210.
16. Seibel, M.J., S.P. Robins, and J.P. Bilezikian, eds. Dynamics of Bone and Cartilage Metabolism: Principles and Clinical Applications. 1999, Academic Press: San Diego.
17. Goldsmith, L.A., ed. Physiology, biochemistry, and molecular biology of the skin. 2 ed. 1991, Oxford University Press: New York.
18. Fung, Y.C., Biomechanics: Mechanical Properties of Living Tissues. 2 ed. 1993, New York: Springer-Verlag.
19. Scott, P.G., et al., Chemical characterization and quantification of proteoglycans in human post-burn hypertrophic and mature scars. Clinical Science, 1996. **90**(5): p. 417-425.
20. Vogel, K.G., M. Paulsson, and D. Heinegard, Specific-Inhibition of Type-I and Type-Ii Collagen Fibrillogenesis by the Small Proteoglycan of Tendon. Biochemical Journal, 1984. **223**(3): p. 587-597.
21. Hammond, T.H., S.D. Gray, and J.E. Butler, Age- and gender-related collagen distribution in human vocal folds. Annals of Otology Rhinology and Laryngology, 2000. **109**(10): p. 913-920.
22. Sato, K., M. Hirano, and T. Nakashima, Age-related changes of collagenous fibers in the human vocal fold mucosa. Annals of Otology Rhinology and Laryngology, 2002. **111**(1): p. 15-20.
23. Garg, H.G., et al., Inseparable iduronic acid-containing proteoglycan PG((IdoA)) preparations of human skin and post-burn PG scar tissues: Evidence for elevated levels of ((IdoA))-I in hypertrophic scar by N-terminal sequencing. Carbohydrate Research, 1996. **284**(2): p. 223-228.
24. Thibeault, S.L., D.M. Bless, and S.D. Gray, Interstitial protein alterations in rabbit vocal fold with scar. Journal of Voice, 2003. **17**(3): p. 377-383.
25. BodeLesniewska, B., et al., Distribution of the large aggregating proteoglycan versican in adult human tissues. Journal of Histochemistry & Cytochemistry, 1996. **44**(4): p. 303-312.
26. Lemire, J.M., et al., Distinct rat aortic smooth muscle cells differ in versican/PG-M expression. Arteriosclerosis Thrombosis and Vascular Biology, 1996. **16**(6): p. 821-829.
27. Laurent, T.C. and J.R.E. Fraser, Hyaluronan. Faseb Journal, 1992. **6**(7): p. 2397-2404.
28. Miserocchi, G., et al., Development of lung edema: Interstitial fluid dynamics and molecular structure. News in Physiological Sciences, 2001. **16**: p. 66-71.
29. Thibeault, S.L., et al., Instability of extracellular matrix gene expression in primary cell culture of fibroblasts from human vocal fold lamina propria and tracheal scar. Annals of Otology Rhinology and Laryngology, 2002. **111**(1): p. 8-14.

30. Chakravarti, S., Functions of lumican and fibromodulin: Lessons from knockout mice. Glycoconjugate Journal, 2003. **19**(4-5): p. 287-293.
31. Cheng, F., et al., Patterns of Uronosyl Epimerization and 4-/6-O-Sulfation in Chondroitin/Dermatan Sulfate from Decorin and Biglycan of Various Bovine-Tissues. Glycobiology, 1994. **4**(5): p. 685-696.
32. Hildebrand, A., et al., Interaction of the Small Interstitial Proteoglycans Biglycan, Decorin and Fibromodulin with Transforming Growth-Factor-Beta. Biochemical Journal, 1994. **302**: p. 527-534.
33. Brettell, L.M. and S.E. McGowan, Basic Fibroblast Growth-Factor Decreases Elastin Production by Neonatal Rat Lung Fibroblasts. American Journal of Respiratory Cell and Molecular Biology, 1994. **10**(3): p. 306-315.
34. Davidson, J.M., O. Zoia, and J.M. Liu, Modulation of Transforming Growth-Factor-Beta-1 Stimulated Elastin and Collagen Production and Proliferation in Porcine Vascular Smooth-Muscle Cells and Skin Fibroblasts by Basic Fibroblast Growth-Factor, Transforming Growth Factor-Alpha, and Insulin-Like Growth Factor-I. Journal of Cellular Physiology, 1993. **155**(1): p. 149-156.
35. Boak, A.M., et al., Regulation of Lysyl Oxidase Expression in Lung Fibroblasts by Transforming Growth Factor-Beta(1) and Prostaglandin E(2). American Journal of Respiratory Cell and Molecular Biology, 1994. **11**(6): p. 751-755.

Chapter 3. Collagen and Fibronectin Glycoproteins

3.1 Introduction

Recognition of the impact of the glycoprotein collagen on normal vocal fold lamina propria (LP) function has led to a number of histological studies of collagen in the human LP. The distribution of collagen fibers throughout the human LP has been well studied with respect to age and gender [1-6], and electron microscopy has been used to assess LP collagen fiber thickness and ultrastructure [3, 5]. Similarly, the collagen distribution of several potential animals model LPs has been histologically evaluated and qualitatively compared to that of human LP [7, 8].

Despite these advances, significant unknowns remain. For example, concentration of collagen in the vocal fold LP has not yet been quantified. Moreover, a number of second-order biochemical features which can have significant impact on tissue health and function, such as the collagen types present in the LP and their distributions, are currently not well-characterized, particularly in potential animal models.

The glycoprotein fibronectin has been shown to be present throughout the human LP in various disease states [9-11]. In dogs and rabbits, the staining for fibronectin in the LP has been shown to increase with scarring [12, 13]. Due to marked alterations in fibronectin concentration associated with LP scar, it is desirable that the normal LP fibronectin presence in human and in potential animal models be understood.

This study expands upon previous work on the collagen and fibronectin content of the normal human vocal fold LP. Hydroxyproline analysis has been used to quantify total collagen in human LP. Since human vocal fold scarring is generally limited to the superficial LP [14], quantitative histology has been used to calculate the percentage collagen in specific LP regions. In addition, the distributions of several collagen types and of fibronectin in normal human LP have been histochemically evaluated. Similar biochemical and histological analyses have been carried out on dogs, pigs, and ferrets towards identifying an appropriate animal model for implant evaluation.

3.2 Materials and methods

3.2.1 Tissue samples and preparation

The tissue specimens and controls used in this study and their preparation for biochemical or histological assays were the same as in Chapter 2.

3.2.2 Biochemical analyses

3.2.2.1 Tissue digestion and total protein quantitation

Specimens allocated for biochemical analyses were digested with proteinase K (Worthington Biochemical, Lakewood, NJ) for 24 hrs at 60°C as described in Chapter 2. Total protein in the sample digests was quantitated in triplicate via amino acid analysis by AAA Service Laboratory, Inc. (Boring, OR), as detailed in Chapter 2.

3.2.2.2 Total collagen quantitation

Specimen digest hydroxyproline levels were quantitated in duplicate by the Texas A&M University Protein Chemistry Laboratory (College Station, TX) and independently in duplicate/triplicate runs by AAA Service Laboratory, Inc (Boring, OR). These two amino acid analysis services use different detection techniques, one based on pre-column derivatization and the other based on post-column derivatization [15]. Both methods were used to quantitate the hydroxyproline content of digested samples to minimize the possibility that buffer or sample contaminants were significantly altering the measured amino acid values. Milligrams total collagen in the LP specimens were calculated from milligrams hydroxyproline by dividing by 0.13, a conversion factor that assumes the dominant collagen type to be collagen type I [16]. For hyaline cartilage controls, a conversion factor of 0.12, which assumes collagen type II to be the primary collagen type [16], was used.

3.2.3 Histochemical analyses

3.2.3.1 Immunohistochemical staining

The antibodies, epitope retrieval methods, and dilutions used in the present study are noted in Table 3.1. Unless otherwise stated, immunohistochemical steps took place in a humidified environment at room temperature, and immunohistochemical reagents were purchased from Biocare Medical (Walnut Creek, CA).

Tissue sections exposed to only enzyme-based epitope retrieval were deparaffinized in xylene, taken to water using graded ethanol baths, and then blocked with peroxidase for 10 minutes. If pretreatment with chondroitinase ABC (ABC) was indicated, the tissue sections were then digested with 0.1 U/mL ABC (Seikagaku America, Falmouth, MA) dissolved in 100mM Tris 10mM EDTA, pH 8.0 for 30 minutes at 37°C. When appropriate, 0.1% pepsin (LabVision, Fremont, CA) or 0.19% trypsin was applied for 7 minutes.

For tissues receiving collagen type IV antibody, combining heat-induced epitope retrieval with enzymatic treatment appeared to be more effective for antigen unmasking than either method used alone (data not shown). Since combined heat-induced/enzymatic epitope retrieval strategies tend to be more prone to nonspecific staining, particular attention was paid to the collagen IV control tissues to ensure staining specificity. For these tissues,

deparaffinization, peroxidase blocking, and heat-induced epitope retrieval were carried out simultaneously by exposing slides to Reveal for 20 minutes at 95°C in a temperature controlled pressure-cooker (Biocare Medical, Walnut Creek, CA). 0.1% pronase was subsequently applied for 3 minutes.

Table 3.1: Pre-treatment and antibody dilution factors

Antibody	Clone	Epitope Retrieval	Human Dilution	Dog Dilution	Pig Dilution	Ferret Dilution
Collagen type I	N/A	ABC	1:800	1:300	1:1200	1:3000
		Pepsin	Sniper	Sniper	Sniper	Sniper
Collagen type II	6B3	Pepsin	1:200	1:200	1:200	1:200
			Dako	Dako	Dako	Dako
Collagen type III	N/A	ABC	1:800	1:500	1:4000	1:3000
		Pepsin	Sniper	Sniper	Sniper	Sniper
Collagen type IV	CIV-22	Reveal	1:150	1:150	1:150	1:300
		Pronase	Dako	Dako	Dako	Dako
Fibronectin	IST-3	Pepsin	1:150	1:150	1:150	1:300
			Dako	Dako	Dako	Dako

All slides were treated with Avidin-Biotin block following the appropriate epitope retrieval steps. After incubation with blocking agent Terminator for 10 minutes, tissue sections were lightly drained, and the appropriate antibody, diluted either in Sniper or general antibody diluent (Dako Cytomation, Carpinteria, CA), was applied. Collagen type II antibody was applied at room temperature for 1 hr, whereas all other antibodies were applied overnight at 4°C.

Following primary antibody application, goat anti-mouse or goat anti-rabbit IgG secondary antibody and streptavidin-HRP were applied sequentially for 10 minutes each. Bound antibody was detected using chromagen DAB.

Epiglottis sections served as positive controls for each antibody. Negative control vocal fold sections involved application of negative control serum or antibody diluent in place of primary antibody following appropriate enzymatic pretreatment.

3.2.3.2 Picrosirius staining

To examine the distribution and orientation of collagen in the LP, tissue sections were picrosirius stained. Briefly, after being washed in tap water (10 minutes) and in distilled water (2 minutes twice), tissues were treated with 0.2% phosphomolybdic acid for 5 minutes and then with 0.1% Sirius Red in saturated aqueous picric acid for 90 minutes. The sections were rinsed in tap water for 3 minutes, treated with 0.01N HCl for 2 minutes, dehydrated, and coverslipped.

3.2.3.2.1 Bright field information

When picrosirius stained tissues are viewed in bright field, fibrillar collagens, collagen type IV, and amyloid, if present, appear red. Amyloid is a protein that is primarily deposited in connective tissues under pathological conditions. In tissues where amyloid presence can be considered negligible in comparison to that of collagen, such as in many normal connective tissues, the extent of Sirius Red dye binding can be used to quantitate total collagen levels in tissue sections [17, 18]. Bright-field picrosirius staining will thus be used for quantitative histological assessment of LP total collagen following the method of Kratky et al. [18].

3.2.3.2.2 Cross-polarized information

When viewed under cross-polarized light, picrosirius staining is specific for fibrillar collagen. In early papers on picrosirius staining, it was proposed that collagen type could be determined from the fiber color observed under cross-polarization conditions. Specifically, yellow or orange/red fibers were believed to be collagen type I, green fibers to be collagen type III, and blue to yellow fibers to be collagen type II [19, 20]. It is now understood that observed fiber color under cross-polarization depends on a number of factors other than collagen type, including: 1.) its degree of crosslinking, 2.) its orientation relative to the cut plane, 3.) and, if using cross-polarized light rather than circularly polarized light, the fiber orientation relative to the initial polarizer. As an example of point 2, if a collagen fiber is oriented such that its axis is transverse to the cut plane of the tissue section, this fiber will generally not be visible under cross-polarization [21]. Hence, in this study, the birefringence property of picrosirius staining will be used primarily to study changes in collagen orientation within the LP rather than to identify collagen type.

3.2.4 Histochemical image analysis

3.2.4.1 Image Capture

An Axiolab microscope (Zeiss, Thornwood, NY) coupled to an Axiocam CCD camera (Zeiss, Thornwood, NY) and to an Axiovision image analysis system was used for image recording. All stained tissue sections were imaged as full-spectrum 1030x1300 8-bit color images. Background correction was performed prior to image capture by interactively referencing a blank field using the Axiovision software.

For picrosirius stained tissues, further images were taken under controlled conditions to allow for subsequent extraction of concentration information, according to the method of Kratky et al. [18]. Specifically, a 10nm bandpass interference filter (Edmund Industrial Optics, Barrington, NJ) centered at 540nm was placed between the microscope light source and slide stage during image capture. 1030x1300 8-bit grayscale images were recorded.

3.2.4.2 Semi-quantitative image analysis

To facilitate interspecies comparison of staining patterns, average relative staining intensity for bright-field picrosirius and fibronectin staining has been semi-quantitated on a specimen-by-specimen basis using the methodology described in Chapter 2.

3.2.4.3 Quantitative image analysis

Scarring is often localized to the superficial LP [14], and therefore a quantitative comparison of the composition of the superficial LP relative to the overall LP would be useful in developing/evaluating scar restoration strategies.

To have a reproducible means of separating the LP into layers, MATLAB was used to segment each LP image into three subregions, subject to the following constraints: (1) the muscle underlying the LP formed part of the boundary for only one subregion, (2) the epithelium overlying the LP formed part of the boundary for only one subregion, (3) no subregion bordered both epithelium and muscle, and (4) each subregion constituted approximately 33% of the total LP cross-sectional area. The subregion bordering the epithelium and the subregion bordering the muscle will be referred to as the superficial third (ST) and the deep third (DT), respectively. The remaining subregion will be called the intermediate third (IT).

The overlap of these MATLAB defined ST, IT, and DT subregions with the traditional superficial, intermediate, and deep layers of the human LP, although strong, is not exact. The MATLAB algorithm was used over visual segmentation because it allowed reproducible and objective separation of the LP into subregions with a uniform methodology for all species.

In quantitating the relative antigen concentration within a given tissue region, the concepts of optical density (OD) and integrated optical density (IOD) were used. The negative logarithm of the grayscale value of a pixel divided by the average grayscale value of the background can be defined as the OD of that pixel. The IOD of a region can be defined as the sum of optical density elements in that region. Assuming staining to be stoichiometric to antigen presence, microscope source wavelength to be narrow bandpass, and the microscope and associated camera to be operating linearly, the IOD of a region can be assumed to be linearly related to the mass of the antigen in that same region [18, 22].

Once subregions had been defined, IODs for the overall LP and for each LP subregion were calculated for each picrosirius stained specimen. Since regional IODs and overall lamina propria IODs (LP-IODs) varied among specimens based on differences in staining intensity and in LP dimensions, regional IOD values were normalized by dividing by the overall LP-IOD for that specimen.

3.2.5 Statistical analysis

The total collagen concentration in each animal model LP was compared to that of human LP using an unpaired student t-test. Differences were considered statistically significant at a level of $p<0.05$. Human total collagen biochemical results were broken down further and statistically analyzed with respect to gender (3 male and 3 female specimens).

3.3 Results

3.3.1 Biochemical results

Figure 3.1 illustrates the average LP collagen content per milligram tissue total protein by species. Figure 3.2 presents human LP collagen concentrations analyzed with respect to gender. Results are reported as average $\pm$ standard error of the mean. Whereas average collagen levels in dog and human LP were statistically similar ($p>0.05$), the mean collagen content of ferret and pig LPs were found to be significantly different from that of human LP (pig: $p<0.016$, ferret: $p<0.011$). In addition, a statistically significant difference was observed between male and female human LP collagen levels ($p<0.024$).

For hyaline cartilage controls, the mean collagen concentration was within the range cited in literature for normal hyaline cartilage [23] (data not shown).

3.3.2 Histochemical results

Figure 3.3 displays representative bright field picrosirius images and corresponding cross-polarized images. Alongside these full-spectrum images, the narrow bandpass OD images used in regional collagen quantitation are displayed in pseudocolor to enhance visualization. The MATLAB-defined ST and DT subregions are outlined in yellow in each pseudocolored OD image. Figure 3.4 depicts representative collagen type I and collagen type III staining across species. Figures 3.5 and 3.6 illustrate representative collagen type IV staining and representative fibronectin staining, respectively. Semi-quantitative staining results for total collagen and fibronectin are displayed with respect to the species-specific schematics in Figure 3.7.

In describing the histochemical results, the segmentation of the LP of each species into superficial, intermediate, and deep regions developed in Chapter 2 will be used. As can be seen from Figure 3.5, collagen type IV was primarily found in association with basement membranes. However, collagen type IV also appeared to be present in non-basement

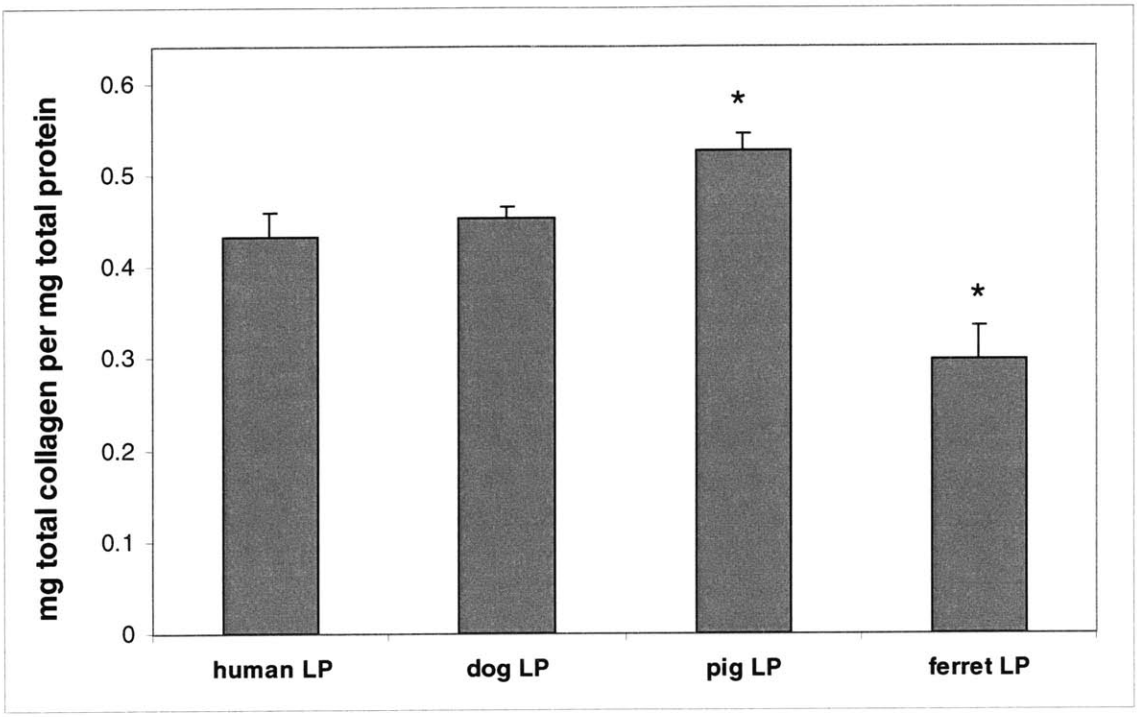

Figure 3.1: Total collagen content by species. Pig and ferret collagen levels were found to be significantly different from human collagen levels, (pig: $p<0.016$, ferret: $p<0.011$).

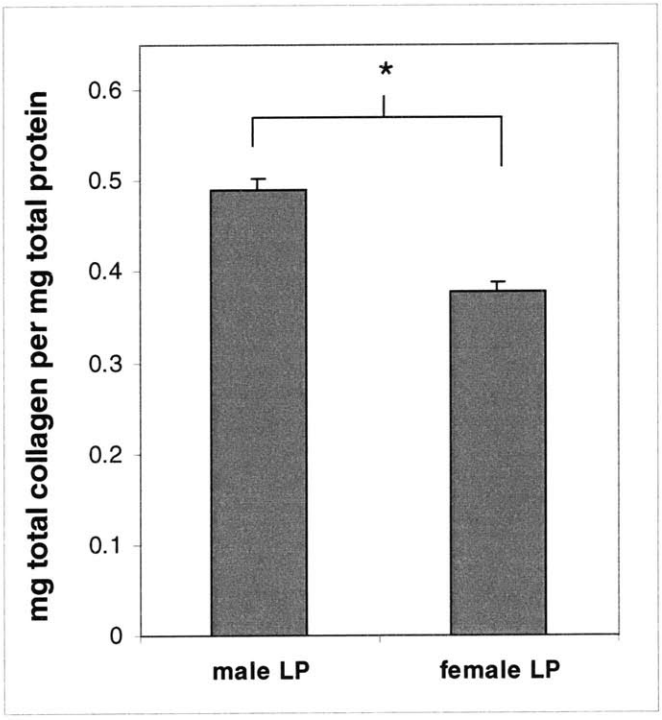

Figure 3.2: Total collagen content by gender. Specimen numbers: males: 3; females: 3. Mean collagen levels in the males were significantly different from that in females: ($p<0.024$).

membrane associated regions of the LP in each species. In dogs and ferrets, collagen type IV staining was extensive throughout the superficial region, and in ferrets staining was also diffuse in the intermediate region. In humans, collagen type IV staining was present in the intermediate and deep LP and tended to be more prominent in the superior regions of these layers than in the inferior regions. Collagen type IV staining was detected throughout the pig LP, although staining tended to be most intense in the superficial and deep LP.

From Figures 3.3 and 3.7, it can be seen that the LP total collagen distribution, as indicated by the bright-field picrosirius stain, was unique for each animal. In dogs and ferrets, collagen staining appeared to be more superficially localized relative to the collagen distributions in humans and pigs.

For pigs, humans, and ferrets, the bright-field LP picrosirius images corresponded well with the cross-polarized images in terms of implied collagen intensity distributions, although for humans the collagen presence in the superficial LP indicated by cross-polarization was occasionally lower than expected based on the bright field images. In dogs, however, bright field and cross-polarized images differed markedly in the degree collagen presence indicated in an extended strip of tissue within the ST (see Figure 3.3d-e). Upon further examination, it appeared that many collagen fiber axes in this region were oriented perpendicular to the cut plane, implying that they would have minimal visibility under cross-polarization. In addition, the superior portion of this strip displayed relatively intense staining for collagen type IV, a collagen type observable in bright field but not generally visible under cross-polarization. Thus, the effects of fibrillar collagen orientation and collagen type IV presence in this region likely combine to account for the discrepancy between dog bright field and cross-polarized picrosirius images.

Figure 3.4 indicates that the staining patterns for collagen types I and III are correlated in humans, pigs, and ferrets, although in humans, collagen type III appears to have a greater percentage of its fibers in the intermediate LP than does collagen type I. In dogs, collagen type III staining tended to decrease from surrounding regions in the oblong subregion of the intermediate region. However, collagen type I staining was not similarly altered in this subregion compared to surrounding tissue. Staining for collagen type II was not detected in the LP of any of the species studied, although staining for collagen type II in the positive control sections was intense (data not shown).

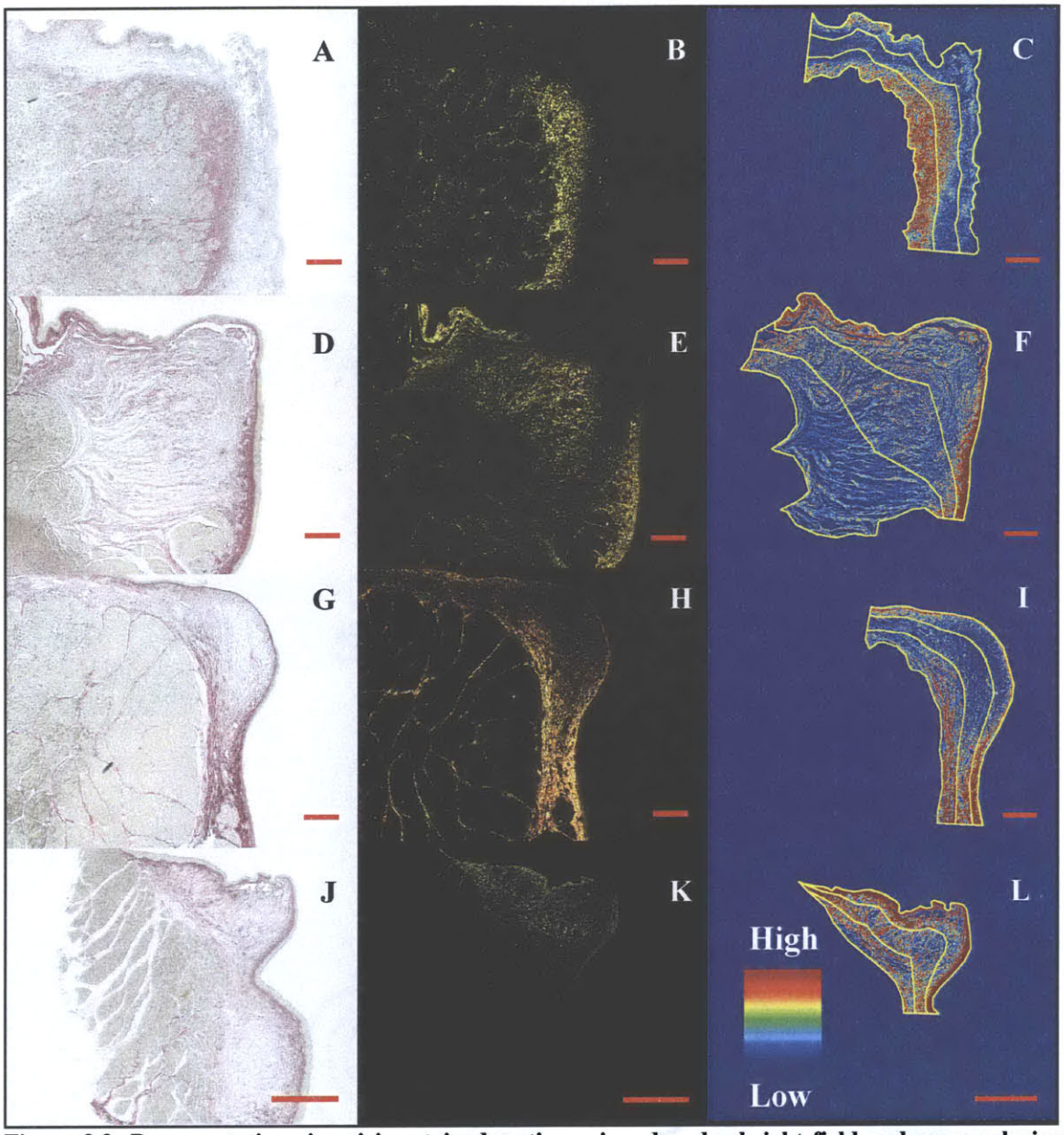

Figure 3.3: Representative picrosirius stained sections viewed under bright field and cross-polarization. (A, D, G, J): bright-field picrosirius staining in human, dog, pig, and ferret LP, respectively; (B, E, H, K): cross-polarized picrosirius images for human, dog, pig, and ferret, respectively. (C, F, I, L): pseudocolored OD images used in collagen quantification in human, dog, pig, and ferret, respectively. The regions outlined in yellow in (C, F, I, L) indicate the ST and DT regions. Scale bars =500 μm.

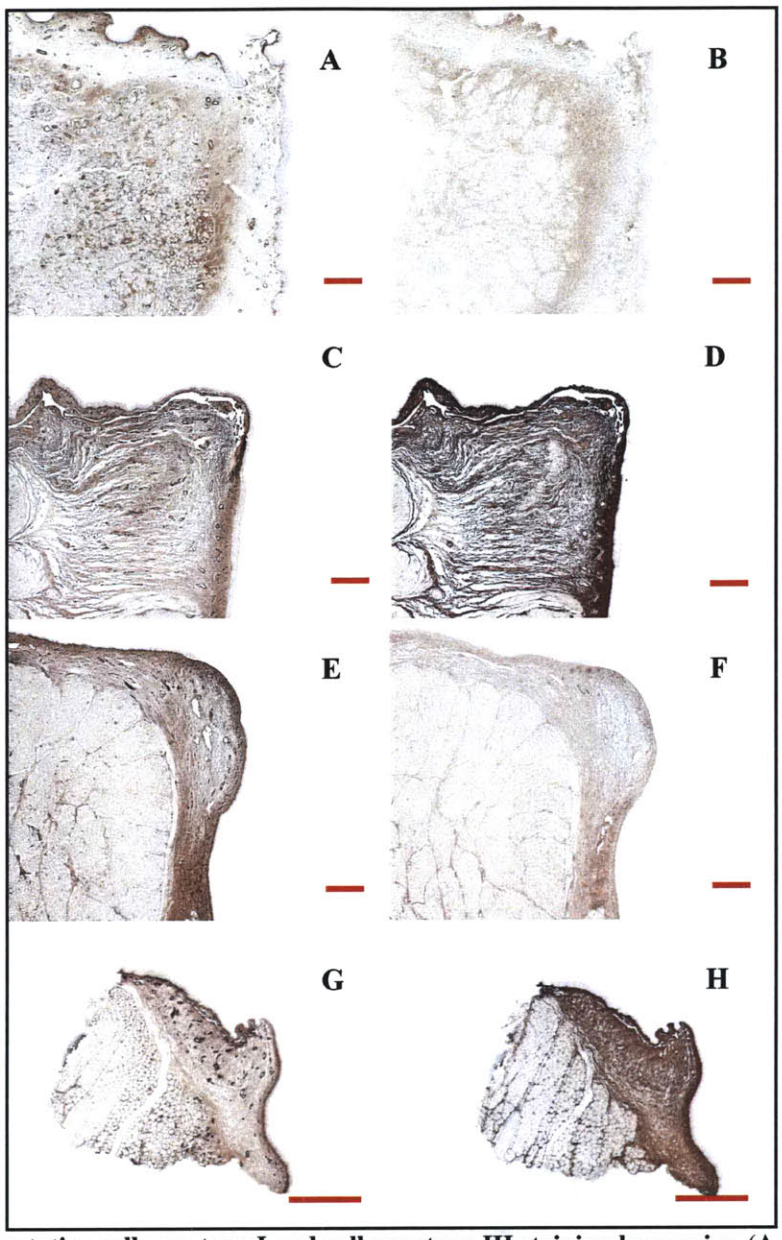

Figure 3.4: Representative collagen type I and collagen type III staining by species. (A, C, E, G): collagen type I staining in human, dog, pig, and ferret LP, respectively; (B, D, F, H): collagen type III staining in human, dog, pig, and ferret, respectively. Scale bars =500 μm.

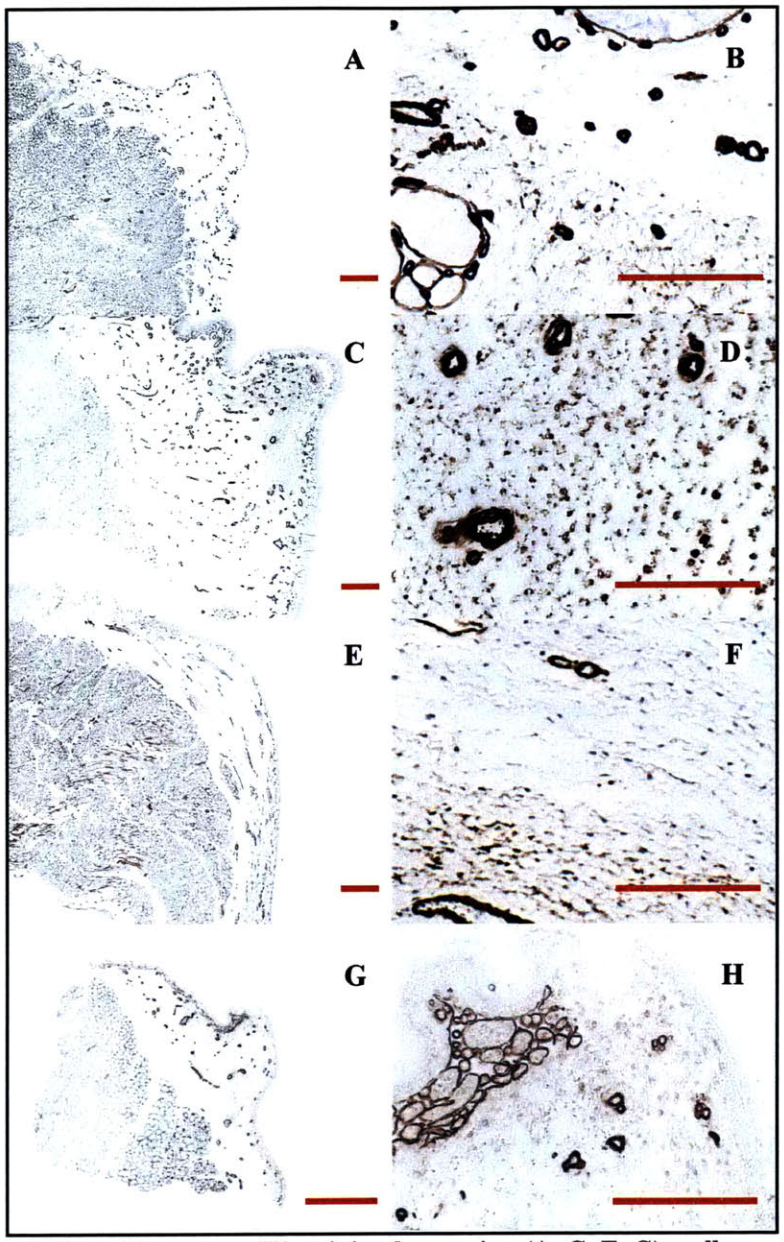

Figure 3.5: Representative collagen type IV staining by species. (A, C, E, G): collagen type IV staining in human, dog, pig, and ferret LP, respectively. Scale bars=500 μm. (B, D, F, H): magnified regions of images of A, B, C, D, respectively, to show fine detail. Scale bars =250 μm.

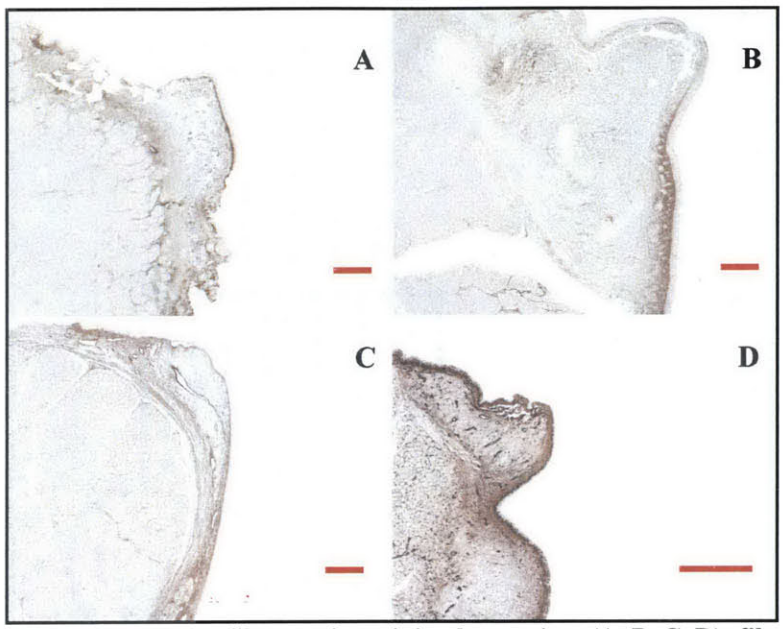

Figure 3.6: Representative fibronectin staining by species. (A, B, C, D): fibronectin staining in human, dog, pig, and ferret, respectively. Scale bars =500 μm.

Fibronectin staining in humans and pigs (Figure 3.6) appeared to closely follow the staining for total collagen, although fibronectin staining in humans tended to be more superficially oriented than the corresponding staining for collagen. In ferrets, fibronectin staining appeared to be most concentrated at the epithelial-LP border and in the deep third of the LP. Dog fibronectin staining was high along the inferior epithelial-LP border and relatively low in the oblong subregion of the intermediate LP.

Figure 3.8 depicts the average fractional IODs for total collagen in the ST, IT, and DT subregions of each species. The corresponding average fractional areas associated with each subregion are indicated in the figure legend. For dogs and ferrets, the quantitative trends in collagen distribution were essentially mirror-images of that seen in humans. In pigs, collagen had a greater superficial presence than in humans. In contrast to total collagen levels, no significant differences in the distribution of collagen in the ST, IT, and DT regions of the human LP were noted with respect to gender (data not shown), although this result may reflect limited specimen number.

The quantitative IOD results can be used to calculate the concentration of collagen in various LP subregions. For example, for humans, the fraction of collagen present in the ST according to IOD calculations is approximately 0.19 ± 0.03, and the overall LP average collagen concentration is approximately 0.43 ± 0.03 mg per mg total protein. The fractional area represented by the ST is about 0.31 ± 0.01. Thus, assuming fractional protein in a region to be proportional to the fractional area of that region, the average collagen concentration in the human ST is approximately 0.26 ± 0.05 mg per mg ST total protein.

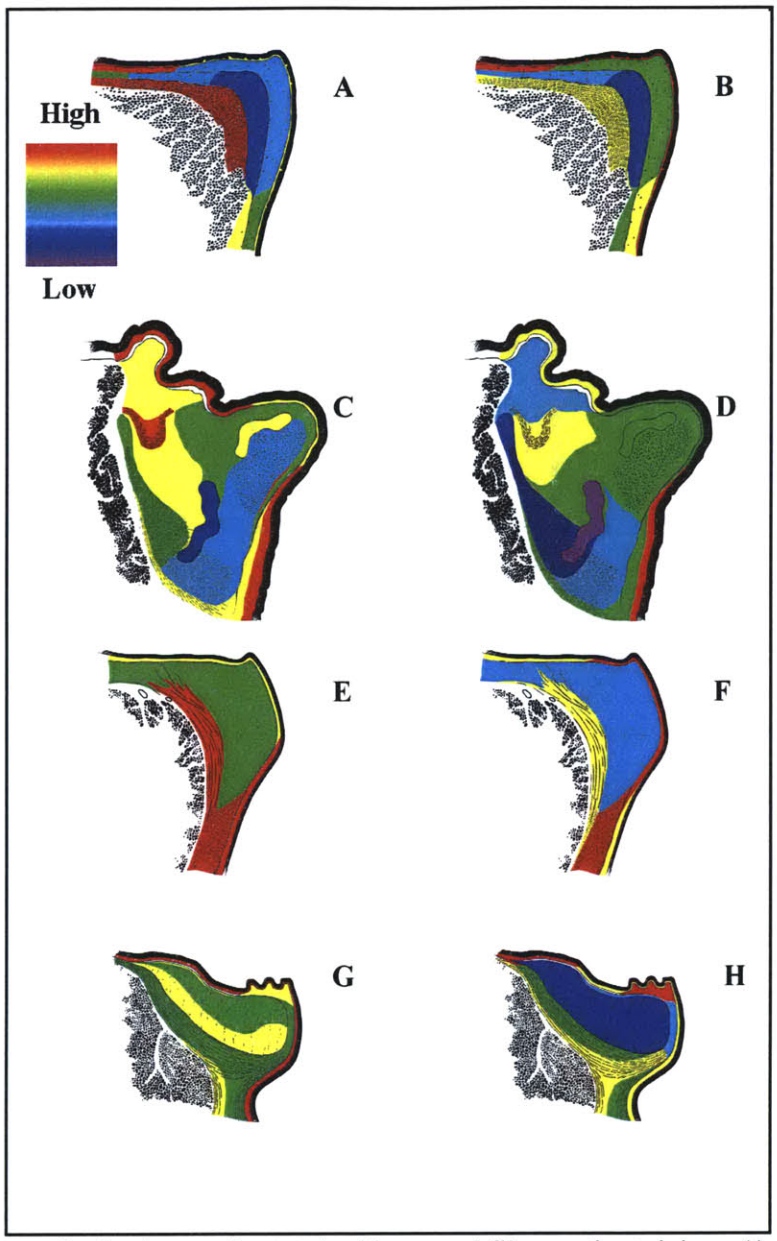

Figure 3.7: Semi-quantitative images for total collagen and fibronectin staining. (A, C, E, G): average relative total collagen staining in human, dog, and pig, and ferret, respectively; (B, D, F, H): average relative fibronectin staining in human, dog, pig, and ferret, respectively.

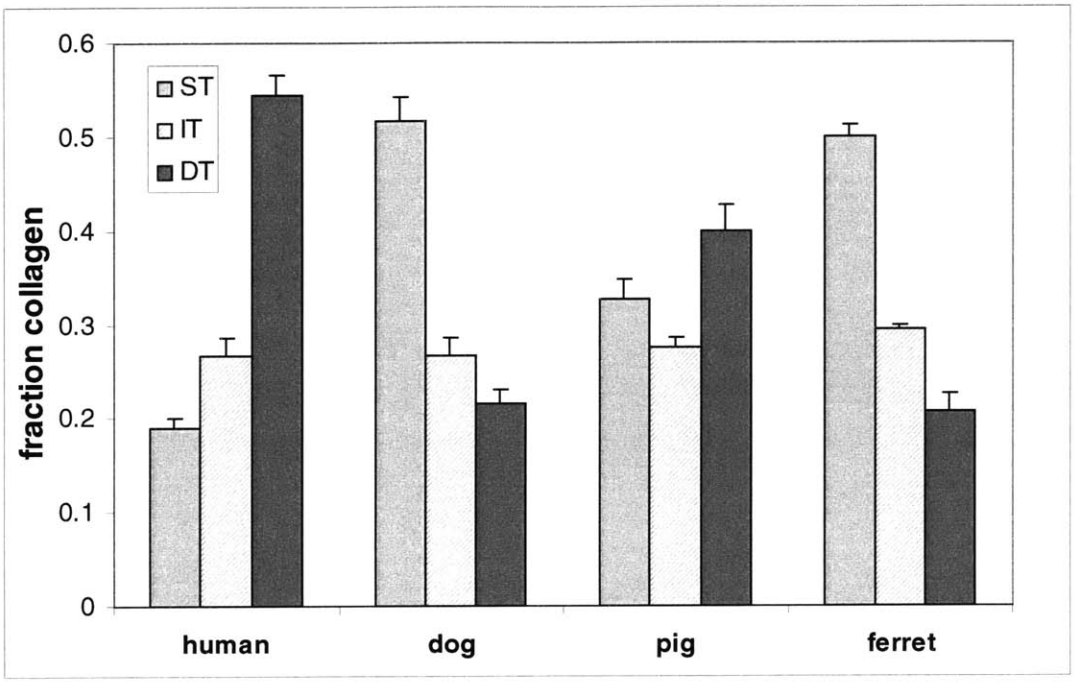

Figure 3.8: Fraction of overall collagen IOD by region. The average fractional areas calculated for each species by region: Human: (ST: 0.307±0.009, IT: 0.360±0.005, DT: 0.333±0.005); dog: (ST: 0.365±0.019, IT: 0.315±0.008, DLP: 0.320±0.019); pig: (ST: 0.294±0.012, IT: 0.382±0.003, 0.324±0.009); ferret: (ST: 0.362±0.019, IT: 0.354±0.004, 0.284±0.019).

3.4 Discussion

3.4.1 Biochemical results

LP total collagen levels varied from a low of approximately 30±3% of tissue total protein in ferrets to a high of approximately 53±2% in pigs. Humans were intermediate in this range with total collagen being approximately 43±3% of LP total protein. These values are in contrast to skin and hyaline cartilage where collagen constitutes approximately 70% [24] and 80% [23], respectively, of tissue total protein. Thus, the collagen concentration in the vocal fold LP is notably lower than that in dermis or hyaline cartilage, a result which has bearing on vocal fold LP biomechanical properties relative to these tissues.

Interestingly, a statistically significant difference between male and female human LP total collagen content was noted, with collagen levels being approximately 49+/-1% for males and 38+/-1% for females. This observed gender difference in collagen concentration supports the histological findings of Hammond et al. [1], in which the observed intensity of human vocal fold LP picric acid staining appeared to be significantly greater in males than in females. Gender differences in collagen and other matrix components are of interest, since they may yield insight into the greater vulnerability of females to LP scarring. However, the collagen

results presented in this paper are based on a relatively small sample set, and more extensive studies are required before broad statements concerning gender differences in human LP collagen content can be made.

3.4.2 Histochemical results

The spatial distributions of total collagen observed in human, dog, and pig LPs in the present study, appear to closely match the collagen staining noted in previous studies for these species [1, 2, 7, 8]. Comparing semi-quantitative results for collagen distribution with those found for decorin in Chapter 2, it can be seen that decorin staining is more superficially localized in the human LP than is the total collagen staining. This observation, as noted in Chapter 2, may be in part related to the documented changes in collagen fiber diameter and density as one progresses from the superficial to the deep LP [1, 3, 4].

When comparing the intensity distribution in cross-polarized picrosirius stained images with that of their bright-field counterparts, changes in collagen orientation within the LP can became visible. Collagen fiber orientation and spatial variations in this orientation can have significant impact on the biomechanical properties of a tissue. In addition, collagen fiber orientation and density tends to be altered in scar tissue, and hence understanding normal spatial variations in LP collagen fiber orientation is desirable. Differences between the bright field and cross-polarized picrosirius images were most striking for dogs in an extended strip of ST tissue. The physiological/functional reasons for this marked regional alteration in dog LP collagen fiber orientation are at present unclear.

According to antibody staining studies, collagen types I and III appear to be the primary collagen types present in the midmembranous vocal fold LP in all species analyzed. Collagen type II does not seem to be a major collagen type in the midmembranous portion of the LP. The dominance of collagen types I and III appears to correlate with high frequency shearing, compressive, and tensile forces that this tissue must withstand while maintaining resilience [25, 26].

As expected, collagen type IV has been found in association with the basement membrane zone and blood and lymphatic vessels in the LP. What is interesting about the observed collagen type IV staining is its apparent presence in non-basement membrane associated regions of the LP, with staining extending into the deeper portions of human and pig LPs. In dogs and ferrets, the collagen type IV distribution was still extensive but tended to be more superficially limited. Collagen type IV is generally found in tissue regions that are required to withstand high shear stresses [27]. Thus, the presence of collagen type IV in the LP ECM may be a reflection of the shear stresses sustained by this tissue. The collagen type IV results also appear to support the relatively extensive LP staining for heparan sulfate described in Chapter 2, since collagen type IV and matrix heparan sulfate proteoglycans are frequently co-localized [28].

Fibronectin is a glycoprotein found in interstitial matrix and plasma, which plays a critical role in cell adhesion, migration, and proliferation and in wound repair [29]. Since fibronectin concentration and distribution appears to be altered in LP scar [13], understanding normal fibronectin distribution is desirable.

The present study is, to the author's knowledge, the first to provide quantitative measures for the total collagen concentration in the human vocal fold LP and in three animal model LPs. Since human vocal fold scarring is generally limited to the superficial LP, quantitative histology has been used to assess the collagen levels this LP subregion. Additionally, the presence and distributions of specific collagen types and fibronectin have been immunohistochemically investigated in the normal LP for all four species.

3.5 Literature cited

1. Hammond, T.H., S.D. Gray, and J.E. Butler, Age- and gender-related collagen distribution in human vocal folds. Annals of Otology Rhinology and Laryngology, 2000. **109**(10): p. 913-920.
2. Madruga de Melo, E., et al., Distribution of collagen in the lamina propria of the human vocal fold. Laryngoscope, 2003. **113**(12): p. 2187-91.
3. Sato, K., M. Hirano, and T. Nakashima, Age-related changes of collagenous fibers in the human vocal fold mucosa. Annals of Otology Rhinology and Laryngology, 2002. **111**(1): p. 15-20.
4. Gray, S.D., et al., Biomechanical and histologic observations of vocal fold fibrous proteins. Annals of Otology Rhinology and Laryngology, 2000. **109**(1): p. 77-85.
5. Ishii, K., et al., Age-related development of the arrangement of connective tissue fibers in the lamina propria of the human vocal fold. Annals of Otology Rhinology and Laryngology, 2000. **109**(11): p. 1055-1064.
6. Sato, K., Reticular fibers in the vocal fold mucosa. Annals of Otology Rhinology and Laryngology, 1998. **107**(12): p. 1023-1028.
7. Garrett, C.G., J.R. Coleman, and L. Reinisch, Comparative histology and vibration of the vocal folds: Implications for experimental studies in microlaryngeal surgery. Laryngoscope, 2000. **110**(5): p. 814-824.
8. Kurita, S., K. Nagata, and M. Hirano, A Comparative Study of the Layer Structure of the Vocal Fold. 1983, College-Hill Press: San Diego. p. 3-21.
9. Gray, S.D., E. Hammond, and D.F. Hanson, Benign Pathological Responses of the Larynx. Annals of Otology Rhinology and Laryngology, 1995. **104**(1): p. 13-18.
10. Thibeault, S.L., et al., Genotypic and phenotypic expression of vocal fold polyps and Reinke's edema: A preliminary study. Annals of Otology Rhinology and Laryngology, 2002. **111**(4): p. 302-309.
11. Hirschi, S.D., S.D. Gray, and S.L. Thibeault, Fibronectin: An interesting vocal fold protein. Journal of Voice, 2002. **16**(3): p. 310-316.
12. Hirano, S., et al., Fibronectin and adhesion molecules on canine scarred vocal folds. Laryngoscope, 2003. **113**(6): p. 966-972.

13. Thibeault, S.L., D.M. Bless, and S.D. Gray, Interstitial protein alterations in rabbit vocal fold with scar. Journal of Voice, 2003. **17**(3): p. 377-383.
14. Rosen, C.A., Vocal fold scar - Evaluation and treatment. Otolaryngologic Clinics of North America, 2000. **33**(5): p. 1081-+.
15. Cooper, C., N. Packer, and K. Williams, eds. Amino acid analysis protocols. Methods in Molecular Biology. Vol. 159. 2001, Humana Press.
16. Miller, E.J. and S. Gay, Collagen - an Overview. Methods in Enzymology, 1982. **82**: p. 3-32.
17. Lopezdeleon, A. and M. Rojkind, A Simple Micromethod for Collagen and Total Protein Determination in Formalin-Fixed Paraffin-Embedded Sections. Journal of Histochemistry & Cytochemistry, 1985. **33**(8): p. 737-743.
18. Kratky, R.G., J. Ivey, and M.R. Roach, Collagen quantitation by video-microdensitometry in rabbit atherosclerosis. Matrix Biology, 1996. **15**(2): p. 141-144.
19. Junqueira, L.C.U., W. Cossermelli, and R. Brentani, Differential Staining of Collagens Type-I, Type-Ii and Type-Iii by Sirius Red and Polarization Microscopy. Archivum Histologicum Japonicum, 1978. **41**(3): p. 267-274.
20. Junqueira, L.C.U., G. Bignolas, and R.R. Brentani, Picrosirius Staining Plus Polarization Microscopy, a Specific Method for Collagen Detection in Tissue-Sections. Histochemical Journal, 1979. **11**(4): p. 447-455.
21. Axer, H., A. Prescher, and D.G.v. Keyserlingk. Evaluation of fiber orientation using polarized light and fuzzy inference. in *European Symposium on Intelligent Techniques*. 1999. Crete.
22. Zhou, R.X., E.H. Hammond, and D.L. Parker, A multiple wavelength algorithm in color image analysis and its applications in stain decomposition in microscopy images. Medical Physics, 1996. **23**(12): p. 1977-1986.
23. Seibel, M.J., S.P. Robins, and J.P. Bilezikian, eds. Dynamics of Bone and Cartilage Metabolism: Principles and Clinical Applications. 1999, Academic Press: San Diego.
24. Goldsmith, L.A., ed. Physiology, biochemistry, and molecular biology of the skin. 2 ed. 1991, Oxford University Press: New York.
25. Thieszen, S.L. and T.H. Rosenquist, Expression of Collagens and Decorin During Aortic-Arch Artery Development - Implications for Matrix Pattern-Formation. Matrix Biology, 1995. **14**(7): p. 573-582.
26. Scherer, R.C., Laryngeal Function During Phonation, in Diagnosis and Treatment of Voice Disorders, J.S. Rubin, et al., Editors. 1995, Igaku-Shoin Medical Publishers, Inc: New York.
27. Thoumine, O., R.M. Nerem, and P.R. Girard, Changes in Organization and Composition of the Extracellular-Matrix Underlying Cultured Endothelial-Cells Exposed to Laminar Steady Shear-Stress. Laboratory Investigation, 1995. **73**(4): p. 565-576.
28. Iozzo, R.V., Matrix proteoglycans: From molecular design to cellular function. Annual Review of Biochemistry, 1998. **67**: p. 609-652.
29. Romberger, D.J., Fibronectin. International Journal of Biochemistry & Cell Biology, 1997. **29**(7): p. 939-943.

Chapter 4. Elastin and Hyaluronan

4.1 Introduction

The contribution of elastin to vocal fold lamina propria (LP) biomechanical properties has long been recognized [1, 2], and recently, the impact of hyaluronan (HA) on LP viscoelasticity has begun to be examined [3]. Several histological studies have investigated the presence of elastin [1, 4, 5] and HA [6] in the human LP, and electron microscopy studies have examined spatial changes in LP elastic fiber thickness and orientation [7-9]. Additionally, the distributions of elastin [10, 11] and total GAG [10] in the LPs of several animal models have been histologically evaluated and qualitatively compared to those of human. Although these studies have significantly advanced the understanding of LP biochemical composition, significant unknowns remain. For example, the concentrations of HA and elastin in normal LP have not yet been evaluated for humans or potential animal models.

This study focuses on characterizing vocal fold LP elastin and HA content. Specifically, quantitative measures of desmosine, an amino acid found only in cross-linked elastin molecules, and of HA in the human vocal fold LP are presented. Since vocal fold scarring is generally limited to the more superficial portions of the LP [12], quantitative histology has been used to calculate the percentage of elastin or HA in specific regions of the vocal fold LP. In addition, the presence of fibrillin-1 in relation to elastin has been histochemically evaluated to gain insight into tensile stress distribution within the LP. Similar analyses have been carried out on dog, pig, and ferret LPs towards defining an appropriate animal model for implant based restoration studies.

4.2 Materials and methods

4.2.1 Tissue samples and preparation

The tissue specimens and controls used in this study and their preparation for biochemical or histological assays were the same as in Chapter 2.

4.2.2 Biochemical analyses

4.2.2.1 Tissue digestion and total protein quantitation

Specimens allocated for biochemical analyses were digested with proteinase K (Worthington Biochemical, Lakewood, NJ) for 24 hrs at 60°C as described in Chapter 2. Total protein in

the sample digests was quantitated in triplicate via amino acid analysis by AAA Service Laboratory, Inc. (Boring, OR), as described in Chapter 2.

4.2.2.2 Desmosine quantitation

Elastin levels were examined indirectly by quantitating desmosine according to the radioimmunoassay protocol described in King et al. [13] Human, dog, and pig digests were measured in triplicate, whereas ferret digests were measured in duplicate due to limited sample. Since desmosine comprises a relatively constant portion of elastin residues in any particular species, desmosine can be used as an indicator of tissue elastin content [14].

Although the desmosine content of elastin extracted from various human, dog, and pig tissues has been quantified [14], the desmosine content of ferret elastin has not been investigated. For this reason, measured LP desmosine concentrations, rather than converted elastin values, will be reported for all species.

4.2.2.3 Hyaluronan quantitation

HA in each human, pig, and dog digest was measured in triplicate and each ferret digest in duplicate using a HA ELISA kit (Echelon Biosciences, Salt Lake City, UT). The post-mortem age of the human specimens prior to preservation was on average about 14 hours greater than that of the animal specimens. Significant extracellular matrix degradation could have occurred during this time period. Since the HA ELISA assay is sensitive to HA degradation, the HA levels presented for humans should be regarded as first-order measures.

4.2.3 Histochemical analyses

4.2.3.1 Hyaluronan staining

To detect HA histologically, serial sections from each LP histology specimen were used. One section from each specimen was exposed to 100 TRU/mL of hyaluronidase from Streptomyces hyaluronticus (EMD Biosciences) for 24 hours at 37°C in a buffer containing 100mM sodium formate, 0.1mg/mL BSA, 0.15M NaCl, 0.1% Triton, pH 3.7, with fresh hyaluronidase being added after 12 hours. The remaining section from each specimen was exposed to sodium formate buffer containing no hyaluronidase for 24 hours at 37°C, with fresh sodium formate buffer being added after the first 12 hours. The tissue sections were then rinsed in deionized water and stained with alcian blue pH 2.5 according to standard protocols [15], although no counterstain was used.

4.2.3.2 Immunohistochemical staining

The antibodies, epitope retrieval methods, and antibody dilutions used in the present study are noted in Table 4.1. Unless otherwise stated, immunohistochemical steps took place in a

humidified environment at room temperature, and immunohistochemical reagents were purchased from Biocare Medical (Walnut Creek, CA).

Tissue sections were deparaffinized in xylene, taken to water using graded ethanol baths, and then exposed to peroxidase block for 10 minutes. If chondroitinase ABC (ABC) digestion was indicated, the tissue sections were then treated with 0.1 U/mL ABC (Seikagaku America, Falmouth, MA) dissolved in 100mM Tris, 10mM EDTA buffer, pH 8.0 for 30 minutes at 37°C. When required, 0.1% pepsin (LabVision, Fremont, CA) was applied for 7 minutes.

Table 4.1: Pre-treatment and antibody dilution factors

Antibody Information	Elastin	Fibrillin-1
Clone	BA-4	12A5.18
Human Epitope Retrieval	Pepsin	ABC
Human Dilution	1:650 Sniper	1:200 Dako
Dog Epitope Retrieval	Pepsin	ABC
Dog Dilution	1:450 Sniper	1:150 Dako
Pig Epitope Retrieval	ABC	ABC
Pig Dilution	1:3000 Sniper	1:200 Dako
Ferret Epitope Retrieval	ABC	ABC
Ferret Dilution	1:500 Sniper	1:200 Dako

All slides were Avidin-Biotin blocked following the appropriate epitope retrieval steps. After incubation with blocking agent Terminator for 10 minutes, tissue sections were lightly drained and the appropriate antibody, diluted either in Sniper or general antibody diluent (Dako Cytomation, Carpinteria, CA), was applied. Elastin antibody was applied overnight at 4°C, whereas fibrillin-1 was applied at room temperature for 1 hr.

Following primary antibody application, goat anti-mouse IgG secondary antibody and streptavidin-HRP were applied sequentially for 10 minutes each. Bound antibody was detected using chromagen DAB.

Epiglottis sections served as positive controls for each antibody. Negative control vocal fold sections involved application of negative control serum or antibody diluent in place of primary antibody following appropriate enzymatic pretreatment.

4.2.4 Histochemical image analysis

4.2.4.1 Image capture

An Axiolab microscope (Zeiss, Thornwood, NY) coupled to an Axiocam CCD camera (Zeiss, Thornwood, NY) and to an Axiovision image analysis system was used for image recording. All stained tissue sections were imaged as full-spectrum 1030x1300 8-bit color images. Background correction was carried out prior to image capture by interactively referencing a blank field using Axiovision software.

For elastin-stained and alcian blue-stained tissues, further images were taken under controlled conditions to allow for quantitative analyses of elastin and HA distributions. Specifically, 10nm bandpass interference filters (Edmund Industrial Optics, Barrington, NJ) centered at 500nm for DAB elastin slides and at 620nm for alcian blue slides were placed between the microscope light source and slide stage during image capture. 1030x1300 8-bit grayscale images were recorded.

4.2.4.2 Semi-quantitative image analysis

To facilitate interspecies comparison of staining patterns, average relative staining intensity has been semi-quantitated on a specimen-by-specimen basis for each antibody/stain using the methodology described in Chapter 2.

4.2.4.3 Quantitative image analysis

Scarring is often localized to the human superficial LP [12], and therefore a quantitative comparison of the composition of the superficial LP relative to the overall LP would be useful in evaluating scar restoration strategies.

Towards this goal, MATLAB was used to separate the LP of each grayscale image into three subregions meant for human specimens to mimick the traditional LP subdivisions, as described in Chapter 3. The subregion bordering the epithelium and the subregion bordering the muscle will be referred to as the superficial third (ST) and the deep third (DT), respectively. The remaining subregion will be called the intermediate third (IT).

In quantitating HA and elastin distributions, the concepts of optical density (OD) and integrated optical density (IOD) were used, as described in Chapter 3. For the alcian blue images, hyaluronidase-treated and non-hyaluronidase treated sections from each specimen were first registered using MATLAB prior to segmentation into subregions. After image registration, the OD for each hyaluronidase treated pixel was subtracted from the OD of the corresponding non-hyaluronidase treated pixel to yield an OD representative of HA presence. This difference OD was used in HA IOD calculations.

Once subregions had been defined, IODs for the overall LP and each LP subregion were calculated for each elastin and HA specimen. The subregional IODs were normalized by dividing by the overall lamina propria-IOD (LP-IOD) for that specimen, yielding regional fractional IODs.

4.2.5 Statistical analyses

Mean HA and desmosine levels in the LP of each animal species were compared to those of human LP using an unpaired student t-test. Differences were considered statistically significant at a level of $p<0.05$.

4.3 Results

4.3.1 Biochemical results

Figures 4.1 illustrates the average LP desmosine content per milligram total protein for all four species. Results are reported as average $\pm$ standard error of the mean. Animal model LP desmosine concentrations were not statistically distinguishable from that of human LP. Due to the dependence of the desmosine content of elastin on species, a statistical similarity between human and animal model desmosine does not necessarily imply similar levels of

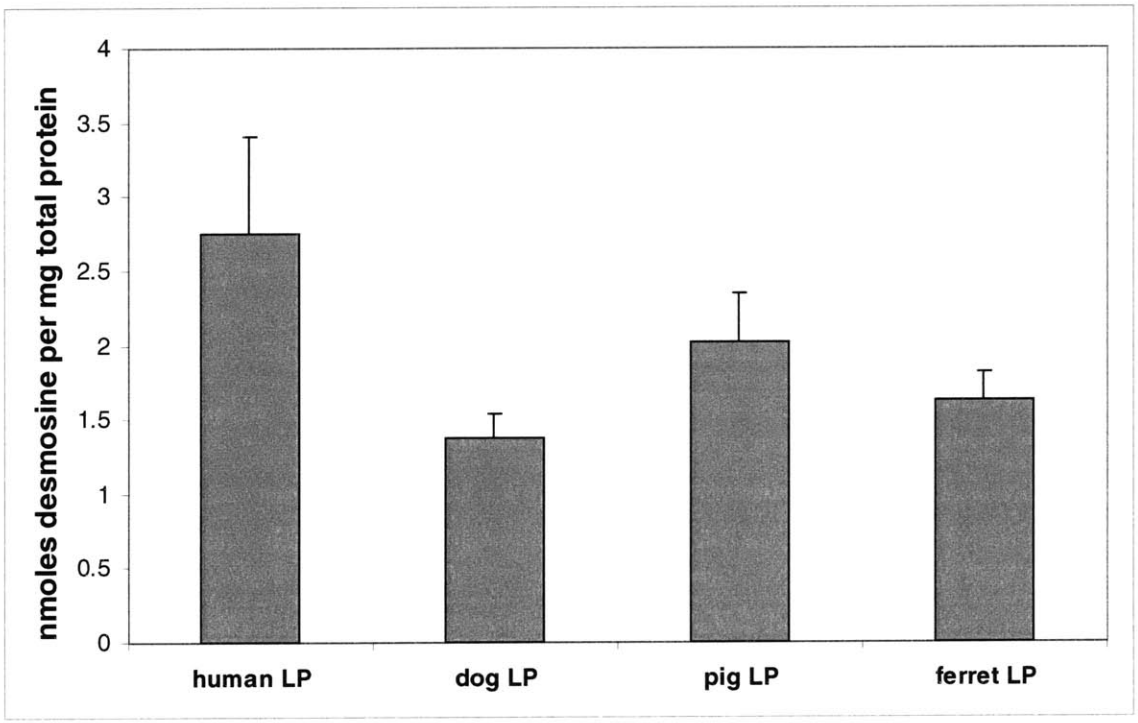

Figure 4.1: Desmosine content by species. No statistically significant differences were found between the mean desmosine levels for pig , dog or ferret and that for humans, $p>0.05$.

elastin. However, a comparison of desmosine levels among species can give an indication of order of magnitude differences in elastin content.

Figure 4.2 depicts average HA concentrations in each species' LP and in the hyaline cartilage controls. The HA levels in the three animal model LPs were significantly different from that of human LP, (dog: $p<3.1x10^{-5}$, pig: $p<1.5 x10^{-5}$, ferret: $p<6.6 x10^{-4}$), although human LP HA content was not statistically distinguishable from that of the hyaline cartilage controls.

No statistically significant differences in human LP desmosine or HA concentrations with gender were noted (data not shown), although this result is likely a reflection of the limited human specimen set. For hyaline cartilage controls, the average HA concentration was within the range cited in literature for normal hyaline cartilage [16]. The desmosine content of the controls was negligible, also in agreement with data for normal hyaline cartilage (data not shown).

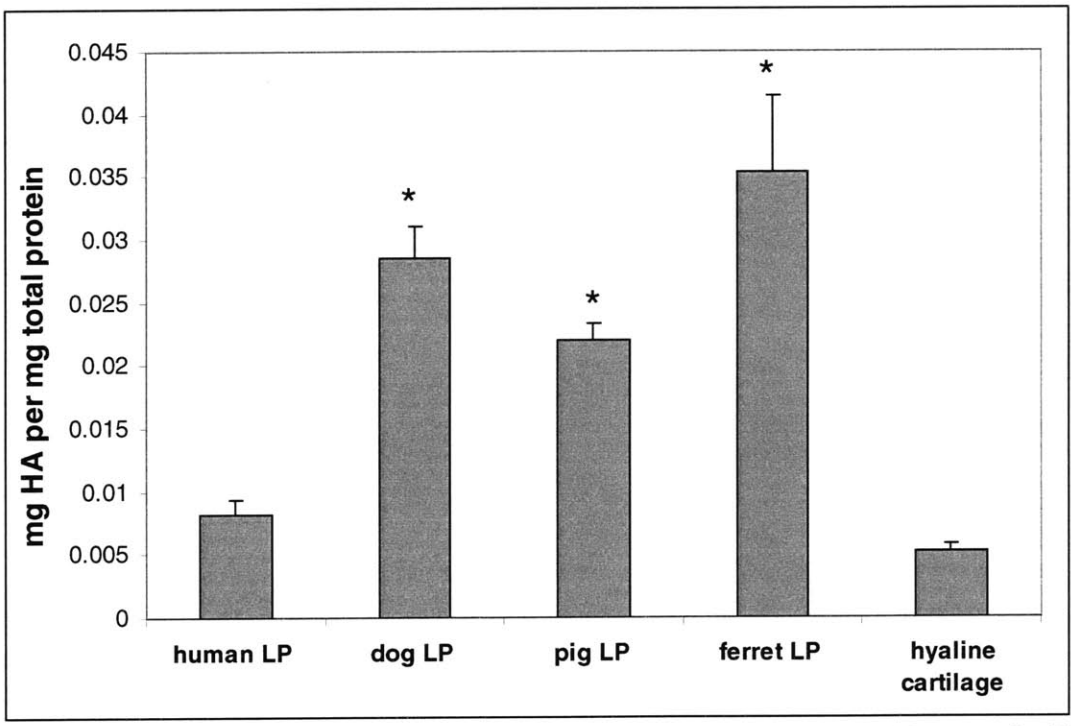

Figure 4.2: Hyaluronan content by species. Mean HA levels in the animal models were significantly different from average human hyaluronan, (dog: $p<3.1x10^{-5}$, pig: $p<1.5 x10^{-5}$, ferret: $p<6.6 x10^{-4}$).

4.3.2 Histochemical results

Figure 4.3 shows representative LP staining for elastin and fibrillin-1. Figure 4.4 displays

representative images of non-hyaluronidase treated and hyaluronidase treated LP sections stained with alcian blue. Alongside these full-spectrum images, the corresponding OD difference images used for HA spatial quantitation have been displayed in pseudocolor to enhance visualization. The MATLAB-defined ST and DT subregions used in image quantitation are outlined in dark blue in each pseudocolored image. Semi-quantitative staining results for elastin, fibrillin-1, and HA are displayed with respect to the species-specific schematics in Figure 4.5.

In describing the histochemical results, the segmentation of the LP of each species into superficial, intermediate, and deep regions developed in Chapter 2 will be used. From Figure 4.5, it can be seen that human, dog, and ferret HA staining tended to be most intense in the intermediate LP. The highest staining for HA in pigs was along the superficial LP-epithelial border and in the inferior regions of the intermediate LP. Elastin appeared to be more superficially-localized in dogs and ferrets than in humans. For pigs, elastin was more evenly distributed throughout the LP than in the other species. In humans, relative staining for fibrillin-1 tended to be low in the IT region stained most deeply for elastin. In addition, the human fibrillin-1 staining distribution was more superficially localized in comparison to elastin staining. Dogs also displayed more superficially oriented staining for fibrillin-1 relative to that for elastin. In ferrets, fibrillin-1 staining was high in the deep regions of the tissue, where elastin staining was relatively low. The pig fibrillin-1 staining more closely followed elastin staining than it did in the other species analyzed. Interestingly, regions staining deeply for both HA and elastin in humans, dogs, and ferrets tended have relatively low staining for fibrillin-1.

Figures 4.6 and 4.7 illustrate the average fractional IODs for elastin and HA, respectively, in the ST, IT, and DT subregions of each species. The corresponding average fractional areas associated with each subregion for each species are indicated in the figure legends. For pigs, elastin was relatively evenly distributed throughout the tissue, whereas the quantitative trends in elastin distribution for dogs and ferrets were essentially mirror-images of that seen in humans. The HA fractional IODs for dogs and ferrets clearly reflected the marked increase in HA staining observed in transitioning from the superficial LP to the intermediate LP in these animals. Although the staining for HA in the majority of the pig IT was relatively low (see Figure 4.4), the fraction HA measured for pig IT reflects the relatively intense staining for HA in the inferior IT region.

These quantitative IOD results can be used to calculate the concentrations of elastin and HA in various regions of the LP. For example, for dogs, the fraction of HA present in the IT according to IOD calculations is approximately 0.47 ± 0.02, and mean HA concentration in the overall dog LP is approximately 0.029 ± 0.003 mg HA per mg total protein. The fractional area represented by the IT is about 0.31 ± 0.01. Thus, assuming fractional protein in a region to be proportional to the fractional area of that region, the average concentration of HA in the dog IT is approximately 0.044 ± 0.005 mg per mg IT total protein.

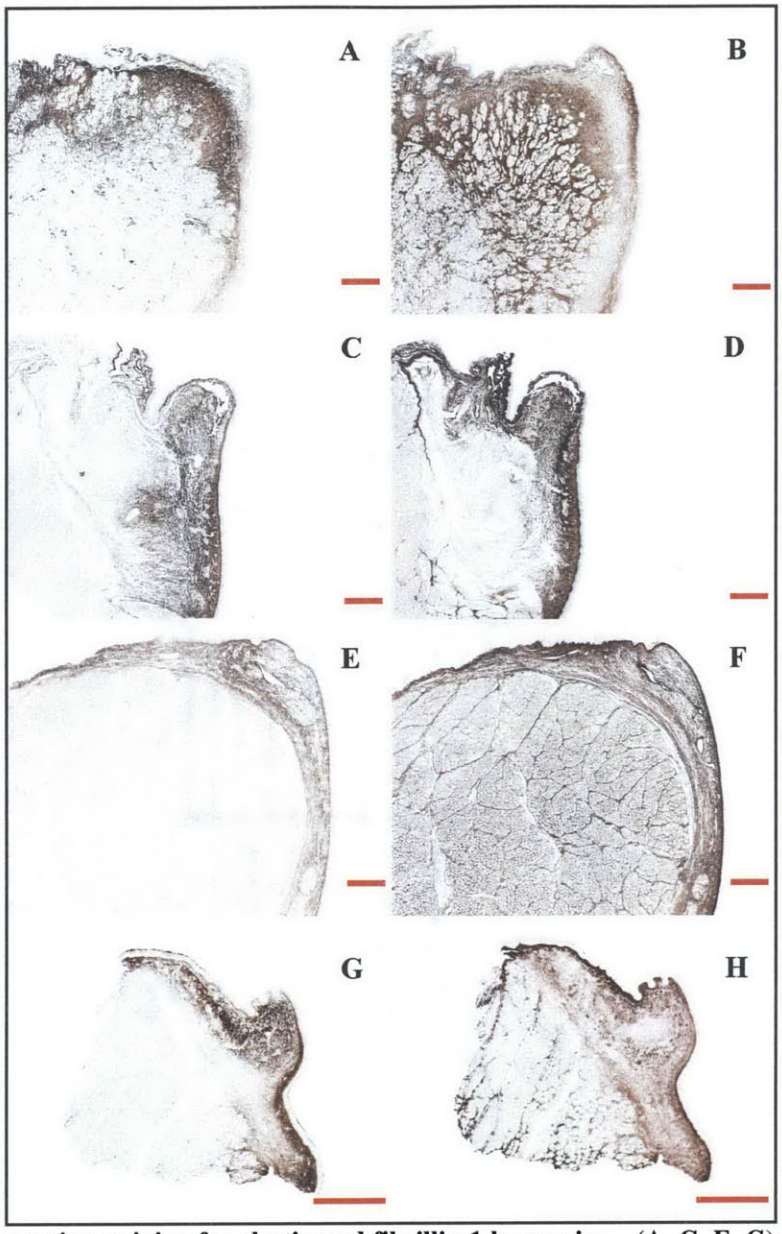

Figure 4.3: Representative staining for elastin and fibrillin-1 by species. (A, C, E, G): elastin staining in human, dog, pig, and ferret, respectively; (B, D, F, H): fibrillin-1 staining in human, dog, pig, and ferret, respectively. Scale bars =500 μm.

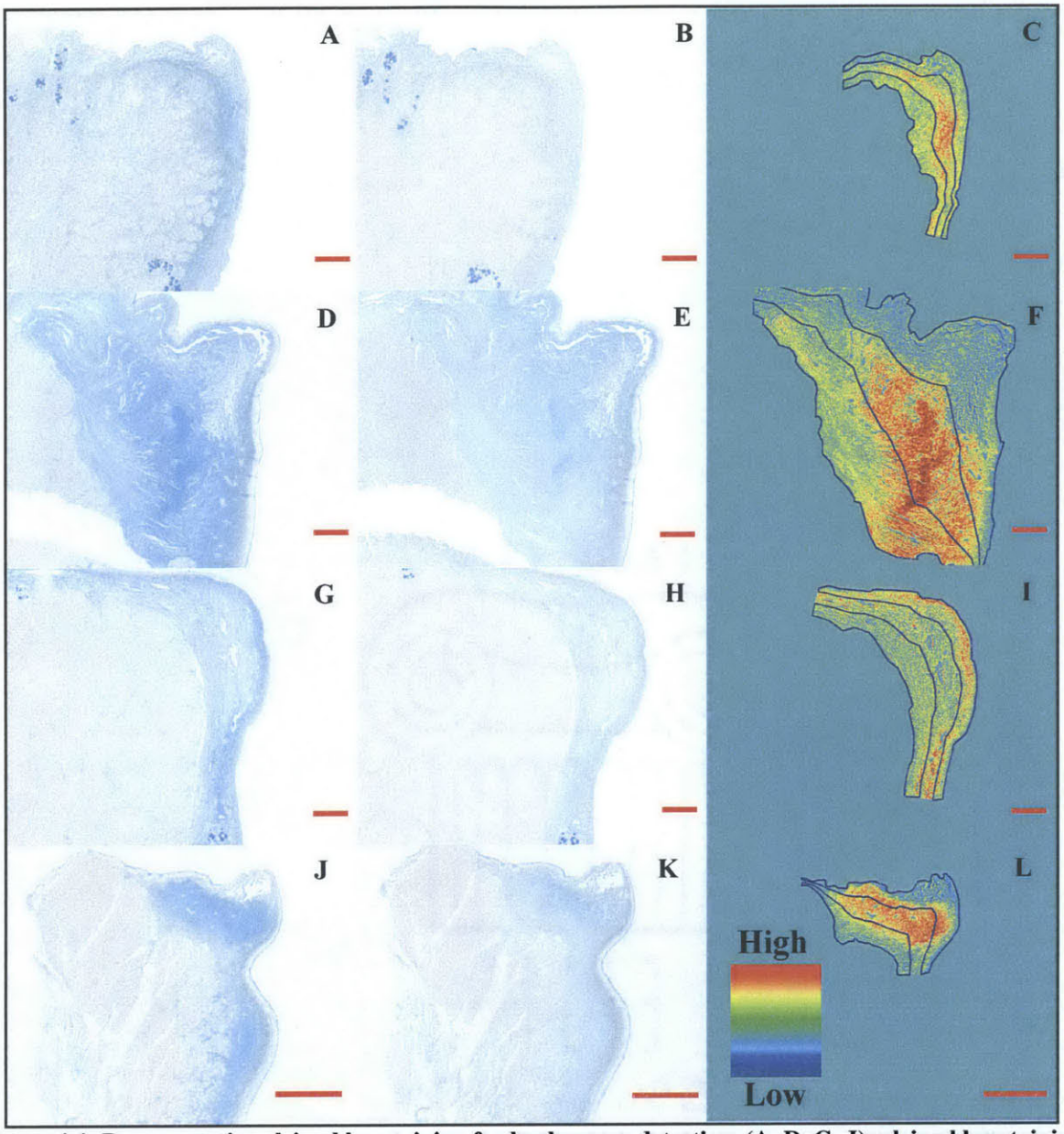

Figure 4.4: Representative alcian blue staining for hyaluronan detection. (A, D, G, J): alcian blue staining of non-hyaluronidase treated human, dog, pig, and ferret LP, respectively; (B, E, H, K): hyaluronidase treated human, dog, pig, and ferret tissues. (C, F, I, L): corresponding pseudocolored OD difference images used in quantitative histology. The regions outlined in dark blue in (C, F, I, L) indicate the ST and DT regions. Scale bars =500 μm.

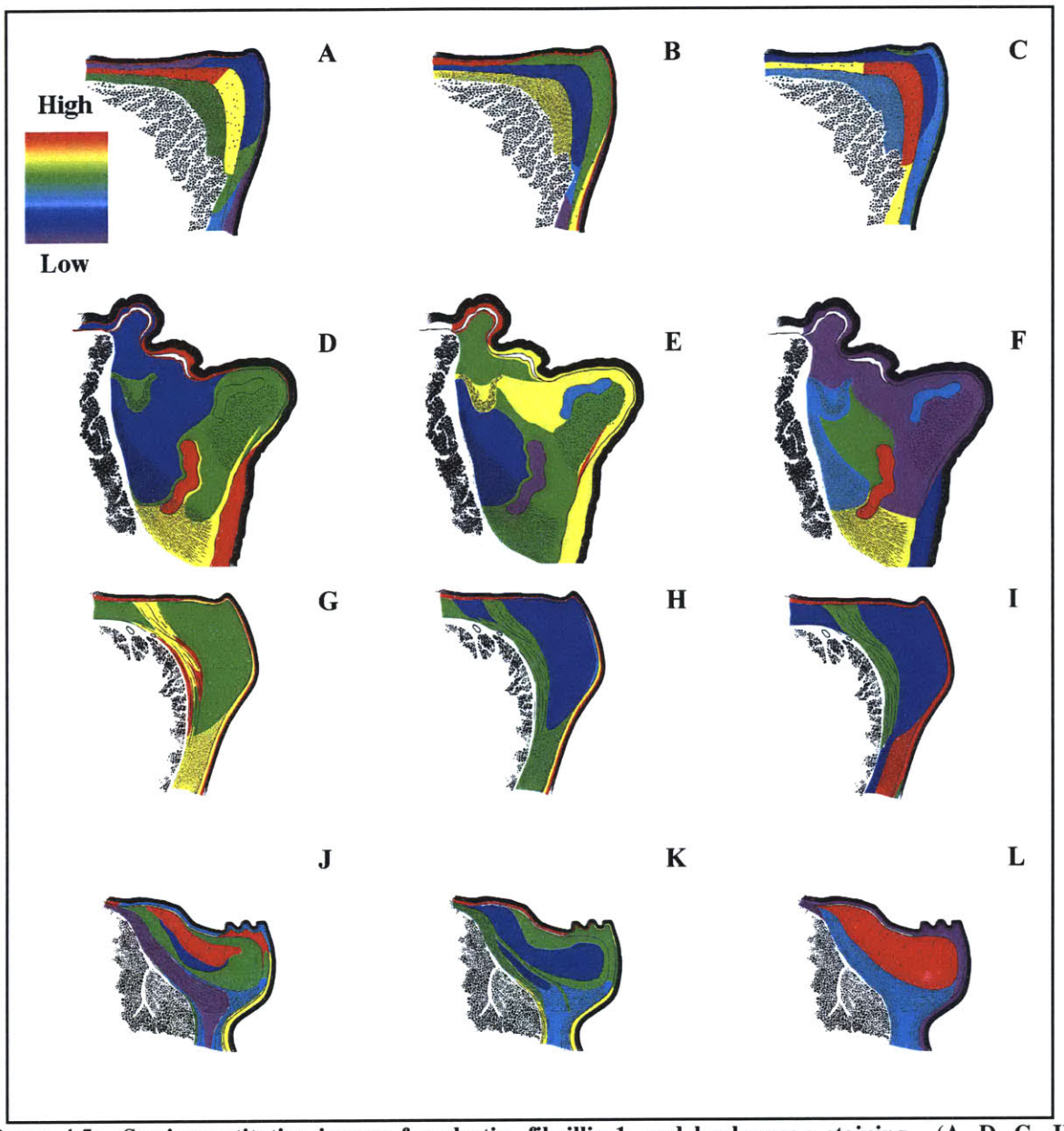

Figure 4.5: Semi-quantitative images for elastin, fibrillin-1, and hyaluronan staining. (A, D, G, J): average relative elastin staining in human, dog, and pig, and ferret, respectively; (B, E, H, K): average relative fibrillin-1 staining in human, dog, pig, and ferret, respectively; (C, F, I, L): average relative hyaluronan staining in human, dog, pig, and ferret, respectively.

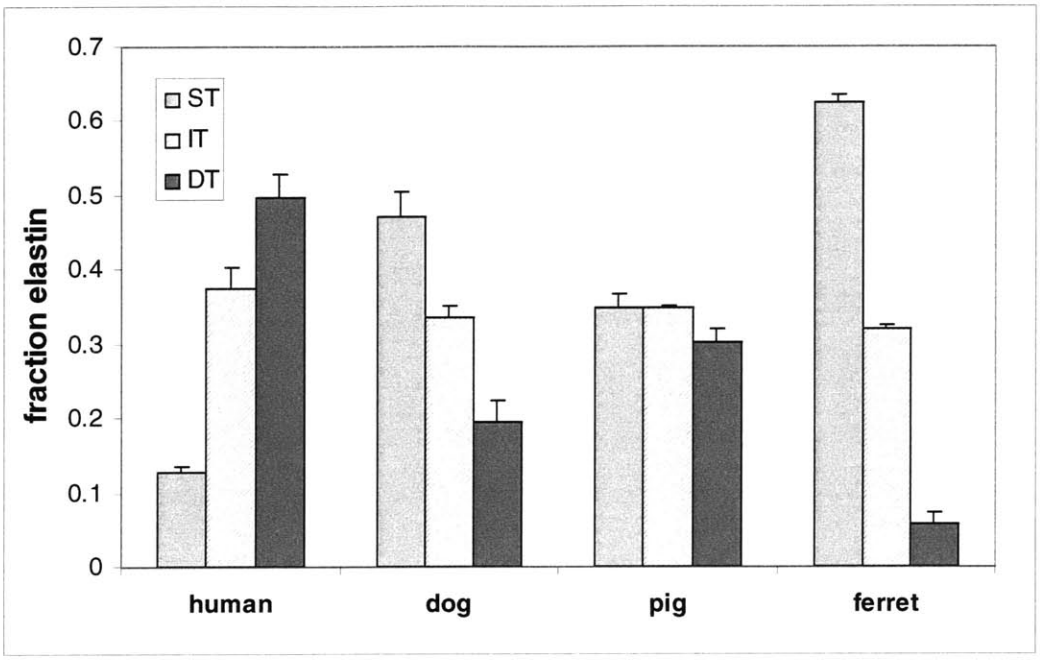

Figure 4.6: Fraction of overall elastin IOD by region. The average fractional areas calculated for each species by region: Human: (ST: 0.312±0.005, IT: 0.358±0.005, DT: 0.330±0.009); dog: (ST: 0.358±0.017, IT: 0.318±0.006, DLP: 0.324±0.019); pig: (ST: 0.304±0.003, IT: 0.375±0.001, 0.321±0.004); ferret: (ST: 0.357±0.012, IT: 0.343±0.003, 0.300±0.015).

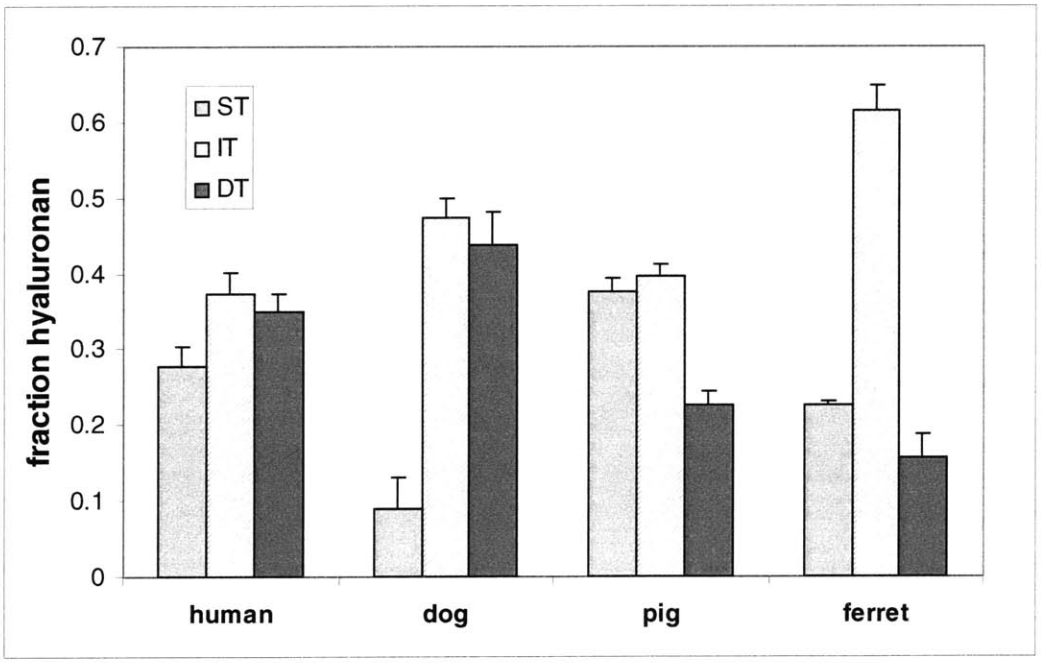

Figure 4.7: Fraction of overall hyaluronan IOD by region. The average fractional areas calculated for each species by region: Human: ST: (0.310±0.010, IT: 0.350±0.008, DT: 0.340±0.014); dog: (ST: 0.351±0.015, IT: 0.312±0.007, DT: 0.337±0.018); pig: (ST: 0.291±0.006, IT: 0.381±0.001, DT: 0.328±0.006); ferret: (ST: 0.327±0.009, IT: 0.363±0.004, DT: 0.310±0.013).

4.4 Discussion

4.4.1 Biochemical results

Desmosine is an amino acid found only in cross-linked elastin [14]. For human aorta, a multiplicative conversion factor of roughly 0.030 has been measured to relate picomoles desmosine to micrograms elastin [14]. For pig and dog aorta, conversion factors of 0.037 and 0.044, respectively, have been measured [14]. Application of these conversion factors to mean LP desmosine values indicate that elastin constitutes approximately 8.5±2.1%, 6.0±0.7%, and 7.5±1.2% of human, dog, and pig LP total protein, respectively. These estimated LP elastin concentrations are on the same order as that of tendon [17].

For humans, the interspecimen variations in desmosine content were greater than those observed for the animal models. Previous histological analyses indicate that the elastin content of the adult human LP increases with age [4]. Thus, the larger interspecimen variability in human LP desmosine levels may be attributable, in part, to the broader age range represented by the human specimens than by the animal specimens. The variability in human desmosine levels may, on the other hand, be a reflection of the natural variability in human LP elastin concentration. The human sample number in this study was not sufficient for these distinctions to be made.

Although the human LP HA content was statistically similar to that of hyaline cartilage controls ($p>0.05$), the mean HA levels in the animal model LPs were approximately 3-4 times greater than that in human LP. The increased post-mortem age of the human specimens may in part account for the observed differences between human and animal model LP HA content, although further studies would be required to clarify the origin of this interspecies variation in LP HA levels. Given these caveats, the HA concentrations presented in this study can be considered to provide order of magnitude assessments of LP HA levels, placing this tissue within the context of other biochemically and biomechanically well-characterized tissues.

4.4.2 Histochemical results

On a qualitative level, the LP elastin distributions observed in human, dog, and pig LPs in the present study closely matched the elastin distributions noted in the literature for these species [1, 2, 4, 6, 10, 11]. From Figure 4.6, dog and ferret appear to follow an elastin concentration profile that is essentially the mirror-image of that of humans, with staining for elastin being lowest in the deep third and relatively high in the superficial and intermediate thirds. This observation could have implications for the suitability of these two animals for evaluating implants meant to restore function to scarred human superficial LP.

Fibrillin-1 is one of the microfibrils associated with elaunin and mature elastic fibers. It is also a constituent of oxytalin, an elastic molecule that contains no elastin component [18]. Oxytalin has been observed to be often associated with tissue regions that bear high tensile stress [18]. If it is assumed that the ratio of fibrillin-1 to other elastin-associated microfibrils remains approximately constant throughout the LP, then the spatial distribution of fibrillin-1, when interpreted in conjunction with elastin staining, gives an indication of the spatial arrangement of oxytalin versus that of elastin-containing elastic fibers.

In humans and dogs, the more superficial localization of fibrillin-1 staining relative to that of elastin seems to indicate that these superficial regions may experience higher tensile stress than underlying LP regions. In ferret LP, fibrillin-1 staining was shifted towards the deep LP relative to elastin staining, implying that ferrets may experience relatively high tensile stress in the deep LP. Interestingly, fibrillin-1 staining tended to the relatively low in humans, dogs, and ferrets in regions of combined high elastin and high hyaluronan staining. The reason for this is unclear, although a distinct microfibril may be responsible for organizing elastin in these regions.

For ferrets, humans, and dogs, HA appeared to be most concentrated in the IT. HA staining in pigs was high along the superficial LP-epithelial border and in the inferior region of the IT, although in the remainder of the IT, HA staining was relatively low. HA is involved in lubrication and in the dissipation of impact and compressive stresses [19]. Thus, these interspecies differences in HA localization may imply corresponding differences in the regional stresses sustained by their LPs.

Comparing HA semi-quantitative staining patterns to those for chondroitin 6-sulfate (C6S) developed in Chapter 2, it appears that C6S staining in both ferrets and dogs is primarily localized to the oblong IT subregion which stains relatively intensely for both elastin and HA. The reasons for the localization of ferret and dog C6S staining to IT subregions are unclear, although it may indicate that the C6S proteoglycan (PG) in this region is a large aggregating PG. Based on the background staining for aggrecan and the disparity between versican and C6S staining distributions in dog and ferret LPs observed in Chapter 2, there seem to be two primary possibilities: either the sulfation of versican-associated chondroitin sulfate side chains varies with LP region, or a distinct PG is responsible for this C6S staining. A similar co-localization of C6S with high HA and elastin staining regions was not noted in humans or pigs.

The present study is, to the author's knowledge, the first to quantify the HA and elastin concentrations in the human vocal fold LP and in three animal model LPs. Quantitative histochemistry has been used to provide a key link between histological and biochemical data, allowing the HA or desmosine content of specific LP subregions to be calculated. The distribution of tensile stresses in the LP, as indicted by fibrillin-1 staining, has similarly been investigated for all four species. These histological and quantitative biochemical results should yield deeper insight into the structure and function of the LP and methods to repair it.

4.5 Literature cited

1. Gray, S.D., et al., Biomechanical and histologic observations of vocal fold fibrous proteins. Annals of Otology Rhinology and Laryngology, 2000. **109**(1): p. 77-85.
2. Kurita, S., et al., The Layer Structure of the Vocal Fold - Age-Dependent Variations. Folia Phoniatrica, 1980. **32**(3): p. 210-210.
3. Chan, R.W., S.D. Gray, and I.R. Titze, The importance of hyaluronic acid in vocal fold biomechanics. Otolaryngology-Head and Neck Surgery, 2001. **124**(6): p. 607-614.
4. Hammond, T.H., et al., Age- and gender-related elastin distribution changes in human vocal folds. Otolaryngology-Head and Neck Surgery, 1998. **119**(4): p. 314-322.
5. Ximenes, J.A., et al., Histologic changes in human vocal folds correlated with aging: A histomorphometric study. Annals of Otology Rhinology and Laryngology, 2003. **112**(10): p. 894-898.
6. Hammond, T.H., et al., The intermediate layer: A morphologic study of the elastin and hyaluronic acid constituents of normal human vocal folds. Journal of Voice, 1997. **11**(1): p. 59-66.
7. Ishii, K., et al., Age-related development of the arrangement of connective tissue fibers in the lamina propria of the human vocal fold. Annals of Otology Rhinology and Laryngology, 2000. **109**(11): p. 1055-1064.
8. Sato, K. and M. Hirano, Age-related changes of elastic fibers in the superficial layer of the lamina propria of vocal folds. Annals of Otology Rhinology and Laryngology, 1997. **106**(1): p. 44-48.
9. Ishii, K., et al., Ultrastructure of the lamina propria of the human vocal fold. Acta Oto-Laryngologica, 1996. **116**(5): p. 778-782.
10. Garrett, C.G., J.R. Coleman, and L. Reinisch, Comparative histology and vibration of the vocal folds: Implications for experimental studies in microlaryngeal surgery. Laryngoscope, 2000. **110**(5): p. 814-824.
11. Kurita, S., K. Nagata, and M. Hirano, A Comparative Study of the Layer Structure of the Vocal Fold. 1983, College-Hill Press: San Diego. p. 3-21.
12. Rosen, C.A., Vocal fold scar - Evaluation and treatment. Otolaryngologic Clinics of North America, 2000. **33**(5): p. 1081-+.
13. King, G.S., V.S. Mohan, and B.C. Starcher, Radioimmunoassay for Desmosine. Connective Tissue Research, 1980. **7**(4): p. 263-267.
14. Starcher, B.C. and M.J. Galione, Purification and Comparison of Elastins from Different Animal Species. Analytical Biochemistry, 1976. **74**(2): p. 441-447.
15. Sheehan, D. and B. Hrapchak, Theory and practice of Histotechnology. 2 ed. 1980, Columbus: Battelle Press.
16. Seibel, M.J., S.P. Robins, and J.P. Bilezikian, eds. Dynamics of Bone and Cartilage Metabolism: Principles and Clinical Applications. 1999, Academic Press: San Diego.
17. Welgus, H., M.D., Elastin, A.A.o. Dermatology, Editor.
18. Ramirez, F. and L. Pereira, The fibrillins. International Journal of Biochemistry & Cell Biology, 1999. **31**(2): p. 255-259.
19. Laurent, T.C. and J.R.E. Fraser, Hyaluronan. Faseb Journal, 1992. **6**(7): p. 2397-2404.

Chapter 5. Cellularity and Extracellular Matrix Turnover

5.1 Introduction

Tissue cellularity is altered during a number of physiological and pathological processes, including growth, aging, degeneration, and repair. Thus, it is important that the normal cellularity of the vocal fold lamina propria (LP) be known in seeking to treat LP scarring. Although several histological studies of vocal fold LP cell types have been published [1-5], the cellular density in the LPs of human and animal models has not been quantitatively assessed.

Also altered in disease states, aging, and repair is the rate extracellular matrix (ECM) turnover in a tissue. Changes in ECM turnover with senescence in rat vocal fold LP have been investigated using RT-PCR [6, 7]. These results have yielded insight into the normal ECM turnover; however, spatial variations in the expression of various enzymes or newly synthesized molecules within normal LP are not captured by these studies. Since scarring tends to be limited to the human superficial LP [8], it is important to understand normal turnover in this LP subregion.

The present study has analyzed the DNA content of human, pig, dog, and ferret vocal fold LP as a measure of tissue cellularity. Spatial variations in vocal fold LP ECM turnover, as indicated by immunostaining for tropoelastin, procollagen type I, and matrix metalloprotease I (MMP-1), have also been investigated.

5.2 Materials and methods

5.2.1 Tissue samples and preparation

The tissue specimens and controls used in this study and their preparation for biochemical or histological assays were the same as in Chapter 2.

5.2.2 Biochemical analyses

5.2.2.1 Tissue digestion and total protein quantitation

Specimens allocated for biochemical analyses were digested with proteinase K (Worthington Biochemical, Lakewood, NJ) for 24 hrs at 60°C as described in Chapter 2. Total protein in the sample digests was quantitated in triplicate via amino acid analysis by AAA Service Laboratory, Inc. (Boring, OR) as described in Chapter 2.

5.2.2.1 DNA quantitation

The Picogreen assay (Molecular Probes) was used to measure the DNA content of human, dog, and pig digests in triplicate and of ferret digests in duplicate. Calf thymus DNA (Sigma-Aldrich) was used as the standard for this assay. Based on combined information from the online Database of Genome Sizes and Gregory [9], the following conversion factors were used to calculate cellular content from measured DNA values: 1.) pigs: 6.6pg DNA/cell, 2.) dogs: 6.3pg DNA/cell, and 3.) humans: 6.9pg DNA/cell. The conversion factor used for ferrets, 6.2pg/cell, was based on average DNA concentrations for measured species within the Order Carnivora [9], of which ferrets are a member.

5.2.3 Immunohistochemical analyses

The antibodies, epitope retrieval methods, and dilutions used are noted in Table 5.1. Unless otherwise stated, immunohistochemical steps took place in a humidified environment at room temperature, and immunohistochemical reagents were purchased from Biocare Medical (Walnut Creek, CA).

For sections receiving heat-induced epitope retrieval, deparaffinization, peroxidase blocking, and epitope retrieval were carried out simultaneously by exposing slides to Reveal for 20 minutes at 95°C in a temperature controlled pressure-cooker (Biocare Medical Walnut Creek, CA).

For slides exposed to enzyme-based epitope retrieval, tissue sections were deparaffinized in xylene, taken to water using graded ethanol baths, and then exposed to peroxidase block for 10 minutes. When required, 0.19% trypsin was applied for 7 minutes.

Table 5.1: Pre-treatment and antibody dilution factors

Antibody	Clone/Antigen	Epitope Retrieval	Human Dilution	Dog Dilution	Pig Dilution	Ferret Dilution
Procollagen type I	M-58	Trypsin	1:650 Sniper	1:450 Sniper	1:3000 Sniper	1:500 Sniper
MMP-1	Recombinant human MMP-1	Reveal	1:200 Dako	1:150 Dako	1:200 Dako	1:200 Dako
Tropoelastin	Ala-Lys-$(Ala)_3$-Lys-$(Ala)_3$-Lys-Tyr	N/A	1:1600 Dako	1:800 Dako	1:1600 Dako	1:800 Dako

All slides were Avidin-Biotin blocked following the appropriate epitope retrieval steps. After incubation with blocking agent Terminator for 10 minutes, tissue sections were lightly drained and the appropriate antibody, diluted either in Sniper or general antibody diluent (Dako Cytomation, Carpinteria, CA), was applied. Procollagen type I antibody was applied overnight at 4°C, whereas remaining antibodies were applied for 1 hr at room temperature.

Following primary antibody application, appropriate secondary antibody and streptavidin-HRP were applied sequentially for 10 minutes each. Bound antibody was detected using chromagen DAB.

Epiglottis sections served as positive controls for each antibody. Negative control vocal fold sections involved application of negative control serum or antibody diluent in place of primary antibody following appropriate enzymatic pretreatment.

5.2.4 Immunohistochemical image analysis

5.2.4.1 Image capture

An Axiolab microscope (Zeiss, Thornwood, NY) coupled to an Axiocam CCD camera (Zeiss, Thornwood, NY) and to an Axiovision image analysis system was used for image recording. All stained tissue sections were imaged as full-spectrum 1030x1300 8-bit color images. Background correction was performed prior to image capture by interactively referencing a blank field using the Axiovision software.

5.2.4.2 Semi-quantitative image analysis

To facilitate interspecies comparison of staining patterns, average relative staining intensity was semi-quantitated for procollagen type I, MMP-1, and tropoelastin on a specimen-by-specimen basis using the methodology described in Chapter 2.

5.2.5 Statistical analysis

The LP cellularity of each animal species was compared to that of humans using an unpaired student t-test. Differences were considered statistically significant at a level of $p<0.05$.

5.3 Results

5.3.1 Biochemical results

Figure 5.1 presents cell number per milligram total protein in pig, human, ferret, and dog vocal fold LPs. Results are reported as average $\pm$ standard error of the mean. To place the cell densities in context, the measured cellularity of pig hyaline cartilage controls have been included in Figure 5.1. Cellularity in dogs was statistically indistinguishable from that in humans ($p>0.05$), although pig and ferret cell densities were significantly different from human cellularity (pig: $p<0.018$, ferret: $p<0.033$).

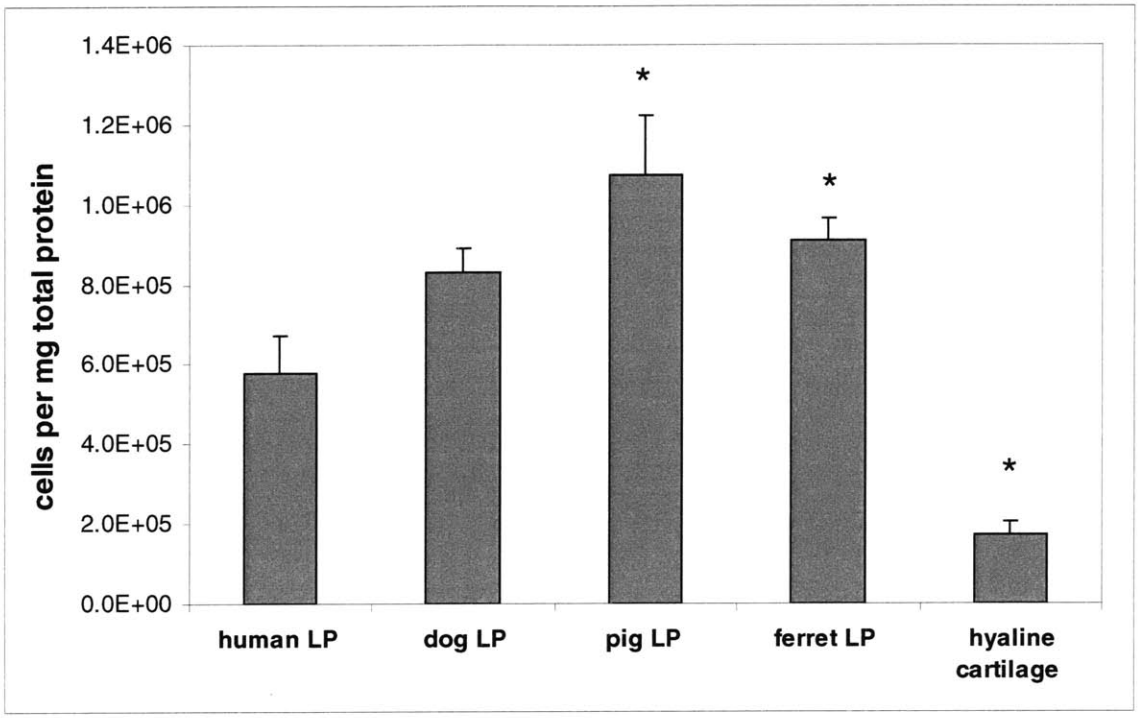

Figure 5.1: LP cellularity by species as compared to hyaline cartilage. Pig and ferret cellularity were significantly different from human cellularity (pig: $p<0.018$, ferret: $p<0.033$). In addition, the cellularity of hyaline cartilage was statistically different from human vocal fold LP ($p<0.011$).

5.3.2 Histochemical results

Figure 5.2 depicts representative tropoelastin and MMP-1 staining for all species, whereas Figure 5.3 illustrates representative procollagen type I staining. Semi-quantitative staining results for tropoelastin, MMP-1, and procollagen type I are displayed with respect to the species-specific schematics in Figure 5.4.

In describing the histochemical results, the segmentation of the LP of each species into superficial, intermediate, and deep regions developed in Chapter 2 will be used. As shown in Figure 5.2, pig tropoelastin staining was relatively evenly distributed throughout the LP, although there was a moderate increase in staining observed in the deep LP. In humans, the tropoelastin distribution was more superficially localized than the elastin distribution described in Chapter 4, although tropoelastin staining was still more intense in the deep LP than the superficial LP. Staining for tropoelastin in dogs and ferrets was most concentrated in the thick superficial rim of tissue along the inferior epithelial-LP border. In the oblong

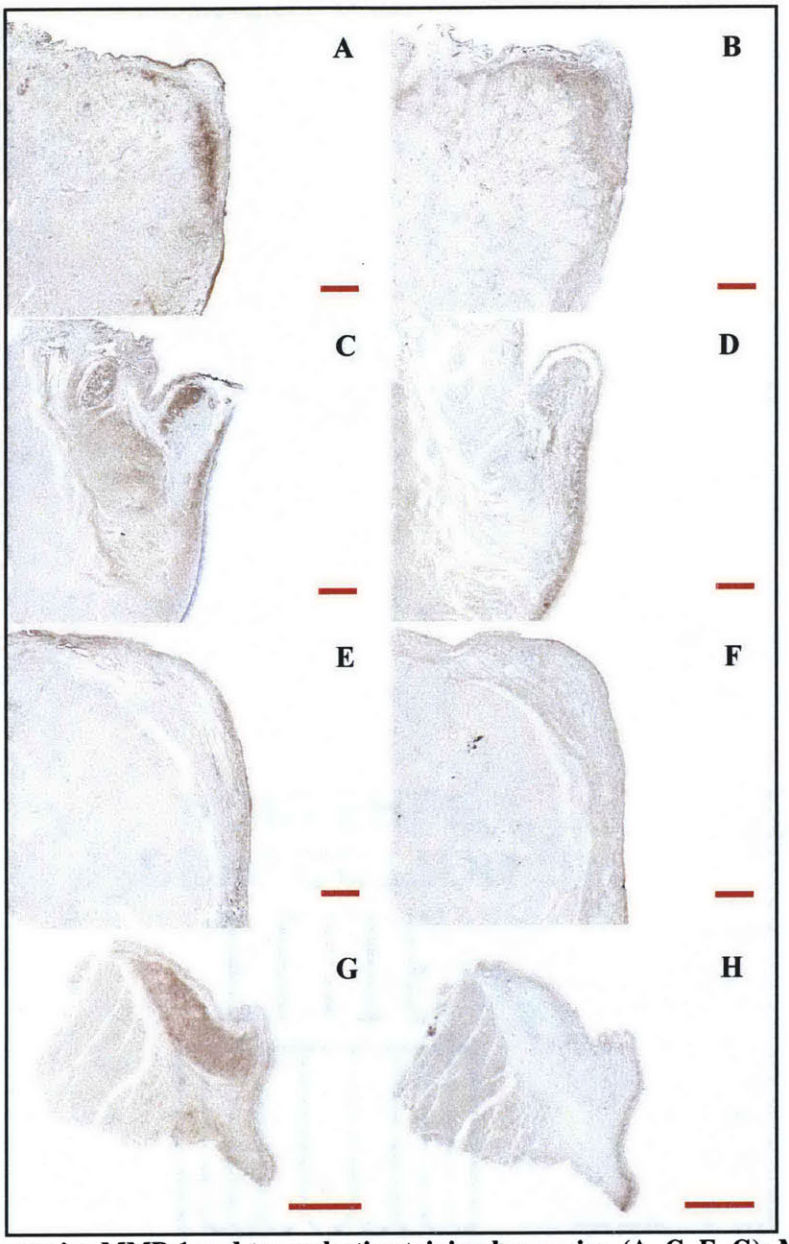

Figure 5.2: Representative MMP-1 and tropoelastin staining by species. (A, C, E, G): MMP-1 staining in human, dog, pig, and ferret, respectively; (B, D, F, H): tropoelastin staining in human, dog, pig, and ferret, respectively. Scale bars =500 μm.

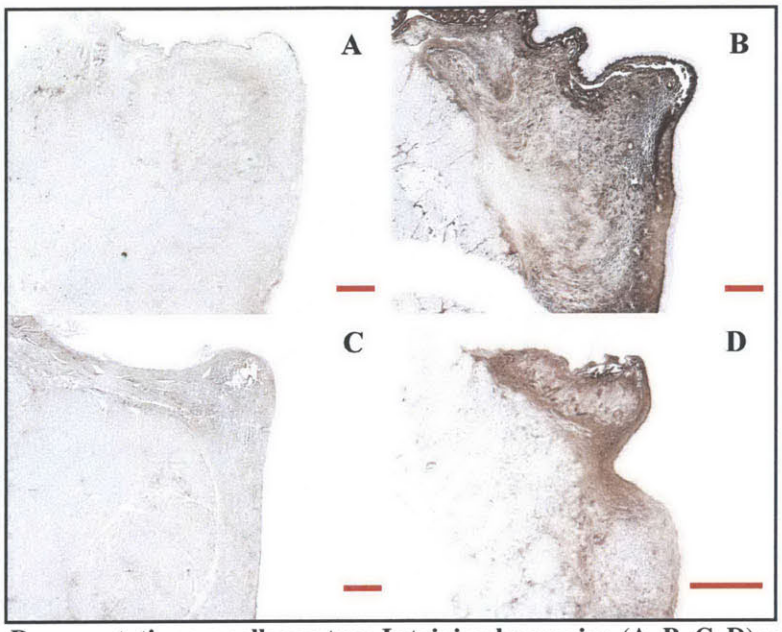

Figure 5.3: Representative procollagen type I staining by species. (A, B, C, D): procollagen type I staining in human, dog, pig, and ferret, respectively. Scale bars =500 μm.

subregion of the dog intermediate LP that stained intensely for hyaluronan and elastin (Chapter 4), tropoelastin staining could not be distinguished from background. In ferrets, however, tropoelastin staining was relatively high in the intermediate LP region of intense elastin and hyaluronan staining (Chapter 4). MMP-1 staining appeared to be high in each species in the regions documented in Chapter 4 to stain intensely for hyaluronan.

Comparing the procollagen type I staining with the bright field picrosirius staining distribution noted in Chapter 3, human LP procollagen type I staining seemed to be more superficially localized relative to total collagen. In pigs, procollagen type I staining tended to be most intense in the superior portion of the LP. In the more inferior pig LP regions, however, staining for procollagen type I tended to be low relative to the picrosirius staining intensity observed in these areas in Chapter 3. Dog and ferret procollagen type I staining appeared to be relatively low in the oblong subregion of the intermediate LP, which stained relatively intensely for hyaluronan in both species (Chapter 4).

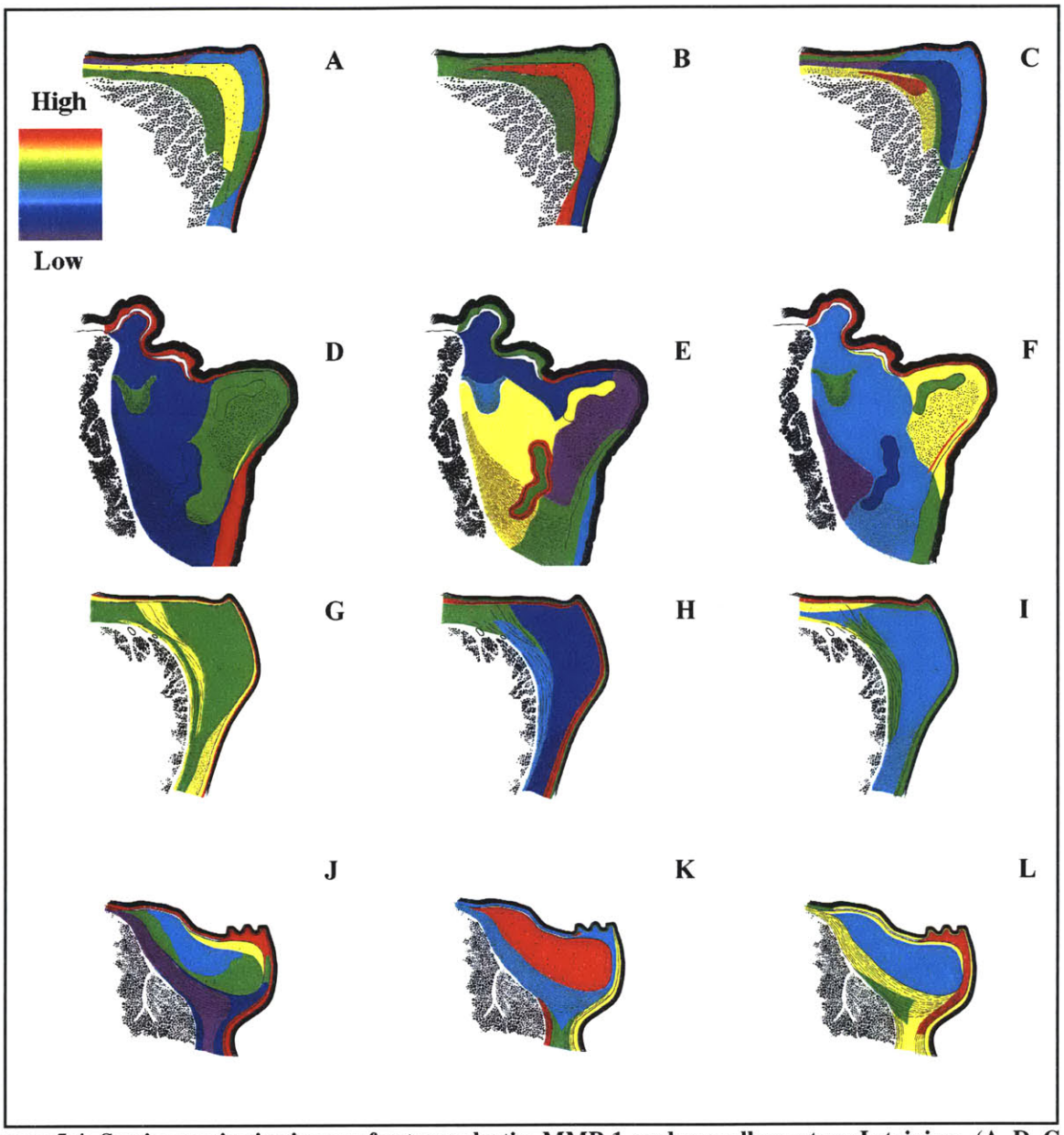

Figure 5.4: Semi-quantitative images for tropoelastin, MMP-1, and procollagen type I staining. (A, D, G, J): average relative tropoelastin staining in human, dog, and pig, and ferret, respectively; (B, E, H, K): average relative MMP-1 staining in human, dog, pig, and ferret, respectively; (C, F, I, L): average relative procollagen type I staining in human, dog, pig, and ferret, respectively.

5.4 Discussion

5.4.1 Biochemical results

It is known that a variety of cell types, including fibroblast-like cells, leukocytes, endothelial cells, and myofibroblasts, are present in the human LP [1]. Approximately 80% of these LP

cells appear to be fibroblast-like cells [1], and these fibroblast-like cells seem to be the primary ECM-producing cells of the LP [3].

In general, when the cellularity of a tissue is discussed, the cited cell density usually refers to the primary ECM-producing cells for that tissue. With respect to this definition, the cell densities measured in this study should be viewed as first-order estimates of the concentration of fibroblast-like ECM producing cells in the LP. The cell densities in this study are not exact measures of LP fibroblast-like cellularity since all cell types present in the dissected vocal fold specimens contributed to the measured DNA levels. In addition to the non-fibroblast-like cells in the LP, the LP specimens analyzed still had the overlying epithelium, which is approximately 3-5 cell layers thick, attached. When the cell number within the epithelium was estimated based on the surface dimensions of the LP specimens and epithelial cell diameter, epithelial cells were calculated to constitute 10-30% of measured cell number, depending on the assumed diameter and number of layers of the epithelial cells (data not shown). Combining the estimated percentage epithelial cells with the percentage of non-fibroblast LP cells reported by Catten et al. [1], it is evident that the present DNA measures provide important, albeit order of magnitude, assessments of LP cellularity.

5.4.2 Histochemical results

With respect to LP ECM turnover, the superficial shift in the tropoelastin staining distribution observed in humans and pigs relative to the corresponding elastin staining distribution (Chapter 4) seems to indicate that the elastin turnover in these species is highest in the more superficial LP regions. Increase in elastic fiber diameter has been linked to decreased elastin turnover. Hence, the present observations may correlate with previous electron microscopy studies of the human vocal fold LP, which have noted an increase in elastin fiber diameter proceeding from the superficial to the deep LP [10].

Procollagen type I staining gives insight into spatial variation in the rate of collagen type I production and turnover. For humans and pigs, procollagen type I staining tended to be more superficially oriented than the corresponding staining for total collagen (Chapter 3), indicating that collagen turnover in the more superficial layers may be higher than in the deeper LP layers. A higher rate of collagen turnover in the superficial LP of humans would be consistent with observations of smaller fiber diameters found in the superficial LP versus the deep LP [11], and these spatial differences in LP turnover may be required for proper human LP biomechanical function. In humans, the combined intermediate and deep LP is frequently referred to as the vocal "ligament", since these layers are assumed to balance the tension between the underlying muscle and the superficial LP [12]. The more highly cross-linked collagen fibers characteristic of the deep LP, which may result in part from lower collagen turnover in the deep LP relative to the superficial LP, may functionally allow this tension to be more effectively transmitted than if the fibers were less highly cross-linked. In the animal models, possible physiological grounds for observed regional differences in procollagen type I production relative to collagen presence are unclear.

MMP-1 is associated with the turnover of a variety of ECM molecules, including collagens type I and III and versican [13]. Comparing semi-quantitative MMP-1 staining distributions with those developed for total collagen (Chapter 3) and versican (Chapter 2), it appears that the MMP-1 staining pattern in all four species is only loosely correlated with those of total collagen and versican. Moreover, the staining patterns for procollagen type I do not seem to follow those for MMP-1 in any of the species analyzed. In dogs, ferrets, and humans, in particular, the staining of MMP-1 was often highest where staining for procollagen type I was correspondingly low. MMP-1 staining did, however, appear to correlate closely with hyaluronan staining in all species studied. This is an interesting observation, since MMP-1 production seems to be inhibited by hyaluronan for certain cell types [14]. Since the MMP-1 antibody used in this study recognizes both latent and active forms of MMP-1, the MMP-1 detected in the hyaluronan rich LP regions may be primarily in latent form.

This chapter has presented first order measures of vocal fold LP cellularity. Additionally, the spatial distribution of several important indicators of ECM turnover have been immunohistochemically analyzed, revealing significant regional variations in MMP-1 levels and in the production of tropoelastin and procollagen type I in the LP. These spatial variations in ECM turnover may be important in maintaining an LP with proper biomechanical function.

5.5 Literature cited

1. Catten, M., et al., Analysis of cellular location and concentration in vocal fold lamina propria. Otolaryngology-Head and Neck Surgery, 1998. **118**(5): p. 663-667.
2. Hirano, M., K. Sato, and T. Nakashima, Fibroblasts in geriatric vocal fold mucose. Acta Oto-Laryngologica, 2000. **120**(2): p. 336-340.
3. Hirano, M., K. Sato, and T. Nakashima, Fibroblasts in human vocal fold mucosa. Acta Oto-Laryngologica, 1999. **119**(2): p. 271-276.
4. Pawlak, A.S., et al., Immunocytochemical study of proteoglycans in vocal folds. Annals of Otology Rhinology and Laryngology, 1996. **105**(1): p. 6-11.
5. Garrett, C.G., J.R. Coleman, and L. Reinisch, Comparative histology and vibration of the vocal folds: Implications for experimental studies in microlaryngeal surgery. Laryngoscope, 2000. **110**(5): p. 814-824.
6. Ding, H. and S.D. Gray, Senescent expression of genes coding tropoelastin, elastase, lysyl oxidase, and tissue inhibitors of metalloproteinases in rat vocal folds: Comparison with skin and lungs. Journal of Speech Language and Hearing Research, 2001. **44**(2): p. 317-326.
7. Ding, H. and S.D. Gray, Senescent expression of genes coding collagens, collagen-degrading metalloproteinases, and tissue inhibitors of metalloproteinases in rat vocal folds: Comparison with skin and lungs. Journals of Gerontology Series a-Biological Sciences and Medical Sciences, 2001. **56**(4): p. B145-B152.
8. Rosen, C.A., Vocal fold scar - Evaluation and treatment. Otolaryngologic Clinics of North America, 2000. **33**(5): p. 1081-+.

9. Gregory, T.R., Nucleotypic effects without nuclei: Genome size and erythrocyte size in mammals. Genome, 2000. **43**(5): p. 895-901.
10. Sato, K. and M. Hirano, Age-related changes of elastic fibers in the superficial layer of the lamina propria of vocal folds. Annals of Otology Rhinology and Laryngology, 1997. **106**(1): p. 44-48.
11. Ishii, K., et al., Ultrastructure of the lamina propria of the human vocal fold. Acta Oto-Laryngologica, 1996. **116**(5): p. 778-782.
12. Kurita, S., et al., The Layer Structure of the Vocal Fold - Age-Dependent Variations. Folia Phoniatrica, 1980. **32**(3): p. 210-210.
13. Somerville, R.P.T., S.A. Oblander, and S.S. Apte, Matrix metalloproteinases: old dogs with new tricks. Genome Biology, 2003. **4**(6).
14. Shimizu, M., et al., Hyaluronan inhibits matrix metalloproteinase-1 production by rheumatoid synovial fibroblasts stimulated by proinflammatory cytokines. Journal of Rheumatology, 2003. **30**(6): p. 1164-1172.

Chapter 6. Final Observations, Summary, and Recommendations

6.1 Final observations and summary

To rationally design an implant material for scar restoration, it is important to have a more complete understanding of vocal fold lamina propria (LP) biochemistry and microstructure than is currently in literature. This dissertation presents the following critical insights into normal human LP biochemical structure:

1.) quantitative analysis of collagen, elastin, hyaluronan (HA), and proteoglycan (PG)/associated sulfated glycosaminoglycan (sGAG) presence;
2.) quantitative examination of the spatial distributions of collagen, elastin, and HA, and qualitative investigation of the spatial distributions of specific PG/sGAG types; and
3.) assessment of cellularity and spatial variations in extracellular matrix (ECM) turnover.

Similar analyses have been carried out on the vocal fold LPs of normal dog, pig, and ferret towards identifying an appropriate animal model for implant trials. Highlights from these biochemical and histological analyses are described below.

6.1.1 Biochemical results

Total collagen, elastin, HA, and sGAG by LP dry weight are shown in Figure 6.1. Focusing collagen and elastin, the human vocal fold LP contains approximately 20% less collagen than the dermis (Table 6.1); however, mean human LP elastin levels are approximately 5 times (by dry weight) the upper range of dermis elastin levels. Thus, the vocal folds may, to a first order, be expected to show a lower tensile strength and a higher elastic response than dermis. These comparisons, although neglecting important microstructural differences between these tissues, serve to place the LP in the context of biochemically and biomechanically well-characterized tissues.

Based on overall LP biochemical similarity alone (i.e., not accounting for differences in LP morphology or in biomolecule distribution and ultrastructure), it would appear that dogs are most similar to humans of the animal models studied. In the author's opinion, however, the more significant interspecies LP differences, in terms of assessing animal model suitability, were observed at the microstructural and morphological levels.

Table 6.1: Collagen and elastin in various tissues by dry weight [1]

	Percent of Dry Weight	
Tissue	**Elastin**	**Collagen**
Dermis	0.6-2.1	71
Lung	3-7	10
Ligamentum nuchae	75	17
Achilles tendon	4-5	86

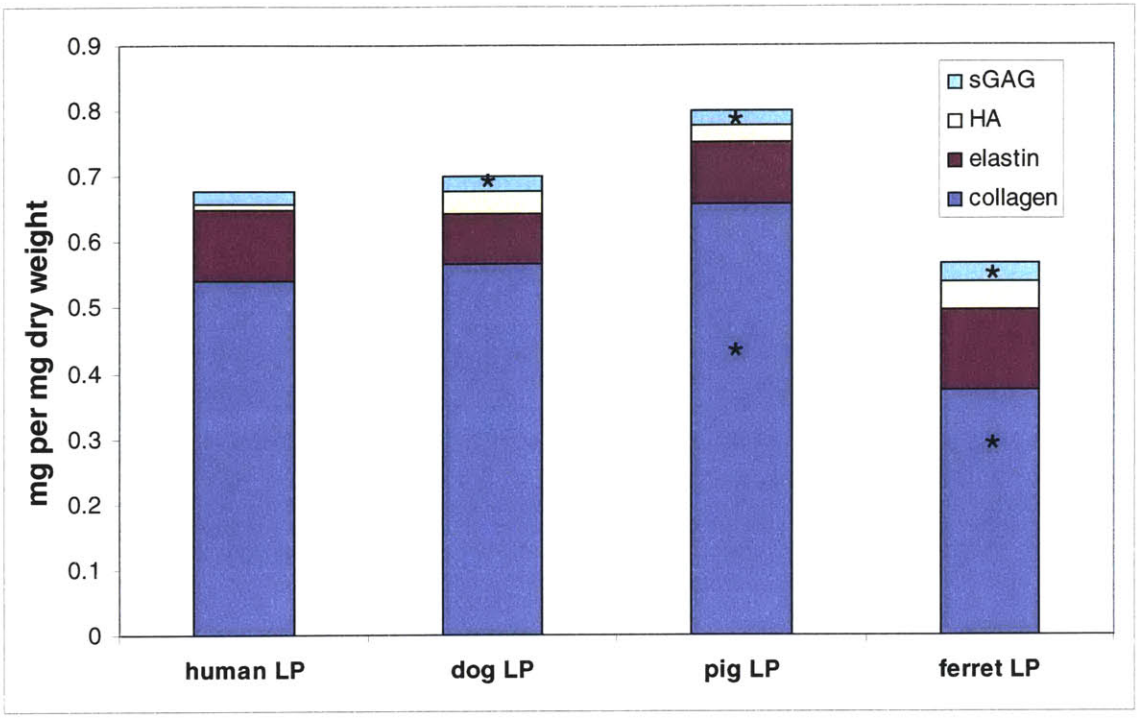

Figure 6.1: Combined LP biochemical results by dry weight. Total protein was assumed to constitute 80% of dry weight on average, matching unpublished observations. Error bars have been excluded for the purpose of clarity. Asterices indicate molecules in a given species found to be present in significantly different levels relative to those in humans. Elastin levels have been estimated from aortic desmosine levels listed in Chapter 3, with the dog conversion factor being used for ferrets.

6.1.2 Microstructural results

From quantitative histological studies described in chapters 3 and 4, the distribution of collagen and elastin within dog and ferret LP was seen to be inversely related to human collagen and elastin distributions. Elastin and collagen in the pig superficial LP also seemed to be more prevalent than in human superficial LP, although the spatial distributions of collagen and elastin in pig more closely matched those of human than did the other two animal models (See Chapters 3,4). Collagen and elastin are critical regulators of tissue biomechanical function. Therefore, marked human versus animal model variations in the LP distributions of these molecules may have implications for the appropriateness of specific animal models for use in human superficial LP restoration studies.

Immunohistochemical analyses described in Chapter 4 indicate that collagen types I and III are the primary collagen types in the midmembranous LP. The dominance of collagen types I and III seems to emphasize the repetitive compressive and tensile forces experienced in the midmembranous LP and the requirements for tissue resilience. The cyclic compressive and impact forces sustained by the LP appear to be further reflected in the diffuse versican staining noted in dog, human, and pig LPs (Chapter 2), and the fibrillin-1 staining observed in

Chapter 3 seems to indicate that tensile stresses, in humans, may be particularly high in the superficial LP. Staining for collagen type IV (Chapter 4) and heparan sulfate PG (Chapter 2) in the LP ECM apart from basement membranes seems to imply significant shear forces may be experienced deep within human and pig LP.

Although total sGAG levels in the LPs of the three animal models could not be statistically distinguished from that of humans ($p>0.05$, Chapter 2), the staining patterns for specific PG/sGAG classes varied significantly with species. In addition, intraspecies comparisons of specific PG/sGAG staining patterns revealed a number of microstructural subdivisions within the dog and ferret LPs that have not, to the author's knowledge, been previously described. These regions were indicated by boundaries or by dashed marks (intended to indicate observed fiber orientation) within the LP schematics developed in Chapter 2. The marked differences in the microstructural organization of human, dog, and ferret LPs documented in these schematics may have bearing on the appropriateness of dogs and ferrets as potential animal models in human LP restoration studies.

6.1.3 Morphological results

In developing the LP schematics introduced in Chapter 2, macroscopic differences in LP geometry among species were also noted. Although some alterations in the overall size and shape of each species' LP from its in vivo state due to the excision of the midmembranous LP from its attachments post-fixation should be expected, certain statements concerning macroscopic differences in LP morphology among species can still be made with confidence. Interspecies LP geometrical variations are particularly evident when one examines the shape of the LP-muscle boundary characteristic for a given species. The muscle-LP boundary in dogs and ferrets tends to be concave relative to the epithelial-LP boundary, whereas the muscle-LP boundary of human and pig LP is convex relative to the epithelial-LP boundary. Thus, if the center of mass of the human LP were calculated, it would lie outside of the LP, in the underlying muscle layer. The same would be true of pigs. The center of mass of dog and ferret LP, however, would be within the LP itself. These basic geometrical/LP mass distribution differences indicate that the observed similarity between human and dog vocal fold vibration [2] may result from different structural origins. This vibratory similarity has been one of the primarily grounds for the historical use of dogs as an animal model in LP research.

6.2 Recommendations

Based on examination of combined biochemical, structural, and morphological information, it is the author's assessment that pigs are the best model of the three potential animal models analyzed for implant studies seeking to restore function to the human superficial LP. Although pigs differ from humans in the distribution of hyaluronan (see Chapter 4) and pig LP molecular organization seems to be more homogenous than that of the human LP, overall,

the composition and microstructure of the pig superficial LP region appears to be more similar to that of humans than do dog and ferret superficial regions.

6.3 Literature cited

1. Welgus, H., M.D., Elastin, A.A.o. Dermatology, Editor.
2. Garrett, C.G., J.R. Coleman, and L. Reinisch, Comparative histology and vibration of the vocal folds: Implications for experimental studies in microlaryngeal surgery. Laryngoscope, 2000. **110**(5): p. 814-824.

Chapter 7. Contributions and Future Directions

7.1 Contributions

To the authors' knowledge, this dissertation presents the first quantitative measures of: (1) total collagen, (2) elastin, (3) hyaluronan (HA), and (4) proteoglycans (PG)/associated sulfated glycosaminoglycans (sGAG) in normal human vocal fold lamina propria (LP). These quantitative measures place this tissue in the context of other well-characterized tissues, establishing bounds on the expected contribution of various extracellular matrix (ECM) components to tissue biomechanical behavior. Immunostaining for specific collagen types and PG/sGAG classes has been carried out, yielding insight into the primary stresses sustained by the LP (see Chapters 2 and 3). Moreover, PG/sGAG types previously believed to be intracellularly or basement membrane localized, such as versican, chondroitin 6-sulfate, and heparan sulfate proteoglycan [1], have been identified in the LP ECM. Since vocal fold scarring is generally localized to superficial LP, quantitative histology has been used to calculate the percent of total collagen, elastin, and HA within specific LP regions (Chapters 3 and 4). Spatial variations in LP ECM turnover, as indicated by immunostaining for tropoelastin, procollagen type I, and matrix metalloprotease I (MMP-1), have also been investigated (Chapter 5), variations which may be important in maintaining proper LP physiology. In addition, total LP cellularity has been quantified (Chapter 5). The results from these analyses significantly advance the understanding of normal human LP biochemistry and microstructure and establish benchmarks for the evaluation of LP scar restoration strategies.

Similar biochemical and histological studies have been carried out on the LPs of three potential animal models: dog, pig, and ferret. Observation of LP biomolecule staining patterns have resulted in identification of microstructurally-related subdivisions in each animal model LP. Recognition of these LP subdivisions may yield insight into the adaptation of LP microstructure to the phonatory needs of each animal, just as the subdivision of human LP into layers heightened understanding of its structure-function relationship.

Comparison of animal and human LP biochemical and histological results seems to imply that dogs, the most common animal model in vocal fold research, may not be the most appropriate for human superficial LP restoration studies. Of the three animal models examined, pigs appear to be the most similar to humans in terms of LP composition, microstructure, and morphology (see Chapter 6).

Moving towards in vitro studies of implant materials, initial methods for vocal fold LP cell isolation and growth have been established (see Appendix B).

7.2 Future directions

Vocal fold research is a relatively nascent field with numerous exciting areas for future research. Potential avenues for future study include:

1.) With the goal of implant design and evaluation:
   a) the use of the developed biochemical and histological benchmarks for implant material evaluation in vitro
   b) analysis of biochemical and histological alterations characteristic of scarred LP
   c) development of appropriate biomechanical measuring equipment and establishment of relevant LP biomechanical benchmarks. Correlation of biomechanical data with the present biochemical and microstructural results may yield deeper insight into the LP structure-function relationship.

2.) On a more basic science level:
   a) investigation of the effects of biomechanical forces on vocal fold fibroblast cellular behavior
   b) quantitation of individual PG/sGAG and collagen types
   c) analyses aimed at understanding the physiology of vocal fold LP fibroblasts relative to that of fibroblast-like cell from other tissues.

7.3 Literature cited

1. Pawlak, A.S., et al., Immunocytochemical study of proteoglycans in vocal folds. Annals of Otology Rhinology and Laryngology, 1996. **105**(1): p. 6-11.

Appendix A. Optical Coherence Tomography Imaging of the Larynx

A.1 Background

In determining whether to pursue development of biochemical versus biomechanical benchmarks for implant design and evaluation, initial feasibility studies were carried out for both approaches. Optical coherence tomography (OCT)-based elastography is one method that was investigated for biomechanical assessment of vocal fold lamina propria (LP). OCT elastography has several advantages over traditional bulk rheological methods, such as cone-and-plate rheometers. Importantly, OCT elastography can potentially give information concerning spatial variations in LP biomechanical properties without requiring removal of the LP from its larynx attachments and from the effects of vocalis muscle tension.

For OCT elastography to be feasible, it is important that landmark LP features at various depths be resolvable and trackable with deformation. However, conventional OCT images of human vocal fold LP were relatively homogeneous in appearance near the vocal fold free edge, making such trackable features difficult to identify (see Figure A.2, which shows an OCT image of the human LP near the free edge. In contrast, Figure A.1 depicts the inferior surface of pig vocal fold LP, which is less homogenous than the free edge due to the presence of glandular structures, but which is not of high interest for biomechanical assessment). Although polarization-sensitive (PS)-OCT, which is sensitive to collagen fiber organization, yielded more differentiated LP images, significant variability in resulting banding patterns was noted across human specimens (the origin of these banding patterns is described below, data not shown). Thus, the relationship of these images to the human LP microstructure was unclear, and larger-scale examination and correlation of ex vivo OCT/PS-OCT vocal fold images with parallel histology would have been required before elastography stress-strain analyses could begin. The actual elastography deformation experiments and their correlation with applied stresses would in themselves require extensive methodology development and verification before biomechanical data could be gathered using this imaging tool. Therefore, the pursuit of OCT-based elastography for biomechanical assessment of the vocal fold LP was determined not to be feasible at that point. The results of these initial OCT imaging studies of the vocal fold are, however, useful to the laryngological community in evaluating the applicability of this imaging technology to the in situ diagnosis and monitoring of laryngeal pathologies and implants, and therefore, important outcomes will be discussed below.

A.2 Optical coherence tomography : introduction

OCT is a relatively new optical imaging modality that allows high resolution, cross-sectional imaging of tissue microstructure. Although OCT was first applied in 1991 to imaging

optically transparent structures, such as the anterior eye and retina [1, 2], subsequent technological advances have enabled high resolution imaging of nontransparent tissue in the cardiovascular system [3] and the gastrointestinal [4], urinary [5], and female reproductive tracts [6]. In addition, the application of OCT to surgical guidance [7] and carcinoma detection [6, 8] has been explored.

The aforementioned imaging studies have demonstrated that OCT is particularly informative in tissues in which non-keratinized epithelium is separated from underlying stroma by a smooth basement membrane zone, suggesting that OCT may have a strong clinical relevance in laryngology. This indication is further strengthened by several features of the OCT system itself: 1) OCT imaging can be performed in situ and nondestructively, enabling the imaging of tissue for which biopsy should be avoided or is impossible; 2) OCT can image with an axial resolution of 1-15 μm and to a depth of 1 to 3 mm in non-transparent tissue; 3) imaging can be performed in real-time, without the need to process a specimen, as in conventional biopsy, and without the need for a transducing medium, as in ultrasound imaging; 4) and OCT is fiber-optically based and can thus be interfaced to a wide range of instruments including catheters, endoscopes, laparoscopes, and surgical probes. Before presenting and discussing OCT images of specific laryngeal structures, it is useful to briefly describe the basis by which OCT systems form subepithelial images.

OCT systems perform high-resolution tomographic imaging by measuring light backscattered or backreflected from internal tissue structures. OCT imaging is analogous to ultrasound B mode imaging, but is based on the detection of infrared light waves, instead of sound. Like acoustic waves, light is characterized by its propagation direction. Light is distinct, however, in that it has an additional vector characteristic known as polarization. The polarization direction is orthogonal to the propagation direction and can be influenced by the medium in which the light propagates. This is known as birefringence. Polarization measurements can be used to provide additional insights into the microscopic structure and integrity of tissues. PS-OCT exploits birefringence as an additional contrast mechanism for imaging tissue, and PS-OCT will be discussed in further detail in a later section.

The analogy with ultrasound is a useful starting point for understanding the basics of OCT. In ultrasound, a high frequency acoustic pulse travels into the tissue and is reflected or backscattered from internal structures having different acoustic properties. The magnitude and the delay time of the echoes are electronically detected, and the structural properties of the internal tissues are determined from the measured signals. In OCT, imaging is performed by measuring the echo delay time and magnitude of light backreflected or backscattered from internal structures with distinct optical properties. Unlike in ultrasound, though, the speed of light is very high, rendering electronic measurement of the echo delay time of the reflected light impossible. OCT systems circumvent this limitation by using low coherence interferometry to characterize optical echoes.

Two or three dimensional images are produced by scanning the light beam across the sample and recording the optical backscattering versus depth at different transverse positions. The

resulting data is a two or three dimensional representation of the optical backscattering of the sample on a micron scale.

A.3 OCT imaging of the larynx: preliminary results

To assess the potential value of OCT imaging technology to improving visualization and pathology diagnosis and treatment of a specific organ, it is essential to first image normal tissue from that organ and then reference the resulting OCT images to parallel histology.

Initial studies of laryngeal imaging using OCT have focused on the free edge and inferior surface of the vocal folds. Figure A.1 presents an OCT image taken along the inferior portion of a pig vocal fold, as evidenced by the transition from free-edge non-glandular LP to subglottal glandular LP observed in the OCT image and corresponding histological section. This OCT image illustrates the ability of OCT to allow visualization of the epithelium, basement membrane, and certain structural features such as glands and vessels. Note in particular that local thickness and transparency of the vocal fold epithelium can be readily deduced from these images, implying that OCT may prove useful for the diagnosis of hyperplasia, early stage keratosis and papillomas, and other pathologies resulting in epithelial abnormalities not normally visible by conventional light endoscopy until an advanced stage. Since many laryngeal pathologies originate at the epithelial-LP border, the ability to observe basement membrane integrity via OCT imaging may have important implications for the use of this technology in aiding the diagnosis and monitoring of such laryngeal disorders.

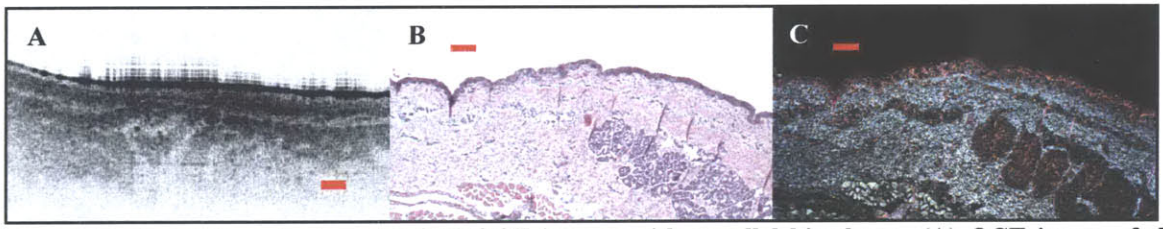

Figure A.1: Correlation of pig vocal fold OCT images with parallel histology. (A) OCT image of the inferior surface of a pig vocal fold; (B) corresponding H&E histology section; (C) phase-contrast viewing of the stained histology section. Scale bars=150μm.

A.4 Polarization sensitive optical coherence tomography

A monochromatic light wave carries three potential sources of information contained in the amplitude, phase, and polarization state of its electric field vector. Conventional OCT, by detecting only the intensity of the interference pattern resulting from interaction of the sample and reference optical beams, fails to quantify the effects of tissue on the polarization state of the sample light beam. An adjunct to conventional OCT, known as polarization sensitive OCT (PS-OCT), therefore, has focused on exploiting the information contained in the

polarization state of the light backreflected or backscattered from the sample relative to that of the reference beam to obtain information about the tissue microstructure.

In order to appreciate the power of PS-OCT and its potential applications, it is helpful to describe briefly the main mechanisms by which tissue alters the polarization state of light. Two mechanisms dominate the changes in the polarization state of light propagating through biological tissue: scattering and birefringence. Scattering changes the polarization of light mainly in a random manner, so it is generally not useful in mapping tissue structure. Organized linear structures, on the other hand, such as collagen fiber bundles with a clear orientation, can exhibit birefringence, resulting in a predictable change in polarization state. Many biological tissues exhibit birefringence, such as tendons, muscle, nerve, bone, cartilage and teeth [9]. Since changes in birefringence may, for instance, indicate changes in functionality, structure, or viability of tissues, PS-OCT images may contain information which can be used to evaluate tissue microstructure and health beyond the level possible with the use of OCT alone [10].

The potential implications for clinical laryngology of the sensitivity of PS-OCT to organized linear structures, such as oriented collagen fiber bundles, are numerous. To illustrate, the human vocal fold LP is generally subdivided into the superficial, intermediate, and deep layers, each layer having a characteristic composition and functionality. The relative thickness and integrity of these various layers appear to have a profound impact on voice. This idea is supported by the fact that the average adult will experience marked thinning of the superficial LP relative to the intermediate and deep layers with increasing age [11], with a concomitant reduction in voice quality.

Histological studies of normal adult human vocal fold tissue have repeatedly noted increased density and orientation of collagen fibers as one progresses from more superficial to deeper LP layers [11]. The collagen fibers present in the superficial layer appear to be loose and randomly oriented. PS-OCT, due to its sensitivity to oriented collagen fiber bundles, may thus allow indirect detection of these LP layers in situ and hence monitoring and possibly improved treatment of voice aging. In the case of vocal fold scarring, the biomechanical integrity of the LP is disrupted, resulting in reduced vocal fold pliability and thus decreased vocal range and quality. Scar tissue has collagen fiber orientation and density that is generally distinct from that of normal tissue, and therefore PS-OCT also may prove useful in visualizing, localizing, and treating vocal fold scar within the LP. These capabilities could have significant impact on the area of voice management.

Figure A.2 compares a PS-OCT image of the free-edge/inferior surface of a human vocal fold with the corresponding OCT image and histological section. Note the banding pattern apparent in the PS-OCT image of the vocal fold: a transition from white to black banding indicates a change in the polarization state of light. In particular, observe the marked increase in thickness of the initial white band in the leftmost portion of the PS-OCT image (corresponding to free-edge tissue) relative to that in the image portion corresponding to increasingly subglottic tissue. The spatial location of this increase in initial white-band

thickness correlates closely with increasing prominence of the vocal fold superficial LP in the same region. Due to lack of an adequate data set, it is not possible for these spatial banding patterns to be definitively interpreted at this point. However, it can be hypothesized that the increased thickness of the initial white band as one moves superiorly from subglottic to free-edge tissue is due in part to the presence of a rich layer of more randomly oriented collagen in the increasingly free-edge region which is not present in the more subglottic space. As such, the more conspicuous this slowed transition from white to black banding in the region of the superficial LP, the more significant the superficial layer may be in terms of overall LP composition.

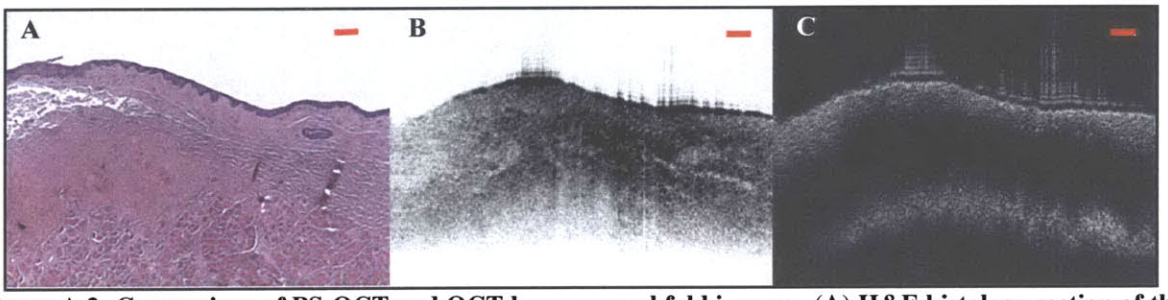

Figure A.2: Comparison of PS-OCT and OCT human vocal fold images. (A) H&E histology section of the inferior surface of a human vocal fold; (B); corresponding OCT image; (C) corresponding PS-OCT image. Scale bar=150μm.

Again, it must be stressed that further studies need to be carried out to determine what the observed vocal fold polarization patterns truly indicate. In the case that these studies show that the relative thickness and/or health of the LP layers can indeed be indirectly assessed by this imaging adjunct, PS-OCT could prove very useful to the study of LP health and in the development of targeted scar treatment strategies.

A.5 Summary

OCT and OCT-adjuncts have potential for improving the diagnosis and management of vocal fold pathology as well as for in vivo implant monitoring. Conventional OCT studies of healthy laryngeal tissues ex vivo have demonstrated that OCT can detect spatial changes in the thickness and transparency of the epithelium; the content of the connective tissues in terms of glands and vessels; pronounced transitions in connective tissue type; and the architecture of the basement membrane. PS-OCT holds promise for permitting indirect "visualization" of the layers of the vocal fold LP as well as of vocal fold scar beds. In addition, a number of other OCT adjuncts, such as spectroscopic OCT [12] and phase dispersion tomography [13] exist or are currently in development, each with distinct imaging advantages and capabilities over conventional OCT imaging.

A.6 Literature cited

1. Hee, M., et al., Optical coherence tomography of the human retina. Archives of Opthalmology-Chicago, 1995. **113**(3): p. 325-32.
2. Swanson, E., et al., In-vivo retinal imaging by optical coherence tomography. Optics Letters, 1993. **18**(21): p. 1864-6.
3. Jang, I., et al., Visualization of coronary atherosclerotic plaques in patients using optical coherence tomography: comparison with intravascular ultrasound. Journal of the American College of Cardiology, 2002. **39**: p. 604-9.
4. Bouma, B., et al., Endoscopic optical coherence tomography of the gastrointestinal tract. Gastrointestinal Endoscopy, 1999. **49**(4 (part 2)): p. 390.
5. Tearney, G., et al., Optical biopsy in human urologic tissue using optical coherence tomography. Journal of Urology, 1997. **157**(5): p. 1915-9.
6. Pitris, C., et al., High-resolution imaging of gynecologic neoplasms using optical coherence tomography. Obstetrics and Gynecology, 1999. **93**(1): p. 135-9.
7. Boppart, S., et al., Intraoperative assessment of microsurgery with three-dimensional optical coherence tomography. Radiology, 1998. **208**(1): p. 81-6.
8. Jesser, C., et al., High resolution imaging of transitional cell carcinoma with optical coherence tomography: feasibility for the evaluation of bladder pathology. British Journal of Radiology, 1999. **72**(864): p. 1170-6.
9. de Boer, J., et al., Polarization Sensitive OCT., in Handbook of optical coherence tomography, B. Bouma and G. Tearney, Editors. 2002, Marcel Dekkar: Basel.
10. Drexler, W., et al., Correlation of collagen organization with polarization sensitive imaging of in vitro cartilage: implications for osteoarthritis. Journal of Rheumatology, 2001. **28**(6): p. 1311-8.
11. Hammond, T.H., S.D. Gray, and J.E. Butler, Age- and gender-related collagen distribution in human vocal folds. Annals of Otology Rhinology and Laryngology, 2000. **109**(10): p. 913-920.
12. Morgner, U., et al., Spectroscopic optical coherence tomography. Optics Letters, 2000. **25**(2): p. 111-3.
13. Yang, C., et al., Phase-dispersion optical tomography. Optics Letters, 2001. **26**(10): p. 686-8.

Appendix B. Vocal Fold Cell Isolation and Culture

B.1 Introduction

The isolation of a tissue's primary extracellular matrix (ECM)-producing cells is a necessary precursor to in vitro analysis of materials to be used for replacement or restoration of that tissue. Thus, two protocols were compared for effectiveness in isolating high purity populations of vocal fold fibroblast-like cells, the primary ECM-producing cells in the vocal fold lamina propria (LP) [1]. In addition, several media types were compared for their effects on vocal fold fibroblast growth, morphology, and viability.

B.2 Cell isolation

Vocal fold fibroblasts were isolated using two different methodologies:

(1) Primary explant:

This procedure relies on cell migration out of the explant tissue. Since fibroblast-like cells have been observed to migrate faster than many other cell types, explant culture has potential for yielding high purity fibroblast populations given appropriate culture conditions [2].

(2) Enzymatic release of cells:

The dermis is a tissue containing many of the same cell types as the vocal fold LP, including myofibroblasts, endothelial cells, leukocytes, and ECM-producing fibroblasts. A commonly used method for isolating dermal fibroblasts involves the following procedure: treatment of the skin biopsy tissue with dispase to dissociate the overlying epithelium from dermis followed by trypsinization of the dermis to release ECM-associated cells [2]. The more rapid proliferation of fibroblasts over contaminant cell types is apparently sufficient to result in high purity fibroblast cell populations after the first several passages.

Ideally, verification of the purity of a primary cell population would involve antibody-based examination of cell types. Although there are no specific cell markers for pig fibroblast-like cells on the market, antibodies specific for many of the potential contaminant cell types, such as leukocytes and endothelial cells, do exist. Thus, the purity of the resulting cell populations can still be assessed by using immunolabelling to verify the absence of contaminant cell populations. The assessments made in this study, however, were based on morphological examination of cell population rather than more rigorous antibody-based examination, due to difficulty in locating appropriate pig negative and positive control cell populations for the antibody-based assays.

Based on visual assessments of cell purity, dispase-trypsin treatment of the vocal fold generally resulted in the significant levels of contaminant cell types that did not appear to be eliminated with passaging. Although fibroblast-like cells were the primary cell types present, contaminant cells would form cell "islands" within surrounding fibroblast-like cells. These cell islands would usually either form raised multicellular structures or flat sheets of fully juxtaposed cells (see Figure B.1), behavior not typically associated with a pure fibroblast population. These cell islands were absent from primary explant cultures, which appeared to yield a relatively uniform cell population in terms of cell morphology and intercellular spacing/organization. These results imply that purity of isolated vocal fold fibroblast-like cell populations may be improved in primary explant versus dispase-trypsin procedures.

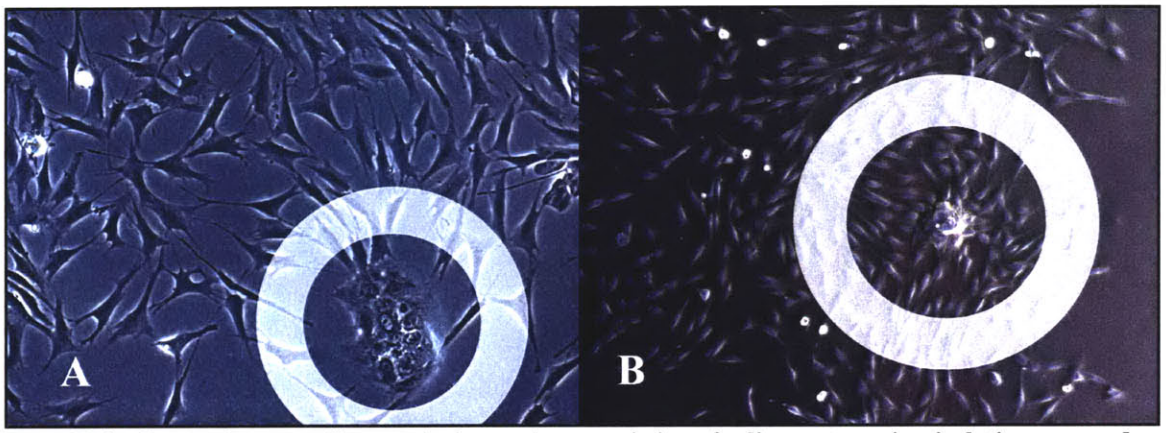

Figure B.1 Contaminant cell populations characteristic of dispase-trypsin isolation procedures. Contaminant cell islands/clusters are circled in white. (A) represents fully-juxtaposed monolayer contaminant cells; (B) represents contaminant cells forming a raised structure.

B.3 Analysis of media types

Previous in vitro studies of vocal fold fibroblasts have used either Dulbecco's Modified Eagle Medium (DMEM) or Eagle's Minimal Essential Medium (MEM) supplemented with fetal bovine serum (FBS) [3-6], both of which are standard media for fibroblast cell culture. However, comparison of the effects of various media types on vocal fold fibroblasts cell morphology and growth has not been carried out. Thus, several different media types were examined for their effects on vocal fold fibroblast proliferation, survival on prolonged exposure to stress, and morphology:

1.) DMEM +10% FBS +
[100 Units/mL penicillin + 100 μg/mL streptomycin] (100 P/S)
2.) DMEM +10% FBS + 100 P/S
3.) MEM + 10% FBS +100 P/S
4.) MEM + 0.1mM non-essential amino acids + 10% FBS +100 P/S
5.) Fibroblast Basal Medium (FBM, Cambrex) +10% FBS +100 P/S
6.) FBM + 1ng/mL hFGF-B + 5 μg/mL insulin + 2%FBS +100 P/S

Results for media 1, 4, 5, and 6 will be focused on in the discussion below. For brevity, the above media will be referred to as: (1) DMEM, (4) MEM+neaa, (5) FBM, and (6) FBM2.

Table B.1 indicates relative proliferation of vocal fold fibroblasts in various media types. Primary pig vocal fold fibroblasts originating from a single passage 6 parent flask were seeded at equal densities among daughter flasks. Groups of daughter flasks received different media types, with media changed every 3 days. After 6 days of growth, cells from each media group were trypsinized, counted using a hemacytometer and tested for viability by trypan blue exclusion. As indicating in Figure 1, cells cultured in media 1,4, and 5 proliferated at a lower rate than those in FBM2. (Cell proliferation in media 2 and 3 was also lower than that in FBM2, data not shown.) The increased proliferation in FBM2 is not unexpected due to the presence of hFGF-B in this media. As can be seen from Tables B.1 and B.2, viability both within 30 minutes post-trypsinization and 3 hours post-trypsinization remained greater than 95% for cells grown in FBM2 media, whereas viability of cells grown in the remaining media types fell to under 90% 3 hours post-trypsinization. Thus cell viability upon extended exposure to stress appears to be higher in FBM2 media than in the remaining media types assayed, a result which is important for ensuring high initial cell viability in encapsulation studies.

In addition to increased proliferative capacity and improved survival, cells grown in FBM2 media were on average smaller and grew more regularly, in terms of cell shape and intercellular spacing, than cells grown in the remaining media types (see Figure B.2). Due at least in part to the increased cell size, cells grown in media 1-5 did not reach the same cell density and number at confluence as those grown in FBM2. The marked alterations in cell size and morphology with media type observed for pig vocal fold fibroblasts were not noted for dermal fibroblasts grown in DMEM versus FBM media. This observation was based on only a single human dermal fibroblast sample, and therefore further and more detailed examination would be required to verify this observation. However, if this disparity between dermal and vocal fold fibroblast responses to media types holds under further experimentation, it may suggest the existence non-environmentally induced differences between dermal and vocal fold fibroblasts.

Table B.1: Cell number and viability by media type. Cell numbers were normalized by FBM2 cell numbers. Cell viability was assessed within 30 minutes post-trypsinization.

Medium	Cells /cells in FBM2	Cell viability
FBM2	1	97%
FBM	.301	93%
DMEM	.250	93%
MEM+neaa	.203	94%

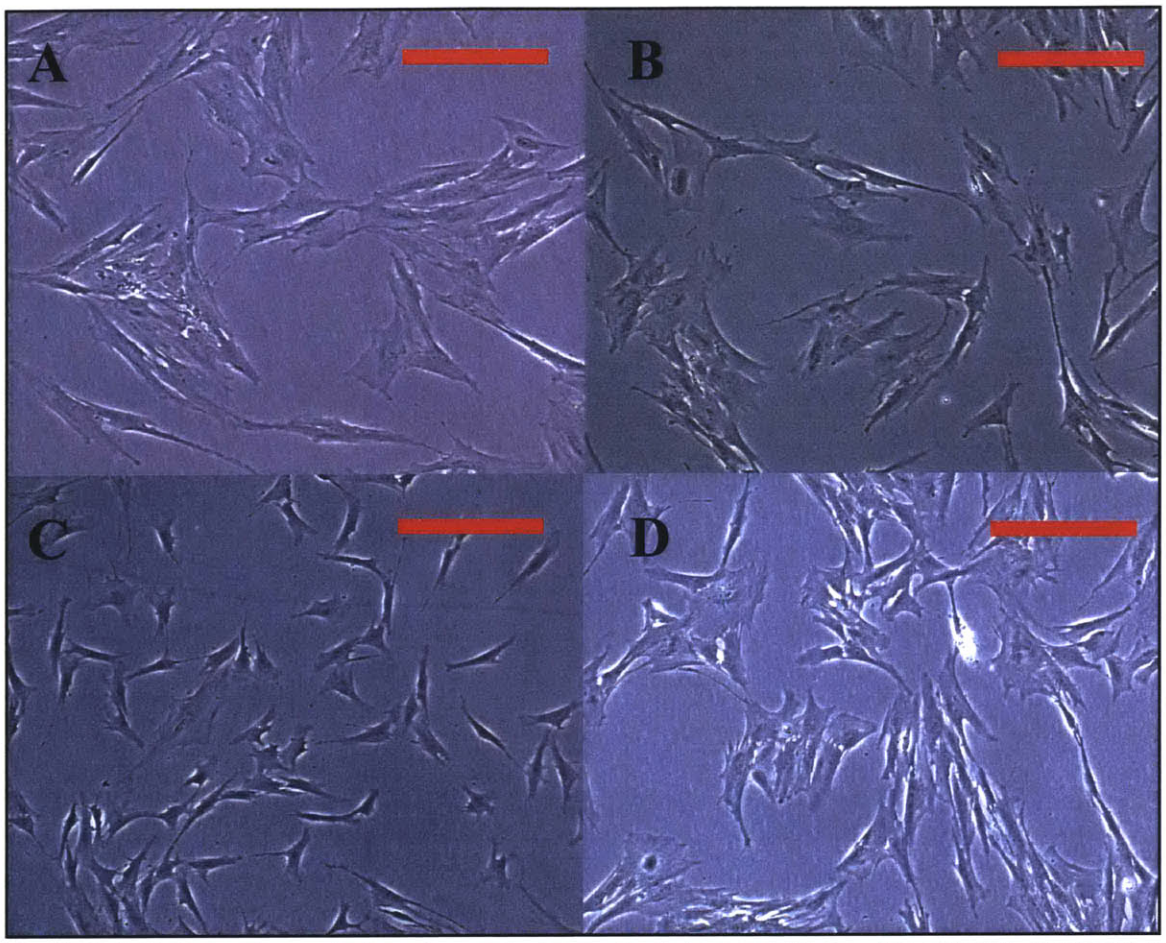

Figure B.2 Cell size and morphology by media type. Scale bars = 200 μm. (A) DMEM, (B) FBM, (C) FBM2, (D) MEM+neaa.

Independent of media type, a noticeable decrease in the proliferation rate of primary explant pig vocal fold fibroblasts generally began following passage 4. Changes in cell morphology were also observed as the cells became senescent. Most notably, increased lamellipodia and intracellular vacuolization were noted with increased age (data not shown).

Table B.2: Cell viability following exposure to prolonged stress. Cell viability was assessed 3 hours post-trypsinization following two centrifugations at 300g for 6 minutes each (typical conditions in initial encapsulation experiments).

Medium	Cell viability
FGM2	97%
FBM	90%
DMEM	87%
MEM+neaa	80%

B.4 Recommendations

Based on the above results, FBM2 appears to be the optimal medium of the media types examined in terms of cells growth up to the point of cell-encapsulation. Aside from yielding improved cell proliferation and viability upon prolonged exposure to stress, FBM2 is attractive because of its reduced levels of FBS, making FBM2 a more defined media than the remaining media types analyzed. However, FBM2 contains hFGF-B and insulin, additives that may not be appropriate for optimal in vitro post-encapsulation studies. The use of this media post-encapsulation requires further investigation, although its utility in these studies will likely depend on experimental design.

B.5 Literature cited

1. Catten, M., et al., Analysis of cellular location and concentration in vocal fold lamina propria. Otolaryngology-Head and Neck Surgery, 1998. **118**(5): p. 663-667.
2. Freshney, R.I., Culture of animal cells : a manual of basic technique. 2000, New York: J. Wiley.
3. Thibeault, S.L., et al., Instability of extracellular matrix gene expression in primary cell culture of fibroblasts from human vocal fold lamina propria and tracheal scar. Annals of Otology Rhinology and Laryngology, 2002. **111**(1): p. 8-14.
4. Hirano, S., et al., Roles of hepatocyte growth factor and transforming growth factor beta 1 in production of extracellular matrix by canine vocal fold fibroblasts. Laryngoscope, 2003. **113**(1): p. 144-148.
5. Hirano, S., et al., Morphological and functional changes of human vocal fold fibroblasts with hepatocyte growth factor. Annals of Otology Rhinology and Laryngology, 2003. **112**(12): p. 1026-1033.
6. Yamaguchi, T., T. Shin, and H. Sugihara, Reconstruction of the laryngeal mucosa - A three-dimensional collagen gel matrix culture. Archives of Otolaryngology-Head & Neck Surgery, 1996. **122**(6): p. 649-654.